

Review

# Analysis, Assessment, and Mitigation of Stress Corrosion Cracking in Austenitic Stainless Steels in the Oil and Gas Sector: A Review

Mohammadtaghi Vakili , Petr Koutník, Jan Kohout  and Zahra Gholami 

ORLEN UniCRE, a.s., Revoluční 1521/84, 400 01 Ústí nad Labem, Czech Republic;  
petr.koutnik@orlenunicre.cz (P.K.); jan.kohout@orlenunicre.cz (J.K.); zahra.gholami@orlenunicre.cz (Z.G.)  
\* Correspondence: mohammadtaghi.vakili@orlenunicre.cz

**Abstract:** This comprehensive review examines the phenomena of stress corrosion cracking (SCC) and chloride-induced stress corrosion cracking (CI-SCC) in materials commonly used in the oil and gas industry, with a focus on austenitic stainless steels. The study reveals that SCC initiation can occur at temperatures as low as 20 °C, while CI-SCC propagation rates significantly increase above 60 °C, reaching up to 0.1 mm/day in environments with high chloride concentrations. Experimental methods such as Slow Strain Rate Tests (SSRTs), Small Punch Tests (SPTs), and Constant-Load Tests (CLTs) were employed to quantify the impacts of temperature, chloride concentration, and pH on SCC susceptibility. The results highlight the critical role of these factors in determining the susceptibility of materials to SCC. The review emphasizes the importance of implementing various mitigation strategies to prevent SCC, including the use of corrosion-resistant alloys, protective coatings, cathodic protection, and corrosion inhibitors. Additionally, regular monitoring using advanced sensor technologies capable of detecting early signs of SCC is crucial for preventing the onset of SCC. The study concludes with practical recommendations for enhancing infrastructure resilience through meticulous material selection, comprehensive environmental monitoring, and proactive maintenance strategies, aimed at safeguarding operational integrity and ensuring environmental compliance. The review underscores the significance of considering the interplay between mechanical stresses and corrosive environments in the selection and application of materials in the oil and gas industry. Low pH levels and high temperatures facilitate the rapid progression of SCC, with experimental results indicating that stainless steel forms passive films with more defects under these conditions, reducing corrosion resistance. This interplay highlights the need for a comprehensive understanding of the complex interactions between materials, environments, and mechanical stresses to ensure the long-term integrity of critical infrastructure.

**Keywords:** stress corrosion cracking; mechanism; mitigation; austenitic stainless steel



**Citation:** Vakili, M.; Koutník, P.; Kohout, J.; Gholami, Z. Analysis, Assessment, and Mitigation of Stress Corrosion Cracking in Austenitic Stainless Steels in the Oil and Gas Sector: A Review. *Surfaces* **2024**, *7*, 589–642. <https://doi.org/10.3390/surfaces7030040>

Academic Editors: Jaeho Kim, Susumu Yonezawa and Alexey Yerokhin

Received: 25 June 2024

Revised: 5 August 2024

Accepted: 14 August 2024

Published: 16 August 2024



**Copyright:** © 2024 by the authors. Licensee MDPI, Basel, Switzerland. This article is an open access article distributed under the terms and conditions of the Creative Commons Attribution (CC BY) license (<https://creativecommons.org/licenses/by/4.0/>).

## 1. Introduction

Materials with exceptional properties are highly valued in the oil and gas industry due to their ability to withstand diverse and specialized environments. Austenitic stainless steel (ASS), a class of iron-based alloys, is renowned for its versatility. Various grades are tailored for specific applications and are widely utilized in this sector [1]. ASS typically contains approximately 19% chromium and 10% nickel, resulting in a predominantly austenitic microstructure at room temperature. This structural stability endows ASS with exceptional characteristics, including high strain hardening, cleanability, low susceptibility to product contamination, superior impact toughness, plasticity, thermal stability, weldability, corrosion resistance, and extended lifespan [2,3]. These properties make ASS a versatile material well suited for diverse applications, particularly within the oil and gas industry [4].

However, despite their advantages, equipment and pipelines in the oil and gas industry are susceptible to various localized corrosion phenomena, including stress corrosion

cracking (SCC), intergranular corrosion (IGC), crevice corrosion, and pitting. This susceptibility is often attributed to the reversion of high-iron-concentration ASS to its native hydroxide or oxide form following the refining process in blast furnaces [5]. Numerous failures in the oil and gas sector have been linked to localized corrosion processes, particularly SCC, which is widely recognized as a primary failure mode in humid environments, leading to significant economic losses and environmental disasters worldwide.

SCC is a phenomenon observed in metals and alloys, characterized by environmentally induced crack propagation. It primarily affects materials protected against uniform corrosion by passive films. The breakdown of localized passivity due to mechanical stresses can accelerate attacks in specific regions [6]. SCC arises from the synergistic effects of a particular aqueous environment, a susceptible alloy, and tensile stress [7,8]. The vulnerability of pipeline steels to SCC is influenced by a multitude of factors, including the steel's chemical composition, texture, inclusion and precipitate distribution, and microstructure; the pH of the environment surrounding the pipeline; the pH of the transported oil and gas; and other relevant considerations [9]. SCC growth in pipelines can occur unpredictably under constant-load and static tensile conditions, particularly in environments conducive to corrosion. This can alter the mechanical characteristics of carbon steel pipelines, making them more susceptible to SCC and initiating crack formation. Subsequently, cracks can propagate rapidly through the pipeline material, ultimately leading to failure. Laboratory testing combining electrochemical and mechanical measurements is often conducted under controlled conditions before and after electrochemical evaluations to assess SCC susceptibility [5]. Detecting and predicting SCC presents challenges, especially in the oil and gas industry, where unforeseen failures can have significant consequences [10]. SCC growth can initiate and spread to total fracture with little warning, even in corrosion-resistant materials. Fracture surfaces often exhibit severe embrittlement, with numerous small cracks at the time of failure. The industrial significance of SCC lies in the difficulty of eliminating stresses induced during component fabrication, making reliable measurements challenging [11].

SCC is a complex process that uniquely affects material properties, distinguishing it from stress or corrosion alone. This complexity is particularly significant in industries where stresses are commonly induced during fabrication. Removing or accurately measuring these stresses in engineering structures is often challenging or impractical. SCC substantially impacts structural integrity and represents a common cause of failures in various systems and industries, such as oil and gas and petrochemicals [12,13]. Figure 1 schematically illustrates the development of uniform and localized corrosion. Unlike general corrosion, where material loss can be determined based on average corrosion rates, SCC is a localized form of corrosion. The service life of the material is considered complete when the fastest-growing localized corrosion attack leads to the first perforation. Therefore, considering the maximum crack growth rate or the minimum time for crack initiation is crucial in estimating the life of components affected by SCC. In the absence of a crack, a component can be assumed to have an infinite life from the perspective of SCC considerations [6].

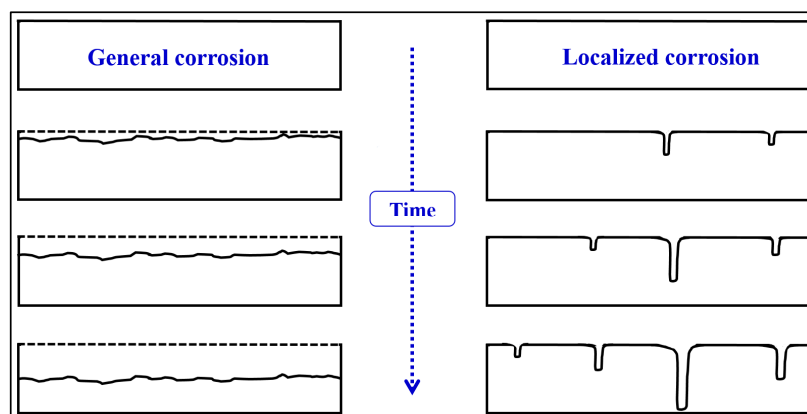


**Figure 1.** Schematic of general and localized corrosion development.

SCC can occur in highly corrosion-resistant alloys, even in seemingly innocuous environments. Detecting tight cracks perpendicular to the tensile stress axis during the initial stages of SCC is challenging using non-destructive techniques. The highly localized nature of SCC is evident from the high aspect ratio of a growing crack, which can reach values as high as 1000. Additionally, SCC exhibits macroscopic brittleness in ductile materials, allowing cracks to initiate and propagate without significant dimensional changes. These features emphasize the potential for unnoticed failures if SCC is not anticipated [6]. In pipeline steel, SCC crack initiation and propagation occur in three stages. Initially, small SCC cracks continuously initiate and coalesce, representing a significant proportion of the pipeline steel's lifetime. Subsequently, these small cracks propagate rapidly, ultimately leading to material failure. A notable feature of SCC in pipeline steels is the branching of cracks, which can be classified into micro- and macro-branching [9].

This review aims to provide a comprehensive overview of SCC in refinery environments, highlighting the importance of research and development in this area. The complexity of SCC and its significant impact on refinery operations, including economic losses and environmental disasters, underscores the urgent need for a thorough understanding of the underlying mechanisms and the development of effective prevention strategies. In this review, the parameters, mechanisms, assessment, and prevention methods of SCC in refinery environments are discussed in detail. Furthermore, chlorine-induced SCC is examined. By combining detailed failure analyses, process optimization, and materials engineering, the refining industry can develop effective strategies to mitigate SCC and ensure the safe and reliable operation of refinery equipment, thereby minimizing the risk of catastrophic failures and their associated consequences.

## 2. SCC Failure Events

SCC has been a major cause of failures in gas and oil transmission pipelines since the mid-1960s. This phenomenon, particularly affecting the external surfaces of buried pipelines, occurs when a susceptible material is exposed to a corrosive environment and tensile stress, either from internal pressure or external forces. SCC poses significant risks, including leaks or ruptures, which can have severe consequences for nearby residents, workers, and the environment. The first documented SCC incident occurred in 1965 in Natchitoches, Louisiana, where a 24-inch natural gas pipeline ruptured, resulting in 17 fatalities. This tragic event spurred extensive research into SCC and led to the introduction of U.S. pipeline safety regulations in 1970 [14].

Since then, SCC has been detected in pipelines across various countries, including Iran, Canada, Pakistan, Australia, the United States, and the former Soviet Union. These incidents have often resulted in catastrophic pipeline failures [15]. For example, the TransCanada pipeline experienced several SCC-related failures in Northern Ontario between 1985 and 1995, leading to two public inquiries by the National Energy Board (NEB) of Canada [16]. The NEB identified the need for improved detection methods and material standards to mitigate SCC risks. In Canada, SCC is a significant issue, with 30 to 40 pipeline failures each year, some resulting in fatalities, such as a 1985 incident where a drainage tile plow ruptured a gas pipeline [17]. These failures highlight the need for stringent regulatory oversight and continuous monitoring of pipeline integrity.

SCC occurrences have also been reported across North America and Europe. In North America, affected regions include Alberta, Ontario, and Saskatchewan in Canada, as well as Arizona, Kentucky, South Carolina, and Tennessee in the U.S. Additionally, SCC has been reported in two southern European countries. The outcomes of these cases vary widely: while only two incidents resulted in ruptures while the pipelines were in service, most were discovered during maintenance or hydrostatic testing [18]. Hydrostatic testing, which involves pressurizing the pipeline with water to a level above its operating pressure, can reveal weaknesses. The most commonly affected pipe grade was X60, known for its widespread use due to its favorable strength and cost characteristics. Notably, 73% of incidents occurred in pipes older than 30 years, primarily constructed between 1956

and 1980, with no SCC incidents reported in pipelines built in the last 32 years [18]. This suggests that newer materials and construction techniques may be more resistant to SCC.

SCC represents a critical threat to energy pipelines, potentially leading to catastrophic failures that endanger human safety, harm the environment, and result in substantial repair costs. For instance, in the 1970s, significant SCC incidents occurred in Canada's Lakehead Pipeline system, particularly in regions with high levels of hydrogen sulfide ( $H_2S$ ), a corrosive component present in some crude oils. In 1978, the Trans-Alaska Pipeline System experienced a major SCC event near Atigun Pass, Alaska, resulting in multiple ruptures, oil spills, and a temporary shutdown. More recently, in 2017, SCC-related failures on the Keystone Pipeline, operated by TransCanada (now TC Energy), caused a significant oil spill in South Dakota, releasing approximately 210,000 gallons of oil. These incidents underscore the ongoing challenges in managing SCC risks [19,20]. Alarming, SCC is responsible for over 50% of failures in gas pipelines [21].

Overall, the threat of SCC to pipelines necessitates a multifaceted approach, including improved materials science, better construction practices, rigorous regulatory frameworks, and ongoing maintenance and monitoring efforts. The industry continues to explore new technologies and methods to predict, detect, and mitigate SCC, ensuring the safety and reliability of pipeline systems worldwide. Notable SCC-related incidents, such as the 2014 gas pipeline explosion in Kaohsiung, Taiwan, which resulted in 32 fatalities and 321 injuries, and the 2013 oil pipeline explosion in Qingdao, China, which caused 136 injuries and 62 deaths, illustrate the global nature of the SCC problem and the need for international collaboration in research and technology sharing. In 2020, the Enbridge Line 5 pipeline, which transports oil and natural gas liquids between the United States and Canada, also failed due to SCC, further emphasizing the vulnerability of critical energy infrastructure to this type of corrosion [22].

### 3. Required Parameters for SCC

SCC is a multifaceted phenomenon influenced by several critical parameters. These include sensitized materials such as carbon steels, copper alloys, and high-carbon-content stainless steels, as well as the presence of various types of tensile stress (residual, thermal, or applied stress). Specific environmental conditions, including high-temperature water, chloride or acidic solutions, moisture, and aqueous environments, also play pivotal roles. The interaction among these factors is crucial for both the initiation and propagation of SCC [23]. Figure 2 illustrates the primary contributors to SCC, emphasizing the intricate interplay among these variables [24,25]. These factors will be discussed in more detail in the subsequent sections.

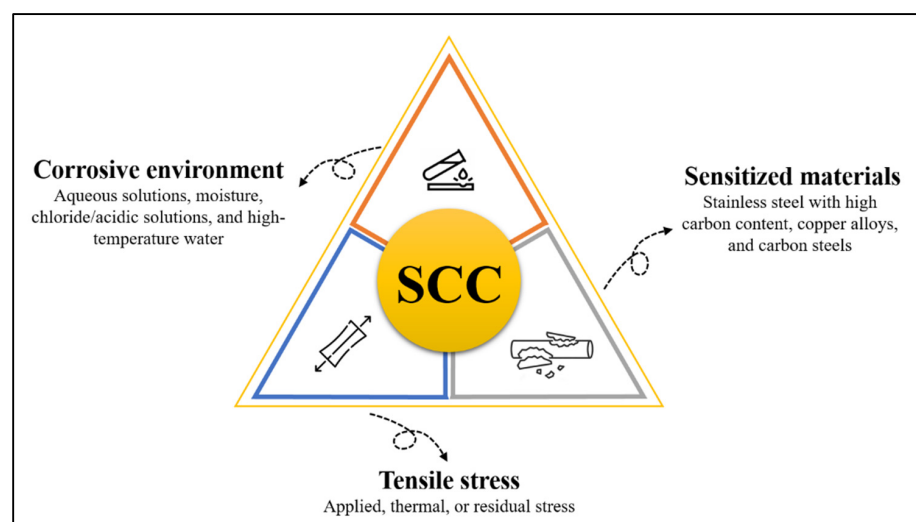


Figure 2. Requirements for SCC.

### 3.1. Stress

SCC arises from the interplay of two primary stress factors: internal residual stresses and external mechanical forces [23]. Internal stresses, also known as residual stresses, are inherent in materials and stem from processes such as plastic deformation, thermal treatments, and manufacturing techniques [5,26,27]. These residual stresses can be classified into distinct categories based on their scales: Type I (macroscopic), Type II (microscopic), and Type III (atomic level).

Type I residual stresses occur at a macroscopic level due to phenomena such as differential cooling, while Type II stresses manifest on a microscopic scale and are associated with features like banded microstructures. Type III residual stresses operate at the atomic level and result from chemical segregations and small coherent phases within the material [26]. Research indicates that internal residual stresses significantly influence SCC. For instance, Chen's study examined the impact of Type I residual stresses on neutral-pH SCC in pipeline steels, demonstrating that plastic deformation and anodic dissolution can mitigate SCC under such conditions. Beavers et al. [28] also found that the likelihood of SCC occurrence is greater in regions with elevated residual stresses. Their study indicated that residual stress in areas close to SCC colonies was nearly double that in regions farther away from near-neutral-pH SCC colonies, highlighting the significant role of tensile residual stress in SCC initiation. Similarly, Van Boven et al. [23,29] investigated the interplay between residual stress and cyclic loading in pipeline materials. Their findings revealed that cyclic loading from bending forces increased residual stress at the pipeline's surface, significantly heightening the steel's susceptibility to crack initiation in a near-neutral-pH environment. Tensile stresses, particularly those induced by welding and mechanical processes, play a critical role in SCC fracture mechanisms [29].

External stresses, especially tensile stress, and mechanical actions during a material's operational life markedly affect its susceptibility to SCC. These stresses encompass forces applied to the material during service, such as tensile, compressive, or shear stress, which can cause the stretching, compression, or deformation of the material, thereby compromising its structural integrity and increasing susceptibility to corrosion-induced cracking [23,29]. For instance, external tensile stresses can induce SCC in buried pipelines transporting hydrocarbons, particularly if the protective coating is compromised, leading to a wet environment conducive to corrosion-induced cracking [5]. Tensile stresses are pivotal in SCC fracture processes, whether applied directly or as residual stresses from thermal processes [30]. Welding and mechanical actions such as cold deformation and machining introduce residual stresses, thereby contributing to SCC susceptibility [30,31].

SCC can occur at stress levels below the material's ultimate tensile strength, with the rate of crack propagation influenced by the magnitude of stress applied. Controlled compressive stresses, such as those induced by shot peening on component surfaces, can mitigate SCC initiation [6]. The strain rate at the crack tip is critical, with SCC more likely to occur within specific strain rate ranges. The stress threshold for SCC varies depending on the material and environmental conditions. For instance, ASS components may experience SCC in hot water at stress levels close to the material's breaking point, while lower stress levels may suffice in hot chloride environments. Effective understanding and prevention of SCC require careful consideration of both external forces and internal residual stresses, particularly in applications involving ASS components [23].

### 3.2. Environment

SCC poses a significant threat to engineering materials, particularly in environments where aqueous conditions and specific aggressive ions, such as chlorides, are present. These environments play a crucial role in both the initiation and propagation of SCC. The susceptibility of an alloy to SCC is determined by both the nature of the material and the aggressiveness of the surrounding environment. However, while a corrosive environment is necessary, not all conditions induce SCC. Specific ions, such as chlorides, are particularly harmful to alloys with protective films. For instance, copper alloys are vulnerable to SCC

in ammonia-rich environments [32], whereas stainless steel and aluminum alloys are more prone to chloride-induced cracking [33]. The ASS 300 series, in particular, exhibits high susceptibility to SCC in chloride-rich conditions, especially at temperatures above 70 °C, where cracking occurs primarily in a transgranular manner [34,35].

Various aggressive ions, including chlorides, caustic substances, and polythionic acid, can accelerate SCC. Chlorides are notorious for penetrating the passive layer of stainless steel, leading to the breakdown of protective films and the onset of SCC, even at ambient temperatures, particularly in heavily machined components [36,37]. In environments where ASS is exposed to caustic substances or acidic conditions, such as in regions with intergranular welding, the risk of SCC is significantly heightened [35]. In chemical and petrochemical plants, the presence of polythionic acid, a byproduct of sulfur in feed gas, is a known cause of intergranular SCC (IGSCC) in ASS, especially in moist conditions [36,38]. Aluminum and titanium alloys also show susceptibility to SCC in environments such as liquid metals, organic liquids, and aqueous solutions, including water vapor and methanolic solutions [35].

Pipeline materials, particularly those made from API 5L X60, X65, and X70, are often exposed to harsh conditions involving high levels of H<sub>2</sub>S, carbon dioxide (CO<sub>2</sub>), and low-pH water, all of which promote accelerated corrosion and hydrogen absorption. These conditions are prevalent in environments like seawater, where atmospheric corrosion due to salt and chloride ions can become severe if the pipeline's coating is compromised, particularly under deep-sea hydrostatic pressure [39,40]. Studies, such as those by Sun et al., show varying SCC susceptibilities at different depths, with lower susceptibility at 1500 m but higher susceptibility at 3000 m [41]. Pipelines buried in soil face SCC challenges influenced by anodic dissolution in high-pH solutions and hydrogen embrittlement (HE) in near-neutral-pH environments [42–46]. The electrolyte composition, especially in carbonate-rich or dilute solutions, significantly affects whether the cracking will be intergranular or transgranular [47].

Sulfur compounds further complicate the SCC landscape. They not only contribute to hydrogen-induced cracking (HIC) by forming manganese sulfide (MnS) inclusions, which act as stress concentration sites [48,49], but also create corrosive conditions that exacerbate SCC. Research by Fan et al. highlights increased SCC susceptibility in L360NS pipeline steel in sulfur environments, linking it to hydrogen ion permeation, the degradation of protective films, and the subsequent loss of mechanical properties under stress [50]. The transition from a benign to a corrosive environment conducive to SCC can be driven by changes in temperature, aeration, or the concentration of ionic species. The stability and solubility of the reaction products in the environment significantly affect crack propagation. Cracks often initiate from the surface oxide film, displaying a transgranular pattern, emphasizing the importance of understanding crack morphology in SCC.

The resistance of an alloy to cracking largely depends on the stability of its surface film, a condition described as borderline passivity, which is critical for crack initiation and is achievable only within specific electrochemical potential ranges [51]. In pipeline steels, SCC is influenced by stress intensity factors arising from both external loads and stresses induced by the oxide film. These film-induced stresses are crucial in developing SCC cracks, with initiation and propagation occurring when these stresses exceed a critical threshold [52]. Figure 3 demonstrates SCC cracks initiated from the oxide film.

Achieving and maintaining borderline passivity, which is influenced by environmental conditions and alloy characteristics, is essential for mitigating SCC risks. Understanding the complex interplay between alloy susceptibility, environmental aggressiveness, and protective film formation is vital for preventing SCC across various industrial applications. For a detailed summary of environments that cause SCC in commonly used alloys, refer to Table 1 [35].

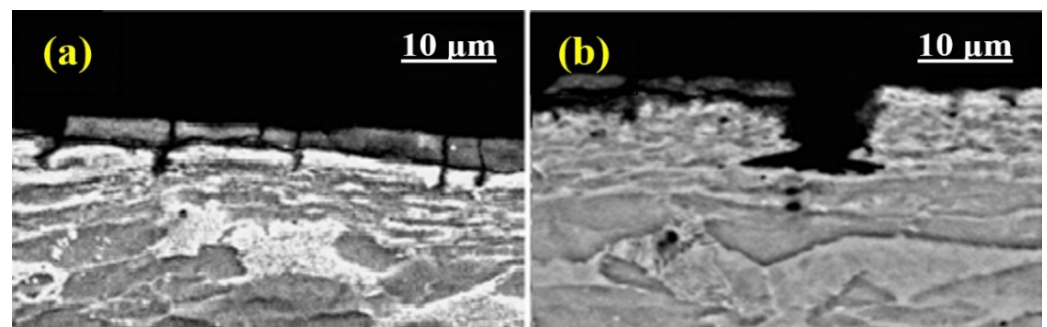


**Figure 3.** Initiation of transgranular stress corrosion cracking (TGSCC) induced by surface oxide. (a) Overview of the crack initiation; (b) Detail of the transgranular crack intersecting a ferrite grain boundary. (Reprinted/adapted with permission from Ref. [41]. 2024, Elsevier).

**Table 1.** Summary of environments associated with SCC of various alloys [25].

Metal	Environment
Titanium alloys	Methanol-HCl Seawater
Stainless steels	Red-fuming nitric acid Condensing steam from chloride waters NaOH-H <sub>2</sub> S solutions H <sub>2</sub> S Seawater NaCl-H <sub>2</sub> O <sub>2</sub> solutions Acidic chloride solutions
Steels	Carbonate–bicarbonate solutions Seawater Acidic H <sub>2</sub> S solutions Mixed acids (H <sub>2</sub> SO <sub>4</sub> -HNO <sub>3</sub> ) Calcium, ammonium, and sodium nitrite solutions NaOH-Na <sub>2</sub> SiO <sub>4</sub> solutions NaOH solutions Fused caustic soda
Nickel	Distilled water
Magnesium alloys	Seawater Rural and coastal atmospheres NaCl-Na <sub>2</sub> CrO <sub>4</sub> solutions
Lead	Lead acetate solutions
Inconel	Caustic soda solutions
Gold alloys	Acetic acid–salt solutions FeCl <sub>3</sub> solutions
Copper alloys	Water or water vapor Amines Ammonia vapor and solutions
Al alloys	Seawater NaCl solutions NaCl-H <sub>2</sub> O <sub>2</sub> solutions

### 3.3. Material

Environmental conditions critically influence SCC, but the metallurgical condition of the material is equally pivotal in its initiation and propagation. SCC requires a specific metallurgical state shaped by factors such as alloy composition, strength levels, the presence of secondary phases, and grain boundary segregation. These factors can either enhance or diminish the material's resistance to SCC [5,6]. For instance, ASS becomes susceptible to IGSCC when sensitized, even in seemingly benign environments like high-purity water at elevated temperatures, especially if oxygen is present. Surface impurities and irregularities significantly contribute to SCC and failure occurrences. However, reducing trace impurities

such as phosphorus, sulfur, and arsenic in ASS substantially improves its resistance to SCC [5].

Impurities like nitrogen and carbon at grain boundaries can influence caustic IGSCC in carbon steel by disrupting passive film formation and affecting plasticity. This segregation results in localized corrosive conditions, illustrating the intricate relationship between metallurgical factors and SCC susceptibility [6]. In welding applications, preventing selective corrosion in austenitic steels requires controlling the carbon content within its solubility limits in austenite. Even low-carbon chromium-nickel austenitic steels are not entirely immune to the adverse effects of welding thermal cycles [53,54]. Research shows that low-carbon steels containing nitrogen are particularly vulnerable to SCC, as nitrogen forms solid interstitial solutions with iron and other metals due to its small atomic radius [55,56].

Several studies have examined how various elements impact the SCC behavior of pipeline materials, identifying phosphorus, manganese, and carbon as primary elements of concern [9,57]. During steel solidification, these elements tend to segregate toward the center of the slab thickness, forming hard phases and structures like martensite and bainite. The segregation ratio of manganese is directly correlated with the carbon content. Notably, low-strength carbon steels exhibit greater resilience to the detrimental effects of phosphorus segregation compared to high-strength alloy steels [9,57].

Manganese significantly enhances austenite stability in steel, leading to increased supercooling and reduced critical quenching rates, which improve the steel's hardenability. However, as the manganese content increases, the SCC resistance of high-strength martensitic steel decreases. Manganese's ability to trap nitrogen within the crystal lattice, combined with carbon's preference for dislocations along grain boundaries, reduces the SCC resistance of high-strength steels [53,58]. Adding calcium to pipeline steel helps control sulfur levels, forming spherical sulfide-based inclusions that prevent the formation of elongated MnS particles, which are typical sites for crack nucleation [59–62].

Copper also plays a crucial role by enhancing steel's strength and SCC resistance through the formation of fine copper-enriched precipitates. These precipitates improve mechanical properties and reduce crack formation. Copper creates a protective barrier on the steel surface that limits hydrogen diffusion into the steel matrix, enhancing resistance to HE [63]. Baba et al. [64] demonstrated that the addition of copper significantly reduces hydrogen permeation in sour environments by forming a thick barrier on the steel surface.

Elements that form stable compounds with nitrogen and carbon, which are soluble in both  $\alpha$ - and  $\gamma$ -iron, profoundly impact SCC resistance. Strong carbide formers like titanium, molybdenum, niobium, and vanadium improve the SCC resistance of low-carbon steels by forming carbides that hinder crack propagation. Among these, titanium and molybdenum have the most significant effects [53,58].

Niobium-stabilized austenitic steels show superior resistance to knife-line corrosion compared to titanium-stabilized steels due to niobium's greater resistance to dissolution in austenite at high temperatures. Niobium binds carbon at grain boundaries, preventing chromium carbide ( $M_{23}C_6$ ) formation, whereas titanium carbides dissolve more readily during tempering, increasing lattice stresses. Niobium-stabilized steels also exhibit better corrosion resistance near the fusion line. For instance, 08Cr17Ni5Mn9Nb steel joints showed no knife-line corrosion, even with some niobium-forming nitrides [53].

Chromium is essential for enhancing the corrosion resistance of steel alloys. Its passivation leads to the formation of a protective oxide layer, significantly increasing corrosion resistance. Stainless steel requires at least 13–15% chromium by mass to maintain these properties [53,58]. Conversely, higher nickel content can reduce SCC resistance. Silicon plays a crucial role in preventing carbide coagulation during tempering, enhancing the stability of sorbitol structures, and slightly increasing the strength and yield strength of steel [53,58].

Metallurgical factors and microstructural characteristics critically influence SCC in metals. Hard and brittle phases within the microstructure, particularly in steel, exacerbate susceptibility to SCC crack propagation [9]. Zhu et al. [65] highlighted the relationship between SCC cracks and local microstructure in X80 pipeline steel. In high-pH environments, abundant bulky granular bainite and polygonal ferrite microstructures primarily lead to intergranular cracking. As the microstructure transitions to fine granular bainite and acicular ferrite, both intergranular and transgranular SCC (TGSCC) cracks are observed. The pH of the solution significantly affects the likelihood of transgranular crack propagation [65].

Beyond microstructural considerations, Gonzalez et al. [66] examined high-strength low-alloy steel and underscored the significant influence of microstructure on SCC crack propagation. Their findings highlight the roles of grain size and grain boundary characteristics in the development of intergranular cracking. Sulfide stress cracking (SSC) susceptibility is closely related to the steel's hardness, microstructure, and chemical composition, typically propagating along grain boundaries but sometimes transgranularly [9]. Despite traditional mitigation methods like micro-alloying and heat treatments, recent research has focused on crystallographic texture as a novel approach to reducing SCC susceptibility in pipeline steels. Studies suggest that texture plays a significant role in mitigating SCC [67–69].

### 3.3.1. Carbon and Low-Alloy Steels

Carbon and low-alloy steels, including those that are quenched and tempered or possess a ferritic–pearlitic microstructure, exhibit susceptibility to SCC across a variety of environmental conditions. These conditions include chloride, carbonate–bicarbonate solutions, ammonia, alkanolamines, hydroxide, and hot nitrate [70]. The predominant failure mode in these steels is intergranular cracking, which occurs along the prior austenite grain boundaries. However, transgranular cracking can also manifest in environments containing hydrogen ( $H_2$ ),  $H_2S$ , or high-temperature water.

The SCC resistance of these steels is inversely related to their strength level or hardness; as the strength or hardness increases, the resistance to SCC typically decreases. Extensive research has been conducted on the influence of steel composition on SCC susceptibility. However, real-world applications often present complexities due to interactions among welding properties, material strength, and heat-treatment responses [71].

The susceptibility of carbon and low-alloy steels to SCC is also affected by the distribution of potential–pH domains across various environmental conditions and temperatures [70]. These domains are critical for understanding the initiation and propagation mechanisms of SCC in these materials. The presence of  $Fe_3O_4$  (magnetite) is often indicative of conditions conducive to SCC, suggesting its role in the cracking process. Additionally, phases such as  $FeCO_3$  (siderite) and  $Fe_3(PO_4)_2$  (vivianite) can influence SCC behavior in specific environments. A key aspect of SCC susceptibility is the relationship between the pitting corrosion potential and crack initiation, underscoring the significance of localized factors. Although SCC mechanisms can vary, understanding these potential–pH domains provides valuable insights into the processes driving SCC in carbon and low-alloy steels. Moreover, these steels are prone to SCC even in environments that are typically considered passivating or conducive to forming protective oxide films. For instance, environments like high-temperature water, ethanol, carbonates, nitrates, phosphates, and strong caustic solutions, which usually foster the formation of passive layers on carbon steels, have induced SCC in these materials.

These challenges pose significant economic and safety concerns due to the extensive use of carbon steels in industrial applications. For example, the catastrophic failure of an ammonium nitrate plant, resulting from nitrate-induced cracking, led to severe financial losses and major safety incidents. Similarly, caustic cracking in steam-generating boilers made from low-alloy steels remains a persistent problem, causing repeated emergency shutdowns in facilities like ammonia plants [30,70].

### 3.3.2. High-Strength Steels

High-strength steels, characterized by hardness levels above 440 HRC, exhibit heightened susceptibility to IGSCC, even in typically non-corrosive environments such as moist air. Environments containing chlorides are particularly detrimental, as they promote SCC in these materials. HE is widely recognized as the primary mechanism of SCC in high-strength steel. The presence of cathodic poisons such as sulfur, tellurium, selenium, and arsenic exacerbates SCC by impeding hydrogen recombination and increasing hydrogen absorption by the steel. Moreover, these steels are susceptible to SCC in the presence of organic compounds and in environments that produce hydrogen. Temperature significantly influences SCC kinetics in hydrogen gas environments, with the steel's strength level critically affecting susceptibility. Maraging steels generally exhibit better resistance to SCC than high-strength steels due to their microstructural refinement and hydrogen-trapping capabilities. However, the specific mechanism by which HE induces SCC in high-strength steels remains unclear and necessitates further investigation.

Due to their inherent sensitivity to SCC, isolating high-strength steels from corrosive environments is advisable whenever possible. Despite variations in SCC resistance among different high-strength steels, it is prudent to limit the specified yield strength to meet minimum requirements. Regarding intergranular cracking, chemical composition and reactions at grain boundaries are critical factors influencing material susceptibility to SCC. Impurity elements such as antimony, tin, arsenic, and phosphorus can promote temper embrittlement and increase susceptibility to SCC. However, microstructural modifications, including martensite structure refinement and increased dislocation densities, can mitigate SCC by reducing hydrogen accumulation and enhancing resistance to embrittlement. Understanding the interplay among composition, microstructure, and SCC mechanisms is essential for developing effective mitigation strategies for high-strength steels. Current research endeavors aim to elucidate specific SCC mechanisms in these materials, offering insights into potential mitigation techniques and enhancing the reliability of high-strength steel components in corrosive environments [71].

### 3.3.3. Stainless Steels

Stainless steels, characterized by a chromium content of at least 11%, exhibit diverse microstructures, including austenitic, ferritic, martensitic, and duplex phases. The susceptibility of these steels to SCC is influenced by factors such as thermal history, microstructure, and alloy composition. The SCC susceptibility of various stainless steel grades depends on specific environmental conditions. ASSs are prone to cracking in hydroxide- and chloride-rich environments, while duplex stainless steels can experience cracking in sour gas and chloride-rich environments. Ferritic and martensitic stainless steels are vulnerable to cracking under both cathodic and anodic conditions. The exact mechanisms of SCC in these systems vary but are typically associated with specific environmental triggers, such as chloride-induced SCC or caustic SCC.

Extensive research has investigated SCC in austenitic, ferritic, martensitic, and duplex stainless steels. The nickel content and sensitization of these steels significantly influence their susceptibility to SCC, with higher nickel content generally enhancing resistance. Sensitized stainless steels are prone to IGSCC, whereas non-sensitized steels typically experience transgranular cracking. The behavior of ASS in chloride-containing environments shows a temperature-dependent threshold below 50 °C, beyond which susceptibility to SCC increases. This susceptibility arises from localized corrosion processes such as pitting, crevice corrosion, and trench formation, which lead to acidification at the crack tip and accelerate crack propagation through corrosive species and enhanced electrochemical reactions.

The presence of delta-ferrite in ASSs enhances their resistance to SCC by impeding crack growth. In contrast, duplex stainless steels exhibit superior resistance due to the cathodic protection provided by the ferrite phase. In high-temperature water, SCC in weld heat-affected zones (HAZ) presents a significant challenge, necessitating predictive

modeling and mitigation strategies. IGSCC induced by polythionic acid in sensitized stainless steels can be mitigated by reducing sensitization and adjusting plant shutdown conditions. Anodic and cathodic polarization techniques also offer preventive measures against polythionic acid SCC, operating within a narrow potential range. Other sulfur species, such as sulfate, thiocyanate, and thiosulfate solutions, can also induce SCC in sensitized stainless steels [71].

#### 3.3.4. Nickel Alloys

Nickel and its alloys are frequently chosen for their resistance to SCC, although susceptibility can arise under specific environmental, microstructural, and stress conditions. IGSCC is prevalent in environments such as high-temperature water, gaseous hydrogen, sulfur-containing atmospheres, and acidic and basic solutions. Nickel-based alloys have applications in various industries, including Ni-Fe-Cr alloys for power generation, Ni-Cr-Mo alloys for chemical processing, and Cu-Ni alloys for seawater applications. Precipitation-hardenable alloys like X750 and 718 are utilized for their high-strength properties.

Alloy 600, a well-studied nickel-based alloy, primarily experiences IGSCC. Precipitation-hardenable alloys are more susceptible to SCC due to the formation of intermetallic phases during aging, which enhances material strength. Carbide precipitation and sensitization from chromium depletion along grain boundaries significantly contribute to SCC susceptibility across different environments. Nickel-based alloys exhibit heightened susceptibility to SCC at elevated temperatures in high-purity water, particularly under deaerated conditions, whereas they demonstrate resistance to SCC at high temperatures in solutions with elevated chloride concentrations.

Hydrogen absorption can accelerate crack propagation in nickel-based alloys, particularly under various hydrogen charging conditions. Hydrogen-assisted mechanisms and anodic dissolution contribute to SCC, with local grain boundary sliding identified as a significant factor in crack initiation. High-strength nickel-based alloys are prone to hydrogen-assisted cracking, potentially influenced by the Slip Dissolution Viscous Creep (SDVC) mechanism, which promotes local grain boundary sliding under specific SCC conditions [71].

#### 3.3.5. Copper Alloys

Copper alloys, such as brass, are particularly susceptible to SCC, especially in environments where moisture condensation facilitates the rapid formation of cupric complexes and tarnish films predominantly composed of  $\text{Cu}_2\text{O}$  [71]. This phenomenon, known as seasonal cracking, has historically been observed during rainy seasons, notably affecting brass cartridges used by the British Army in India. Brass, primarily composed of copper and zinc (Cu-Zn) alloy, exhibits varying degrees and modes of cracking depending on its zinc content [32,72].

Research on SCC in copper alloys has primarily focused on moist air conditions. However, SCC has been documented in various other environments, including those containing chlorides, nitrites, nitrates, sulfates, and even pure water [71]. Pure copper, especially when exposed to solutions containing acetate and nitrite, also shows susceptibility to SCC. Cathodic polarization suppresses SCC, while general corrosion is exacerbated under noble potentials. Conversely, the anodic polarization of copper alloys from their free corrosion potential significantly increases SCC. Additionally, the temperature dependence of SCC in copper alloys follows an Arrhenius-type behavior, characteristic of thermally activated processes.

The mechanism of SCC in these alloys is complex, involving both intergranular and transgranular cracking mechanisms. IGSCC typically proceeds through a detachment or film breakage process, while TGSCC may involve discontinuous cleavage initiated by an epitaxial film, such as a dealloyed layer or oxide at the crack tip [32,72]. In TGSCC, dealloying becomes critical when the alloy exceeds specific limits, approximately 14 atomic percent (a/o) for Cu-Al alloys and 18 a/o for Cu-Zn alloys, which dictate their susceptibility

to SCC. It is noteworthy that while alloys with higher zinc content commonly exhibit TGSCC, those with lower zinc content may display IGSCC [32,71,72].

### 3.3.6. Aluminum Alloys

Aluminum and its alloys are renowned for their exceptional corrosion resistance, which is attributed to the formation of a protective oxide film on their surfaces. This oxide film, typically consisting of two layers, provides stability within a pH range of approximately 4 to 8.5. However, exposure outside these pH values can lead to aluminum corrosion, resulting in the generation of  $\text{Al}^{3+}$  or  $\text{AlO}_2^-$  ions due to the solubility of aluminum oxides in various acids and bases [71]. The SCC phenomenon in aluminum alloys has been extensively studied, revealing its complexities and influencing factors. Second phases, often intermetallic compounds, are common in aluminum alloys, ranging from negligible amounts to about 20%. These phases precipitate predominantly along grain boundaries and significantly affect the corrosion behavior of aluminum alloys due to their varying electrode potentials relative to the matrix. IGC, frequently observed in these alloys, arises from electrochemical potential gradients between adjacent grains and grain boundaries, with the anodic path showing compositional variations across different alloy compositions. The susceptibility of aluminum alloys to SCC is notably influenced by IGC and pitting corrosion. Alloys containing soluble alloying elements (e.g., zinc, silicon, magnesium, and copper) are particularly prone to SCC, where intergranular pathways facilitate crack propagation under stress and environmental conditions. However, mitigation strategies such as cathodic protection or specific heat treatments can modify the microstructure and reduce SCC susceptibility [71,73,74].

In the context of SCC in aluminum alloys, water and water vapor are critical environmental factors contributing to its development. Halide ions, especially chlorides, significantly exacerbate the susceptibility of these alloys to SCC. Generally, in alkaline solutions, the susceptibility to SCC is relatively low compared to neutral and acidic environments. The fundamental principles of SCC involve localized anodic dissolution occurring at grain boundaries under the synergistic influence of stress and environmental factors, along with hydrogen ingress or adsorption contributing to crack propagation. The non-uniform progression of cracks in SCC-susceptible aluminum alloys suggests that continuous anodic dissolution alone cannot fully explain crack propagation [71].

Aluminum and its alloys are prone to failure via intergranular cracking when subjected to significant stresses and exposed to specific environmental conditions. Notably, the 2xxx, 5xxx, and 7xxx series of aluminum alloys exhibit heightened susceptibility to SCC due to their inherent chemical compositions and microstructural characteristics. The 7xxx series alloys, widely used in structural, military, and aerospace applications for their exceptional mechanical properties, including high strength-to-weight ratios and fatigue resistance, are particularly vulnerable to SCC. Therefore, carefully considering SCC susceptibility during the design and manufacturing processes is essential to ensure the integrity and reliability of final products [71,73–75].

### 3.3.7. Hexagonal Alloys: Magnesium, Zirconium, and Titanium

Materials with a hexagonal close-packed crystal structure, such as zirconium and titanium, exhibit highly negative potentials in aqueous environments, emphasizing the significant role of hydrogen uptake in enhancing their resistance to SCC. Zirconium and titanium form stable hydrides, whereas magnesium hydride decomposes rapidly above 280 °C, displaying lower hydrogen solubility than zirconium and titanium [71].

While titanium alloys generally demonstrate excellent resistance to SCC, specific environments, such as anhydrous methanol, hot salts, and strong oxidizers, can induce SCC [71,76]. In halide solutions, active corrosion trenches initiate cracks that propagate through anodic dissolution or hydrogen-assisted cracking mechanisms. This process can involve the local precipitation of brittle titanium hydride, significantly affecting the mechanical properties of the material [71]. Kiefer and Harple first reported the SCC

susceptibility of commercially pure titanium in aqueous environments, particularly in red-fuming nitric acid (HNO<sub>3</sub>). Subsequent cases of hot-salt cracking were observed in turbine blades made from titanium alloys operating at elevated temperatures. Brown also documented instances of SCC in titanium alloys exposed to room-temperature aqueous environments, highlighting susceptibility in seawater, particularly in the titanium 8-1-1 alloy [30].

SCC in zirconium alloys is confined to specific conditions, such as halogen vapors, concentrated HNO<sub>3</sub>, and oxidizing chloride solutions, with mechanisms akin to those observed in titanium alloys. Additionally, susceptibility to SCC has been noted in methanol environments, primarily affecting methanol and potentially other low-molecular-weight alcohols [71]. Whether cast or extruded, magnesium-based alloys may be susceptible to SCC under diverse conditions, such as purified water and air. Alloys containing aluminum are particularly vulnerable, with increased susceptibility in the presence of zinc. Cracking can occur along grain boundaries or transgranularly, influenced by cathodic regions within the microstructure. TGSCC in magnesium alloys typically manifests along twinning planes or cleavage, often exhibiting extensive branching. Proposed SCC mechanisms include the brittle hydride model, developed based on observations of stress-induced magnesium hydride phases. Cathodic polarization generally mitigates SCC susceptibility, whereas anodic polarization exacerbates it [71].

### 3.3.8. Austenitic Stainless Steel (ASS)

ASS is susceptible to SCC in environments containing polythionic acid, caustic solutions, and chlorides. Sensitization occurs when ASS with more than 0.03 wt.% carbon is heated, leading to the precipitation of M<sub>23</sub>C<sub>6</sub> at grain boundaries [77]. This sensitization reduces the chromium content along grain boundaries, making them prone to rapid preferential dissolution and increasing vulnerability to SCC [78]. The stability of the passive film in ASS, crucial for corrosion resistance, is influenced by factors such as temperature, acidity, halide content, and the potential difference between the metal and the solution [79]. Sensitized stainless steels are particularly susceptible to SCC in the presence of halides, including chlorides, bromides, and iodides, which can induce pitting corrosion [80].

ASS sensitization occurs at elevated temperatures, resulting in M<sub>23</sub>C<sub>6</sub> precipitation along grain boundaries [4]. The kinetics of this precipitation depend on the carbon content, with lower carbon content requiring more time for sensitization. Chromium and nitrogen increase carbon solubility, delaying or reducing precipitation, while molybdenum and nickel promote it. The presence of nitrogen can also reduce carbide precipitation in ASS [81]. Elements enhancing passive film stability contribute to resistance against pitting, crevice corrosion, and SCC [35].

Table 2 presents the chemical compositions of frequently used ASSs in various industrial applications. ASSs like SS304 and SS316 are widely used in industry for their exceptional properties, enabling the manufacture of corrosion-resistant components and containers. For instance, SS304 and SS316 are employed in high-pressure piping systems and primary circuits of Boiling Water Reactors (BWRs) and Pressurized Water Reactors (PWRs), respectively. SS316, modified with additional elements such as titanium, silicon, and phosphorus, is used in light water reactors for fuel cladding tubes [82,83]. These alloys exhibit outstanding mechanical properties, including an elongation of 66.5%, yield strength of 410 MPa, and tensile strength of 691 MPa [4,84].

The resistance of ASS to pitting corrosion is influenced by the alloy composition, which can be quantified using the Pitting Resistance Equivalent Number (PREN). A higher PREN value indicates improved corrosion resistance. For example, due to its molybdenum content, SS316 (PREN = 25) exhibits superior pitting corrosion resistance compared to SS304 (PREN = 20). Other grades, such as SS310 and SS321/SS347, are utilized to mitigate cold work hardening, withstand high temperatures, and facilitate welding in high-temperature applications. However, designers must be cautious of high sulfur levels in tubing, which aid in welding but compromise corrosion resistance [85–87].

**Table 2.** Chemical compositions of commonly applied ASSs in cooling and piping systems [4].

ASS	Element (wt.%)									
	Cr	Ni	S	P	Mn	Mo	Si	N	C	Others
SS302	17.00	8.00	0.030	0.045	2.00	–	0.75	0.10	0.15	–
SS310	24.00	19.00	0.030	0.045	2.00	–	1.50	–	0.25	–
SS347	17.00	9.00	0.030	0.045	2.00	–	0.75	–	0.08	Nb1.00
SS321	17.00	9.00	0.030	0.045	2.00	–	0.75	0.10	0.08	Ti 0.70
SS316	18.00	10.00	0.030	0.045	2.00	2.00	0.75	0.10	0.08	–
SS304	18.23	8.13	0.004	0.029	1.65	–	0.35	0.10	0.06	–

Pitting corrosion accelerates in chloride environments, forming distinct anodic and cathodic zones. Exposure to chloride aqueous solutions disrupts the passive film, which is promptly replenished with a chromium-enriched layer. The thickness of the passive film increases over time due to elevated  $\text{Fe}^{2+}$  levels in the oxide layer with prolonged exposure at elevated temperatures. Increased chloride ion concentration within the typical atmospheric humidity range exacerbates pitting corrosion [88,89]. Given the susceptibility of ASSs to SCC in chloride environments, chloride ions play a critical role in initiating and propagating SCC. The interaction between chloride ions and sensitized stainless steel surfaces accelerates passive film breakdown, leading to localized corrosion and eventual crack formation under stress. Understanding these mechanisms is crucial for mitigating SCC risks in chloride-rich environments [88,89].

The resistance of high-strength steels to SCC varies with the tempering temperature. Initially, SCC resistance increases with the tempering temperature but diminishes at specific points. However, further tempering can enhance resistance again. The specific tempering temperature affecting SCC resistance depends on the steel composition. For instance, steels like 08Cr15Ni5Cu2Ti and 13Cr15Ni4NMo3 are most susceptible to SCC after tempering between 425 °C and 475 °C, achieving maximum strength. At lower temperatures (200–350 °C) and higher temperatures (525–560 °C), SCC resistance improves, potentially eliminating cracking. Welded joints exhibit different behaviors based on tempering temperatures; joints welded below 400 °C experience reduced SCC rates, while those welded above 500 °C are less susceptible. The effective pre-treatment of steels like 08Cr15Ni5Cu2Ti at 500–550 °C alters the microstructure, preventing SCC and IGC in welded joints [53].

Low-temperature tempering uniformly forms carbide particles within steel crystals, reducing internal stress and enhancing SCC resistance. Increased tempering temperatures lead to more precipitation and martensite formation from austenite. This results in martensite decay along grain boundaries, creating carbon-depleted zones as cathodes and carbon-enriched areas as anodes. Further tempering extends martensite decay throughout the grain, reducing internal stress and increasing SCC resistance. These mechanisms illustrate how the tempering temperature influences the SCC resistance of high-strength steels, underscoring the importance of composition and heat treatment in mitigating SCC risks [53,55,90].

#### 4. SCC Mechanism

SCC manifests through two primary mechanisms: dissolution-based and cleavage-based. In dissolution-based SCC, materials corrode locally at crack tips, compromising the passive film and initiating cracks, while cleavage-based SCC involves brittle fractures along grain boundaries [71,91].

#### 4.1. Dissolution Mechanism

Dissolution-based SCC initiates through localized corrosion at crack tips, where the passive film breaks down, indicating localized film failure. This process is influenced by three dissolution mechanisms: the pre-existing active path model, the strain-generating active path mechanism, and the corrosion tunnel model [71]. Anodic dissolution at pre-existing grain boundaries, often containing intermetallic and segregated compounds, is exacerbated by tensile stress, a phenomenon known as the mechanoelectric effect. Chromium-depleted grain boundaries are particularly susceptible, leading to intergranular cracking, which is mainly observed in sensitized ASS [35].

In the strain-generating active path mechanism, crack growth proceeds through cycles of passivation and dissolution along slip steps or crack tips. This involves the rupture, dissolution, and repassivation of the passive film on the metal surface [92]. Crack growth may pause at slip steps until repassivation occurs, characterized by arrest marks on cracked surfaces, while smooth surfaces may exhibit cleavage. Additionally, intergranular cracks can form due to grain boundary features on the fractured surface [93,94].

The corrosion tunnel model describes cracks initiating at slip steps and propagating under tensile stress, potentially leading to ductile or mechanical failure. These cracks initially appear as thin tunnels and may progress to mechanical fracture, with surfaces expected to match closely [4]. The dissolution-based model is influenced by the interplay between dissolution and repassivation rates. Accelerated crack growth in chloride-induced SCC occurs when dissolution exceeds repassivation, driven by chloride ions and mechanical stress. Conversely, rapid repassivation thickens the passive film, hindering further slip-step corrosion [95,96].

#### 4.2. Cleavage Mechanism

The cleavage-based mechanism involves crystal fractures propagating along crystallographic surfaces, leading to brittle failure [71]. The adsorption-induced cleavage mechanism occurs when environmental species are adsorbed under stress, resulting in cleavage fracture. Tensile stress weakens atomic bonds along grain boundaries, particularly at crack tips where chloride ions are present [97]. The tarnish rupture mechanism involves cyclic processes of arrest marks, film formation, crack growth, and film fracture. Under tension, cracks initiate due to brittle passive films. Upon exposure to the solution, repassivation halts crack propagation, primarily through transgranular fracture surfaces, enabling IGSCC ahead of the crack tip [98,99].

The film-induced mechanism suggests that passive film formation through dissolution may lead to brittle crack development under tensile stress, propagating beyond film thickness into the metal volume. Crack propagation halts due to the metal's tough microstructure, resulting in blunted cracks through plastic deformation. Factors influencing film-induced cleavage include film thickness, initial cleavage crack velocity, substrate toughness, and the bonding strength between the metal matrix and the passive film [4]. The atomic surface mobility mechanism, which focuses on the role of hydrogen atoms, predicts crack susceptibility under environmental conditions. Vacancy diffusion is critical, as it removes crystal lattice elements near crack tips, enabling atomic migration and crack propagation in the presence of aqueous contaminants [4,100]. Chatterjee [101] notes that multiple mechanisms contribute to SCC rather than a single dominating mechanism. According to the cleavage-based model, hydrogen atoms migrate to crack tips, causing embrittlement and contributing to SCC. The dissolution of oxide films by anodic chloride ions enhances the concentration of acidic species at crack tips [102].

#### 4.3. SCC Development

Crack growth rates depend on loading conditions, environmental aggressiveness, exposure duration, and material sensitization. Mathematically, the crack growth rate is related to the crack length, exposure time, and metal sensitization. Sensitization involves the formation and precipitation of  $M_{23}C_6$  along grain boundaries, depleting the

chromium content and disrupting the protective film (Figure 4 left). Decreased chromium content leads to a sudden discontinuity in the passive film. ASS sensitization, often resulting from welding or exposure to high temperatures, diminishes SCC resistance and accelerates crack propagation, even under low-stress conditions. Figure 4 right illustrates specific crack paths observed in anodic solutions, depicting the distinctions between IGSCC and TGSCC [103].

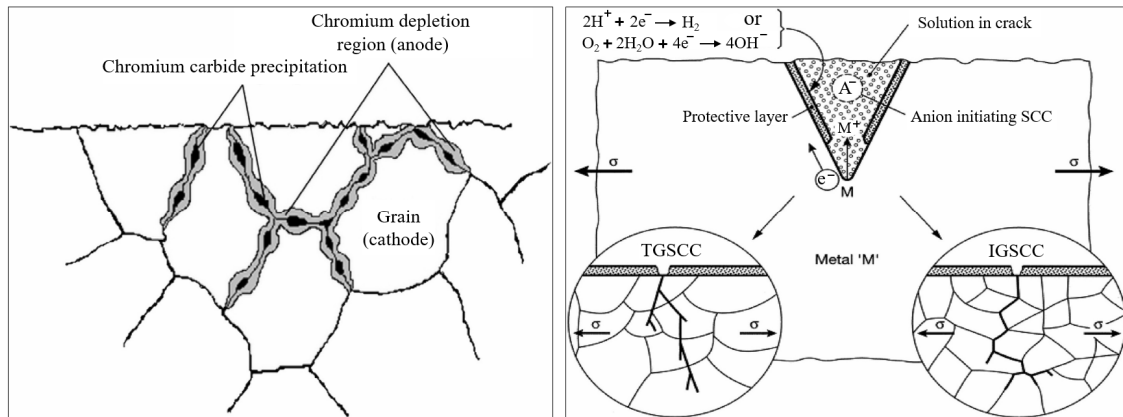


**Figure 4.** (left) Chromium carbide precipitation at grain boundaries in sensitized stainless steel and (right) SCC mechanism: interaction between anodic solution and material resulting in IGSCC and TGSCC [4].

ASS components in BWRs and PWRs are susceptible to Irradiation-Assisted SCC (IASCC) and IGSCC [104]. BWRs' thermally sensitized ASS components are particularly prone to IGSCC, which is exacerbated by neutron exposure that initiates and propagates cracking [105]. Conversely, TGSCC typically originates on the exterior surfaces of ASS components.

Chloride contamination creates aqueous environments that are ideal for crack propagation, often facilitated by thermal insulation, water ingress, or wetting. This environment fosters pitting or crevice corrosion concurrently with SCC, particularly under tensile stress conditions [106]. ASS components are prone to SCC under suitable corrosive conditions. Parkins identified three stages in the stress corrosion spectrum of various materials exposed to diverse corrosive solutions: pre-existing active paths, strain-induced active paths, and specific subcritical stress location adsorption [4]. According to the Parkins model, SCC progresses through initiation, propagation, film rupture, and pitting [103]. Elevated-temperature interactions between applied tensile stress and corrosive solutions disrupt local passive films, leading to pitting and subsequent crack initiation. Stress localization profoundly impacts pit formation, influencing the crack length and material properties (Figure 5).

Hänninen [71] suggested that Cl-SCC is typically absent in non-sensitized ASSs below 50 °C under near-neutral conditions. However, low-pH conditions can induce Cl-SCC, even at room temperature. In chloride solutions, pits or localized corrosion often initiate cracks, whereas crevice corrosion acidifies crack tips, hydrolyzing dissolved metal ions [99,107]. Xie et al. [108] studied SCC in SS316 under simulated PWR conditions through solution treatment and cold working. The introduction of chloride ions significantly increased SCC susceptibility. The mechanism involves the cyclic rupture and regeneration of the oxide film through metal atom diffusion, producing dissolved chlorides that form microcracks and accelerate the initiation and propagation of TGSCC. Dissolved oxygen enhances crack growth in cold-worked SS316 by promoting anion diffusion at crack tips, thereby accelerating SCC.

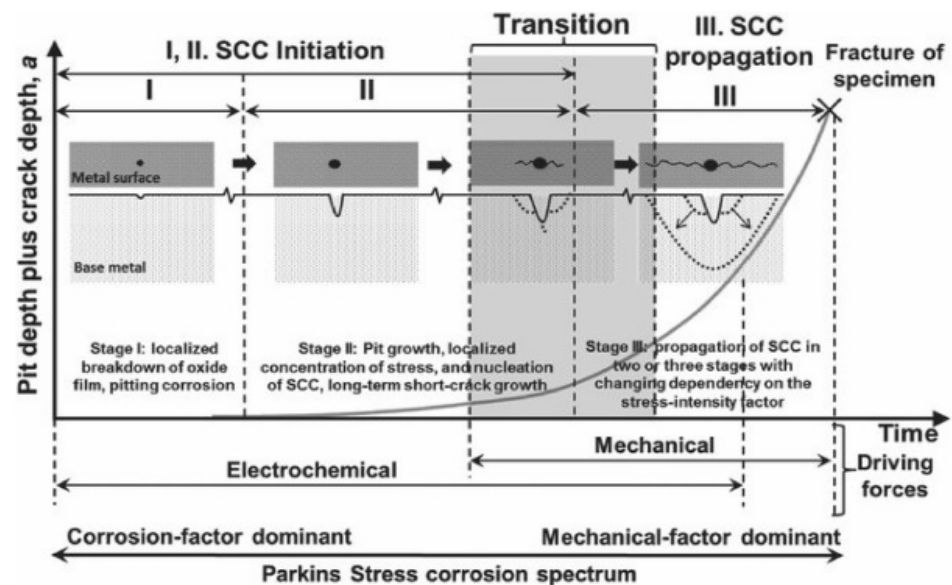


**Figure 5.** A three-stage model for SCC progression (Reproduced/reprinted/adapted from Ref. [4], 2024, licensed under an open access Creative Commons CC BY 4.0 license).

Once initiated, Cl-SCC in ASS cannot be completely stopped, but it can be mitigated. Yeom et al. [109] employed cold spray technology to mitigate Cl-SCC in nuclear fuel storage canisters by propelling SS304L powder particles with helium and nitrogen gases, increasing particle velocity. This method penetrated oxide layers, inducing compressive residual stress and effectively sealing crack openings as a physical barrier, which inhibits the progression of Cl-SCC.

SCC is a sudden and severe failure mechanism in materials exposed to corrosive environments, particularly in chloride-rich and high-temperature conditions. ASS sensitization from welding or high temperatures leads to intergranular crack formation along grain boundaries, contrasting with transgranular cracking in unsensitized materials. Parkins's stress corrosion spectrum and dissolution-based models elucidate the contributions of chloride ions to passive film breakdown and crack propagation.

### 5. Chloride-Induced Stress Corrosion Cracking (Cl-SCC)

Chloride-induced stress corrosion cracking (Cl-SCC) occurs when metals, particularly ASS and nickel alloys, are exposed to corrosive environments under tensile stress [110]. The kinetics of transient oxidation in Cl-SCC systems are complex and depend on the interplay of material properties, environmental factors, and loading conditions [111]. Shallow pits, although easily inspected, can act as stress concentrators, potentially initiating SCC [112]. In petroleum refining, environments containing polythionic acids, amines, ammonia, caustics, and molten chlorides are commonplace. Chlorides, in particular, are known to induce TGSCC in ASS and nickel alloys [113]. Despite the prevalence of sulfates, chlorides are considered more aggressive in promoting SCC. Understanding the composition and origin of deposits in refining environments is crucial [110].

The initiation of Cl-SCC in refineries typically stems from chloride-containing compounds present in crude oil, refining processes, or external sources such as seawater ingress. Upon contact with metal surfaces, subsequent cooling and moisture absorption lead to the formation of a corrosive layer, fostering localized corrosion and potential SCC under stress conditions [4]. Externally initiated Cl-SCC involves electrochemical mechanisms followed by a propagation stage influenced by electrochemistry and metal separation [114]. Cl-SCC can lead to deterioration and potential structural failures in industrial applications, impacting safety through partial or through-wall corrosion and cracking [115]. This poses a significant risk to ASS, especially in chloride-rich

environments where transgranular cracking predominates, although sensitized steels may experience intergranular cracking [113].

Various parameters influence Cl-SCC in refinery settings, reflecting diverse operational and environmental conditions. Critical environmental factors include chloride content, pH, temperature, impurity concentrations, and the formation of chloride-containing moisture films. Relatively low temperatures (below 100 °C) can catalyze SCC in corrosive solutions [4]. Deliquescent chlorides, capable of absorbing moisture, form highly concentrated films on equipment surfaces, with deliquescence relative humidity (RH) playing a pivotal role in film initiation [116,117]. External sources of chlorides, such as rain, coastal fog, deicing salts, and process leaks, significantly contribute to chloride exposure on metal surfaces, particularly in industries located near coastal areas. Over time, equipment performance can be adversely affected by corrosion induced by the hygroscopic properties of salts and the deposition of chloride ions as aerosols. These factors can contribute to localized SCC, especially in areas with high residual stresses from welding. Airborne pollutants, dust, and aerosols can deposit on equipment surfaces, leading to localized corrosion attacks [118]. Thermal insulation can exacerbate ASS susceptibility to SCC. While localized corrosion is widely recognized as the primary initiator of Cl-SCC, the mechanisms governing crack propagation remain complex and not fully understood [119]. Crack propagation likely involves electrochemical dissolution and atomic-level fracture mechanisms within the metal structure [120].

In industrial settings, particularly in equipment such as steam generators, coolant systems, heat exchangers, and pipes, ASS faces an elevated risk of Cl-SCC due to prevailing operational conditions and the presence of chloride ions in coolants [82]. Despite the corrosion resistance of 300 series stainless steel, exposure to temperatures above 60 °C increases its susceptibility to Cl-SCC in aqueous environments. This can lead to passive film degradation, pit formation, and cracking under tensile stress [121]. The resulting threat to refinery equipment necessitates proactive measures to mitigate risks effectively [111]. Operational stresses, including cyclic loading, thermal stresses, pressure changes, and potential welding during construction or maintenance, contribute to residual stresses. Tensile stresses induced by welding, particularly in ASS without stress relief treatments, create an environment conducive to the initiation and propagation of Cl-SCC. Despite limited direct measurements, high residual stresses along weld directions increase the material's vulnerability to Cl-SCC. Advances in residual stress modeling underscore the critical role of welding-induced residual stresses in governing Cl-SCC susceptibility in ASS [4].

### 5.1. Factors Affecting Cl-SCC

#### 5.1.1. Materials

Cl-SCC poses a significant challenge in refinery operations, particularly concerning material susceptibility. The spectrum of susceptibility ranges from carbon steel and low-alloy steels, which exhibit lower resistance, to alloys such as 300 series stainless steels, Alloy 400, duplex stainless steels, Alloy 800, Alloy 825, Alloys 625 and C276, and titanium, which demonstrate higher resistance to Cl-SCC.

Cl-SCC occurs when materials susceptible to chloride exposure, such as 300 series stainless steels, encounter chloride salts. This form of corrosion poses a significant threat to piping and equipment integrity across various refining units, including product stabilizer towers, recycle gas systems, Fluidized Catalytic Cracking Units, overhead systems of crude distillation and fractionation columns, hydroprocessing effluent systems, catalytic reforming units, and hydrotreater desulfurizer prefractionators. Reactor effluent streams operating at approximately ~300 °F are especially prone to fouling and corrosion induced by chloride salts. Understanding the metallurgical nuances influencing material susceptibility to Cl-SCC is crucial for selecting appropriate materials and implementing effective corrosion mitigation strategies in refinery environments. Metallurgical considerations are paramount in determining susceptibility to Cl-SCC, with factors such as

alloy composition, microstructure, and grain boundary characteristics playing crucial roles. Carbon steel and low-alloy steels, with higher iron content and susceptibility to sensitization, are more prone to chloride-induced corrosion and cracking than stainless steels and corrosion-resistant alloys. While ASSs, such as the 300 series, offer corrosion resistance, they remain susceptible to Cl-SCC under certain conditions, particularly in chloride-rich environments and under tensile stresses. Duplex stainless steels exhibit improved resistance due to their dual-phase microstructure, combining characteristics of austenitic and ferritic stainless steels [122].

Microstructural effects significantly influence material susceptibility to Cl-SCC, with grain boundaries acting as preferential sites for chloride ion ingress and crack initiation. Sensitization in ASS, characterized by  $M_{23}C_6$  precipitation along grain boundaries, can increase susceptibility to Cl-SCC by depleting the chromium content in the adjacent matrix. Techniques such as grain boundary engineering, involving modification or alloying, can enhance resistance by minimizing grain boundary sensitization and promoting a more corrosion-resistant microstructure. Alloy selection criteria are crucial in mitigating Cl-SCC risk, considering factors including chloride content, temperature, pressure, and mechanical loading. Alloys with higher chromium, molybdenum, and nickel contents, such as Alloys 825, 625, and C276, demonstrate superior resistance compared to carbon steel and low-alloy steels. Titanium alloys offer excellent corrosion resistance in chloride-rich environments due to the formation of a stable passive oxide film on their surface. By comprehending metallurgical factors and integrating this knowledge into alloy selection and design considerations, engineers and materials scientists can develop robust solutions to mitigate Cl-SCC risk in refinery environments [122].

Alloy chemistry and microstructure profoundly influence the susceptibility of stainless steel to SCC. ASSs are particularly vulnerable to Cl-SCC, contrasting with the superior resistance of ferritic stainless steel. Nickel, molybdenum, and nitrogen play pivotal roles in enhancing the SCC resistance of ASSs. Increasing the nickel content above 8% in ASSs can significantly improve their resistance to Cl-SCC. Additionally, molybdenum and nitrogen have been found to enhance SCC resistance, possibly due to their beneficial effects on pitting resistance, a precursor to SCC initiation. Conversely, elevated levels of sulfur and phosphorus within the steel matrix detrimentally affect SCC resistance. Stress corrosion studies have demonstrated that higher phosphorus content in ASS correlates with increased susceptibility to SCC in chloride-rich environments.

Furthermore, the sensitization of ASSs between 500 and 850 °C renders them susceptible to IGC and IGSCC in various environments containing chloride or fluoride ions [6]. The nickel content within stainless steel alloys also plays a critical role in SCC susceptibility. Cl-SCC susceptibility increases with the nickel content up to a certain threshold, typically within the range of traditional AISI 304 and 316 steels. Beyond this threshold, usually around 10% nickel content, nickel demonstrates a mitigating effect on SCC in chloride-rich environments. Alloys containing more than 42 wt.% nickel are immune to Cl-SCC [123].

Further investigations into sensitization processes have revealed insights into the nuanced relationship between sensitization parameters and SCC susceptibility. Prolonged sensitization durations and lower sensitizing temperatures have been associated with heightened susceptibility to IGSCC. This vulnerability has been linked to a reduction in chromium concentration adjacent to grain boundaries, which undermines the stability of passive films and increases the chemical activity of localized regions, facilitating IGSCC initiation [6]. Quantitative assessments using Electron Probe Micro-Analysis (EPMA) and Slow Strain Rate Testing (SSRT) have provided valuable insights into the relationship between the degree of sensitization and IGSCC susceptibility. While a linear correlation is observed between IGSCC susceptibility and EPMA charge values for low degrees of sensitization, complexities arise at higher degrees of sensitization. Conversely, IGSCC susceptibility increases with a decrease in sensitizing temperature for a given

EPMA charge value, highlighting the intricate interplay of multiple factors in governing SCC behavior [6].

In industrial applications, selecting structural materials is critical due to the aggressive chloride-rich environments involved. Alloys with PRENs exceeding 50 have emerged as promising candidates, demonstrating notable resistance to Cl-SCC. Nickel content has been identified as a decisive factor, with alloys featuring higher nickel content exhibiting enhanced resistance to Cl-SCC [123]. Investigations into SCC susceptibility within supercritical water (SCW) environments have provided additional insights into the interplay of environmental parameters and material behavior. The chloride concentration within SCW has been identified as a critical determinant of SCC susceptibility, with higher chloride concentrations correlating with heightened susceptibility. Conversely, higher chromium content has been associated with reduced IGSCC susceptibility, highlighting the role of alloy composition in dictating material performance under aggressive environmental conditions [124].

In conclusion, the susceptibility of stainless steels to SCC represents a multifaceted phenomenon governed by alloy composition, microstructure, and environmental factors. Continued interdisciplinary research efforts are essential for deepening our understanding of SCC mechanisms and developing robust mitigation strategies to safeguard critical infrastructure against the perils of SCC.

#### 5.1.2. Temperature and Limiting Relative Humidity

Factors influencing Cl-SCC primarily include temperature and RH. The impact of temperature on corrosion is multifaceted: within a certain range, it can facilitate both localized corrosion and SCC. However, beyond this range, elevated temperatures may hinder corrosion by reducing surface RH below the limiting relative humidity (RHL), thereby preventing the formation of deliquescent salts necessary for corrosion [121,125]. Conversely, lower temperatures can elevate surface RH to levels where deliquesced solutions become too diluted to sustain corrosion [115].

ASSs are prized for their general corrosion resistance but are highly vulnerable to localized forms such as pitting, crevice corrosion, and SCC, especially in chloride-rich environments. Chloride ions, pervasive in water and industrial settings, catalyze SCC. Elevated temperatures exacerbate SCC, particularly in sensitized ASSs that are susceptible to IGSCC, even at ambient temperatures. While a consensus on the critical temperature for SCC initiation remains elusive, evidence suggests a significant increase in crack growth rates above 80 °C. However, SCC can occur at lower temperatures, particularly when surface impurities, such as embedded iron particles, create sites for chloride accumulation.

Determining a threshold chloride concentration below which SCC is mitigated is challenging due to the localized nature of the corrosion process. Chloride accumulation within crevices or under deposits on ASS surfaces exacerbates SCC, with chloride often leaching from thermal insulation, thereby increasing the risk. ASSs can typically withstand water with less than 1000 ppm chloride under flowing conditions, assuming no concentration mechanisms are active. However, the permissible chloride content in insulation depends on its silicate content. Therefore, mitigating SCC requires a thorough understanding of how local environmental factors influence chloride accumulation and corrosion initiation on ASS components [6].

Understanding the detailed effects of temperature on corrosion kinetics is crucial for Cl-SCC. Temperature influences electrochemical and diffusion kinetics, resulting in varied corrosion rates. Experimental findings support this observation in exposure tests conducted at different temperatures. For instance, SS304 exhibits significantly longer failure times under applied stress (~400 MPa) at 50 °C compared to 80 °C. Additionally, lower temperatures generally reduce electrochemical and diffusion kinetics, thereby lowering corrosion rates [126].

RH is also critical in atmospheric chloride SCC. Exposure tests indicate that RH above the RHL is essential for chloride salt deliquescence and subsequent SCC initiation [115]. Studies suggest a critical RH threshold of 15% for Cl-SCC in materials like SS304 and SS316 up to 80 °C. However, laboratory tests replicating realistic environmental conditions suggest that variations in humidity may not necessarily accelerate Cl-SCC, even with elevated surface chloride concentrations [116].

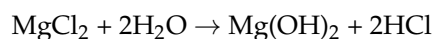
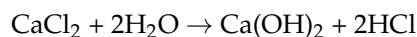
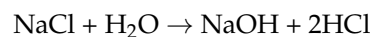
Comparisons between natural and accelerated test conditions underscore the importance of realistic environmental simulations in assessing SCC risks. For example, SCC propagation rates differ significantly between natural and accelerated testing conditions, with a two-order difference in propagation rates [127]. Despite these insights, neither set of conditions precisely mirrors in-service environments, highlighting the complexity of predicting actual failure occurrences.

Furthermore, findings from exposure tests reveal additional nuances. For instance, cracking severity increases with exposure time at lower temperatures, with more specimens developing cracks and longer crack lengths observed. This underscores the dynamic nature of Cl-SCC and its sensitivity to environmental variables.

A comprehensive understanding of the effects of temperature and RH on Cl-SCC involves delving into the underlying electrochemical kinetics, diffusion processes, and material responses. Higher temperatures facilitate the diffusion of corrosive species to material surfaces, promoting localized corrosion initiation. Conversely, fluctuations in RH influence the availability of water and chloride ions at surfaces, affecting corrosion kinetics and the formation of protective films.

### 5.1.3. Types of Salts

Chloride ions, originating from sources such as hydrogen chloride (HCl) resulting from chloride salt hydrolysis, are pivotal in initiating and propagating Cl-SCC. In refinery operations, chloride salts like NaCl, magnesium chloride (MgCl<sub>2</sub>), and calcium chloride (CaCl<sub>2</sub>) undergo hydrolysis at elevated temperatures, releasing corrosive HCl:



Additionally, organic chloride decomposition contributes to HCl formation, further exacerbating corrosion within refinery systems. The presence of salts in refinery processes introduces complexities, as factors such as temperature, pressure, and the chemical composition of organic compounds influence the kinetics of Cl-SCC [122].

Experimental studies have demonstrated a direct correlation between the chlorine concentration and Cl-SCC incidence. Higher concentrations of chloride ions create a more corrosive environment, accelerating the degradation of passive films on stainless steel surfaces and facilitating SCC initiation. Sensitized SS304 specimens have exhibited crack formation when exposed to elevated chlorine concentrations, such as 1 and 10 g/m<sup>2</sup>. Similarly, as-received SS304 specimens show increased susceptibility to crack initiation with higher levels of chlorine deposition. Conversely, when chlorine concentrations are below certain thresholds, typically around 1 g/m<sup>2</sup>, occurrences of cracks on SS304 specimens are significantly reduced. It is crucial to note that chlorine exposure can occur through various means, including direct contact and indirect infiltration from atmospheric deposition or industrial emissions. A comprehensive assessment of environmental factors and potential sources of chloride contamination is essential for effective corrosion management [115].

The types of salts significantly influence the Cl-SCC phenomenon. Several studies have underscored the critical role of salt types in corrosivity, with varying sensitivity observed toward changes in ion concentrations. Laboratory experiments involving chloride mixtures have shown that  $\text{MgCl}_2$  induces failure in stainless steel specimens most rapidly, followed by  $\text{CaCl}_2$ , while  $\text{NaCl}$  exhibits the slowest corrosive action. This disparity can be attributed to solubility and chloride activity differences among various salts.  $\text{MgCl}_2$  and  $\text{CaCl}_2$ , being more soluble than  $\text{NaCl}$ , exhibit heightened corrosive potential. Despite  $\text{MgCl}_2$  demonstrating faster reactivity than  $\text{CaCl}_2$  in certain studies, extensive research consistently identifies  $\text{CaCl}_2$  as the primary contributor to Cl-SCC among sea salts at room temperature. The corrosive impact of salt deposits depends on the equilibrium chloride concentration within the electrolyte formed on the surface due to water vapor absorption.  $\text{CaCl}_2$  demonstrates greater corrosiveness than  $\text{MgCl}_2$  due to its ability to generate solutions with higher concentrations at specific relative humidities [128,129].

At chloride concentrations below 0.5 g/L, sulfide salts synergistically exacerbate Cl-SCC, particularly evident in SS316 and SS304, where significant transgranular cracking has been observed [115]. Sulfides typically reduce resistance to crevice corrosion and pitting in stainless steel across various grades. The susceptibility to Cl-SCC increases with higher sulfur content, leading to a denser distribution of sulfide inclusions that serve as initiation sites for SCC and pits. Under typical ambient conditions and in the absence of  $\text{H}_2\text{S}$ , such low chloride concentrations generally do not induce cracking [115].

#### 5.1.4. Residual Stress

Cl-SCC manifests through crack initiation and propagation under the combined influence of tensile stress, exposure to chloride-rich environments, and elevated temperatures. While pitting corrosion typically initiates slowly, residual stress can expedite degradation mechanisms, accelerating crack growth rates. Previous studies on SCC in dry storage conditions have predominantly utilized U-bend specimens, which may not fully replicate stress distributions in actual canister welds. Nevertheless, these investigations offer valuable insights into stress-related phenomena. By simulating stress distributions akin to real canister environments, researchers have estimated the potential impact of residual stress on SCC development [115].

To investigate the relationship between residual stress and time to rupture, experiments were conducted using sensitized and as-received SS304L and SS304 specimens subjected to varying applied stresses. The results indicated a decrease in rupture time with increasing applied stress ( $\sigma_{ap}$ ) for SS304, with rupture times of 100 h at 510 MPa and 531 h at 147 MPa. The threshold stress for SCC initiation was identified at 74 MPa, highlighting the significant role of residual stress in SCC susceptibility mitigation. Interestingly, under the tested conditions, aging treatments at 650 °C for 10 min did not substantially alter SCC susceptibility in SS304 and SS304L materials [107]. SS304L exhibited marginally longer rupture times than SS304, particularly at higher stress levels, suggesting slightly enhanced resistance to SCC.

#### 5.1.5. Sensitization and Failure

Sensitization in stainless steels occurs when  $\text{M}_{23}\text{C}_6$  precipitates at grain boundaries, reducing the chromium content within grains and compromising corrosion resistance. This phenomenon is commonly induced during welding processes, particularly in the HAZ, where residual stresses are highest post-welding due to melting and solidification. Despite efforts to mitigate sensitization, its effects persist, making sensitized stainless steels vulnerable to rapid cracking and corrosion initiation in benign environments like moist air or water, particularly along susceptible grain boundaries [115]. Experimental studies on sensitized SS304 at 80 °C and 35% RH demonstrated heightened susceptibility to SCC. Below the proof stress (approximately 290 MPa), sensitized SS304 exhibited significantly shorter rupture times compared to the as-received material, attributed to elevated residual stresses induced during sensitization [107].

### 5.1.6. Localized Corrosion Potentials

Localized corrosion potentials are crucial in influencing crack propagation in Cl-SCC, particularly within crack or crevice environments in chloride solutions where pH levels drop drastically to around 1–2. This acidic environment promotes SCC growth [130,131]. A study conducted by Tani et al. [132] investigated the anodic polarization behavior of SS316 and SS304 in synthetic seawater at pH 1 and 80 °C, revealing distinct peaks in the active dissolution current at around  $-0.25$  V for each stainless steel sample. Notably, both specimens experienced SCC failure after approximately 500 h of testing. Furthermore, overlapping anodic polarization curves in passivation and transition zones indicated similar pitting potential behavior, suggesting comparable failure tendencies.

Temperature significantly influences localized corrosion potentials. Generally, crevice corrosion potentials are lower than pitting potentials across different specimens. Studies by Mayuzumi et al. [116], along with Tani et al. [132], on the temperature dependence of localized corrosion potentials in saturated synthetic seawater for SS316 and SS304 demonstrated an inverse relationship between the surface temperature and localized corrosion potentials, including the open-circuit potential (OCP). Lower surface temperatures elevated localized corrosion potentials and the OCP, while higher temperatures reduced the dissolved oxygen concentration on the metal surface, thereby lowering the corrosion potential. Anodic polarization curve analysis highlighted considerable variability in SS304's pitting potential at 80 °C, underscoring measurement challenges in assessing localized corrosion potentials accurately and their implications for SCC.

## 5.2. Cl-SCC Mechanism

Cl-SCC is characterized by the interplay of residual stress and pitting corrosion, occurring in two primary stages: initiation and propagation.

### 5.2.1. Initiation Stage

The initiation of Cl-SCC involves complex electrochemical processes. The resistance of stainless steel to electrochemical corrosion is primarily due to its protective chromium oxide passive layer, typically 1–3 nm thick [115]. However, chloride ions significantly threaten this passive layer, leading to localized damage [133]. This initiates pitting corrosion when the steel exceeds a critical potential known as the film breakdown potential or pitting potential. Chloride ions locally disrupt the passive film, initiating pitting corrosion [132,134]. Pits formed during pitting corrosion serve as preferential sites for Cl-SCC initiation, causing increased surface roughness and passive film disruption. Residual stresses from manufacturing or mechanical loading can further increase susceptibility to crack initiation, concentrating at pit edges or other surface imperfections [132,134].

In materials science, pitting corrosion is widely recognized as crucial in initiating Cl-SCC. As the passive film breaks down, pits develop on the stainless steel surface, facilitating SCC initiation due to increased surface roughness and the disrupted passive film. Within these pits, aggressive local chemistry promotes the development of tensile stresses through mechanisms such as concentration gradients and stress concentration due to pit geometry [115]. Once tensile stresses exceed the material's SCC threshold, cracks typically initiate from the pit bottom and propagate under the influence of aggressive chemical environments and applied stresses [107].

### 5.2.2. Propagation Stage

The propagation of SCC involves intricate scientific processes primarily influenced by metal dissolution and residual stress. Once a crack initiates at a pit, it rapidly propagates under these conditions, with mechanical factors predominantly influencing the process. Specific threshold conditions must be met for crack propagation to occur. Studies indicate that the rate of metal loss over time significantly impacts SCC progression, underscoring the importance of prolonged exposure to conducive environments [135]. Additionally, environmental factors such as RH levels below 15% can inhibit SCC propagation, high-

lighting the interaction between environmental conditions and crack advancement [116]. The mechanisms underlying crack initiation and SCC involve a combination of mechanical and electrochemical processes. Cracks primarily propagate along grain boundaries, where material microstructure is critical. Crack growth is driven by mechanical loading and chemical reactions at the crack tip, promoting the separation of atomic bonds. Concurrently, the aggressive chemical environment within the crack accelerates metal ion dissolution, further exacerbating crack propagation [135].

## 6. Assessment of SCC

Various techniques are commonly employed to assess SCC, including the SPT, CLT, and SSRT. The SSRT utilizes a constant-extension-rate machine to gradually strain materials, providing controlled insights into SCC behavior under deformation. The CLT applies sustained loads using proof rings to study SCC under constant stress conditions. The SPT employs miniaturized specimens to efficiently assess SCC characteristics, often complemented by electrochemical measurements for comprehensive SCC analysis. The CLT involves exposing specimens to constant tensile stresses in corrosive environments for durations of up to one month. Despite meeting ANSI/NACE TM0177 standards, the CLT has limitations, such as static conditions, the inability to continuously monitor SCC progression, and extended test durations [5].

The SPT is utilized in academic research to evaluate various mechanical properties of metallic materials, including susceptibility to SCC, using acoustic emission and small indentations. This method offers advantages by enabling the assessment of mechanical characteristics in small, inaccessible regions compared to conventional methods. Currently, the SPT is applied to study fracture behavior, creep resistance, ductile–brittle transition temperatures, tensile states, and susceptibility to Environmentally Assisted Cracking (EAC) [5,136,137].

The SSRT is a mechanical approach extensively used to assess SCC in buried pipelines, subjecting steel samples to gradual straining within a simulated service environment. This method provides valuable insights into the susceptibility of pipeline steels to SCC with short experimental durations [5,138]. The SSRT utilizes portable instruments to maintain consistent extension rates, which is crucial for evaluating metals under challenging environmental conditions [139].

### 6.1. SCC Assessment Using SSRT

Evaluating materials for susceptibility to SCC commonly follows standardized methods such as ASTM G129 and NACE TM0198. This process typically involves comparing the mechanical properties of specimens tested in defined environments, such as soils or solutions, against those tested in air. Established equations and criteria are used to quantify the extent of deterioration [5,140,141]. A critical aspect of this assessment is the analysis of ductility parameters, explicitly focusing on the plastic strain-to-failure (PSF) ratio. This ratio is computed by dividing the PSF observed in the testing environment by that observed in ambient air and multiplying by 100 [5]. Ratios below 0.5 indicate higher susceptibility, while ratios between 0.8 and 1.0 suggest lower susceptibility to EAC. Achieving PSF ratios close to 1.0 is recommended to enhance resistance to SCC. Mechanical and spectroscopic assessments are advised to confirm SCC occurrence at PSF ratios below 0.8, with crack properties typically examined along the longitudinal section of the specimen gauge.

Kane and Wilhelm proposed a standardization framework in 1993 to harmonize testing techniques across industrial and academic domains. The SSRT and CLT are the primary methods for assessing SCC susceptibility in carbon steels. The SSRT employs specialized equipment, such as the Inter-Corr M-CERT machine, to apply controlled strain conditions, loads, and extension rates during testing [5]. Test specimens, whether cylindrical or rectangular, are machined to meet specific experimental conditions and the requirements of the tensile testing machine, adhering to detailed specifications outlined in relevant

standards [5,136,140,141]. Commonly recommended test specimens for evaluating SCC in carbon steels include Bent-Beam, pre-cracked cantilever beam, pre-cracked wedge-open-loading-type, U-bend, and C-ring configurations [5]. The CLT involves subjecting specimens to constant tensile stresses in environments conducive to cracking for extended durations, up to 30 days.

For detailed SCC testing procedures, NACE Standard TM0284 provides further guidance [5]. Novel materials such as composite coatings or polymer compounds can be efficiently evaluated for SCC susceptibility using methods that allow relatively short test durations and familiar terminology. Additionally, combining electrochemical techniques with tension tests enables the simultaneous assessment of corrosion processes and material behavior [142]. However, careful consideration of factors such as electric contact isolation from test machine structures is essential, along with acknowledging limitations, such as the oversimplification of crack initiation stages and potential specimen size and cost implications [5,143].

Moreover, Afanasyev et al. [144] proposed cyclic testing to simulate real-world load conditions and understand crack behavior, particularly in the absence of corrosive environments. This methodology involves subjecting field-damaged samples to cyclic loading using four-point loading conditions, replicating pressure fluctuations representative of operational pipelines [5].

#### 6.2. Complementary Test Methods for Assessing SCC

Numerous experimental studies have investigated the phenomena of SCC and their corresponding electrochemical behaviors [5]. Established protocols for supplementary investigations into external SCC adhere to ASTM standards. These include ASTM D4959 for gravimetric analysis to determine moisture content, ASTM G4643 for pH determination, ASTM G187 and ASTM G57 for soil resistivity measurement using a soil resistivity meter, and ASTM G51 for redox potential analysis. Ion chromatography and inductively coupled plasma (ICP) spectroscopy are employed to assess oxygen concentration, texture characteristics, and the presence of anions and metals. Additionally, assessments related to cathodic disbondment and criteria for the cathodic protection of underground pipelines follow standards such as ASTM G95, ASTM G80, ASTM G42, ASTM G8, and NACE Standard TM0497. Holiday detection in coatings is conducted in accordance with ASTM G62, while studies on microbiologically influenced corrosion align with NACE Standard TM0106. Protocols for the external direct assessment of pipelines are outlined in ANSI/NACE Standard RP0502 [5].

Electrochemical data obtained from cyclic tests are complemented by fractographic examinations of cross-sectional samples [144]. Elemental analysis using spectroscopy is utilized to investigate the composition of corrosion products (oxides) and to study SCC phenomena [144]. For internal SCC (I-SCC) evaluation, recommended standards include NACE Standard SP110 for pipelines conveying wet natural gas and NACE Standard SP0206 for directly assessing pipelines transporting dry natural gas [6]. Further internal evaluation tests involve determining metal and anion contents, oxygen concentration, and texture characteristics using ion chromatography and ICP analysis. Redox potential analysis follows ASTM Standard G200, while ASTM Standard D4294 characterizes sulfur-compound-containing petroleum products. Hydrocarbon properties such as API gravity, acid number, density, and viscosity are determined by ASTM D287, ASTM D1298, ASTM D664, and ASTM D5002, respectively. Various water properties, including pH, density, conductivity, resistivity, iron content, and bacterial presence, are also assessed [5].

### 6.3. Non-Destructive Testing

To assess materials for SCC, non-destructive testing (NDT) techniques are employed. NDT is essential for detecting early stages of corrosion and facilitating timely corrective actions, thus extending the lifespan of components. It evaluates materials without causing damage, unlike destructive methods such as the SSRT or CLT, which intentionally induce failure to gather data. Despite meticulous material selection, design, and environmental controls, some corrosion-related degradation is unavoidable. NDT is crucial in both manufacturing and maintenance for inspecting raw materials, sub-components, and finished products without altering the material's properties or functionality [145].

Significant advancements in NDT emerged during World War II, driven by heightened demands for industrial quality control. In the 1950s, enhancements in NDT instrumentation led to improved resolution and defect detection capabilities. The 1960s introduced further advancements through the application of statistical methods and interferometric concepts. By this time, NDT techniques were commonly used to inspect defects such as cracks, voids, porosity, non-metallic inclusions, and forging laps. Over the following decades, developments continued in response to new materials, increasing quality standards, complex geometries, and evolving defect morphologies [146].

One of the key applications of NDT is corrosion-related failure detection, which is crucial for identifying degradation that can compromise structural integrity. This includes forms such as pitting corrosion, uniform corrosion, and microcracking. SCC is particularly challenging to detect due to its often-subtle nature, with cracks potentially developing beneath the surface and remaining invisible to conventional inspection methods, such as visual inspection or dye penetrant testing. NDT methods are required to detect such hidden defects. The integration of various NDT techniques enhances the ability to identify concealed cracks and defects, thus improving safety and reducing the risk of catastrophic failures. This integration is essential for maintaining the integrity of critical infrastructure and ensuring operational safety in industries susceptible to these forms of degradation.

Predicting SCC in materials is crucial, as NDT can reveal imperfections such as variations in the density, size, location, and morphology of defects. Effective NDT techniques for detecting and predicting SCC include ultrasonic testing (UT), acoustic emission testing (AE), eddy current testing (ECT), radiographic testing (RT), and magnetic particle testing (MPT) [147]. These techniques involve applying energy to a component and analyzing the resulting signals with sensitive detectors to identify discontinuities by assessing how energy interacts with the material. Techniques utilize various probing media, including sound waves, electromagnetic fields, and radiation [146].

For SCC prediction, such kinds of methods are particularly valuable due to their ability to detect early signs of cracking. Each NDT technique has specific sensitivities to material properties and conditions, evaluating characteristics such as geometric, mechanical, electrical, magnetic, acoustic, and thermal properties. Many techniques require minimal specimen preparation, use portable equipment, can be automated, and offer good temporal resolution. Additionally, some methods enable online monitoring, which is crucial for ongoing SCC prediction [148].

However, NDT methods have limitations, including detector sensitivity, background noise, and challenges in signal interpretation. Detecting small SCC-related defects can be difficult due to these factors. Higher resolution often increases inspection time and cost. The effective application of NDT for SCC prediction requires prior knowledge of defect characteristics and accessibility to the inspection area. While NDT can identify defects, it does not assess their severity, necessitating further evaluation to determine the appropriate repair actions [146,149].

### 6.3.1. Ultrasonic Testing

Ultrasonic testing (UT) is a widely used NDT method that employs high-frequency sound waves, typically ranging from 0.5 to 10 MHz, to detect internal defects within materials. Sound waves propagate through a medium at a known velocity and reflect off interfaces or boundaries between different media. This principle of reflection is fundamental to UT [147]. In UT, ultrasonic waves are generated and detected by transducers, which convert electrical impulses into mechanical sound waves and vice versa. The transducer emits ultrasonic pulses into the material, and the reflected pulses are captured to measure the time taken for the waves to travel through the material, which aids in identifying internal defects such as cracks and voids [147].

UT is particularly effective for detecting SCC in various structures, including pipelines, pressure vessels, and aerospace components. The technique employs methods such as pulse-echo and shear-wave (angle beam) testing to identify defects. Shear-wave UT is especially useful for detecting SCC, as it can analyze reflections from the edges of cracks, thereby revealing both transgranular and intergranular types of SCC [150]. This capability is crucial for ensuring the integrity of structures exposed to corrosive environments. Recent advancements in UT technology have significantly enhanced its effectiveness in SCC detection. For example, phased-array UT uses multiple transducers to steer the ultrasonic beam and create detailed images of the internal structure. This technique allows for more accurate and comprehensive detection of complex cracks. Additionally, guided-wave UT can inspect large areas of pipes and other structures, providing long-range inspection capabilities and detecting SCC over extensive distances [147,151]. Automated UT systems offer considerable advantages for SCC detection, including increased speed, reproducibility, and the ability to process complex data, such as three-dimensional tomography. These systems are particularly valuable in high-pressure and high-temperature environments, such as offshore facilities, where manual inspection may be impractical or hazardous. Moreover, UT is effective in monitoring corrosion and detecting SCC across various industries, including oil and gas, petrochemical, and aerospace [147,151].

The advantages of UT include the ability to perform inspections from the external surface while structures remain in service, as well as its compatibility with various coatings and linings. It also provides a non-contact alternative through laser-ultrasonic methods, which are useful in high-temperature and hazardous environments. However, UT has its limitations. Calibration must be tailored to specific materials, and flaw orientation is critical for accurate detection. Optimal results are achieved when the sound beam is perpendicular to the flaw's axis; flaws that are parallel or nearly parallel to the beam may be missed. Additionally, UT may exhibit lower sensitivity to very small changes in metal loss compared to some physical or electrochemical methods [148].

In summary, UT is a powerful tool for detecting SCC, offering detailed insights into material integrity without damaging the components. Its ability to provide real-time, non-destructive evaluation makes it essential for maintaining the safety and reliability of critical infrastructure. As technology continues to advance, the role of UT in detecting SCC and other material defects will become increasingly pivotal in ensuring the longevity and safety of structural components.

### 6.3.2. Acoustic Emission

The acoustic emission (AE) technique is a crucial tool for detecting and monitoring SCC and other microscopic defects that arise from stress variations due to changes in process conditions, such as pressure or temperature fluctuations [152]. AE involves the detection of transient acoustic waves produced by the rapid release of energy from localized sources within a material. This technique is particularly effective for evaluating corrosion-related phenomena because it captures the acoustic emissions generated by the development of defects or plastic deformation, providing real-time insight into the structural integrity of materials.

AE sensors detect these transient acoustic waves and convert them into electrical signals. The amount of acoustic energy recorded is influenced by the size of the defect, its location relative to the sensor, and the material's properties. AE monitoring has proven effective in identifying significant issues in a variety of structures, including ASS affected by SCC [153,154]. One notable advantage of AE is that it is not constrained by temperature limits for sensors; these sensors can be connected via metal acoustic waveguides welded to the structure, allowing the sensor to be positioned outside of thermal insulation. AE is particularly effective for evaluating corrosion-related phenomena, such as SCC. SCC involves complex interactions between mechanical stress and a corrosive environment, which can generate significant acoustic emissions. The AE technique can monitor SCC effectively by detecting the acoustic signals associated with crack initiation and propagation. Research has shown that AE signals strongly correlate with SCC initiation and progression. For example, studies on AISI 316L ASS exposed to a 3% NaCl solution have demonstrated that AE signals correlate with the initiation and growth of SCC [155].

Additional research has utilized AE to study SCC in low-carbon type 304 stainless steel under varying corrosive conditions. Tests conducted in 0.01 M and 1 M NaCl solutions with a pH adjusted to 1 revealed that higher AE rates were observed in more concentrated NaCl solutions, correlating with increased SCC damage. Both the applied stress and solution potential influenced AE rates, indicating that AE can detect variations in SCC severity based on environmental conditions and mechanical stress [156,157]. This highlights AE's capability to provide detailed insights into the corrosion processes occurring under different conditions. Crevice corrosion, another corrosion-related phenomenon, involves localized corrosion in confined areas where a metal is exposed to a corrosive environment while other parts of the surface remain protected. AE has proven effective in monitoring crevice corrosion as well. Studies on 304L ASS have shown that AE can detect crevice corrosion initiation, propagation, and repassivation. Changes in AE signals were linked to variations in crevice damage, influenced by factors such as the presence of chloride ions and the mechanical assembly conditions [157]. This demonstrates AE's versatility in monitoring various types of corrosion beyond SCC.

AE is particularly effective for detecting processes associated with SCC, including crack propagation, gas evolution, and plastic zone formation. While some corrosion processes, such as uniform metal dissolution, do not generate AE due to the lack of localized strain, SCC typically produces significant AE signals because of the strain associated with crack formation. Studies by Shaikh et al. [158] have shown that AE can effectively capture the microprocesses of SCC in materials like AISI 316LN stainless steel. These studies reported increased AE counts and energy at SCC initiation, with continuous AE prior to initiation and bursts of AE during crack growth, underscoring AE's capability to monitor SCC in real time.

In a standard AE monitoring setup, a piezoelectric sensor is acoustically coupled to the test object using an appropriate coupling medium. The sensor output is amplified and filtered by preamplifiers before being transmitted to the monitor through shielded coaxial cables. The monitor processes, filters, and amplifies the AE signals, providing data for detailed analysis. The results and raw data are recorded for archival purposes or further evaluation to pinpoint the location and nature of the AE signals [159].

Overall, AE offers several advantages, such as its ability to provide real-time responses to SCC development and detect discontinuities across an entire structure with limited access. However, AE also has limitations, including its sensitivity to background noise and its primary focus on detecting dynamic processes. AE cannot detect static discontinuities unless they are actively propagating. Despite these limitations, AE remains an essential tool for assessing SCC and other corrosion-related phenomena, offering valuable insights into material integrity and structural health [147].

### 6.3.3. Eddy Current Testing

Eddy current testing (ECT) is an NDE method widely employed to assess the integrity of conductive materials, including those susceptible to SCC. The technique operates by passing an alternating current (AC) through a coil, which generates an alternating magnetic field. This field induces eddy currents within the material, and variations in these currents can provide insights into material integrity [160]. ECT is especially effective for detecting SCC when high-frequency coils are used, as they enhance sensitivity to surface and near-surface cracks, which are indicative of SCC. Regular inspections using ECT can monitor changes in metal loss and corrosion over time, although achieving high sensitivity in real-time applications remains a challenge.

ECT includes several advanced methodologies tailored to specific inspection needs. Surface ECT focuses on scanning the material's surface to identify surface-breaking defects and discontinuities, making it effective for detecting SCC on exposed surfaces. Tubular ECT involves inserting a probe into the interior of conductive tubes to detect internal flaws and corrosion, which is useful for identifying I-SCC. Weld ECT evaluates welds to find defects such as incomplete fusion or cracks, which may suggest SCC in welded joints. ECT employs multiple coils activated sequentially or simultaneously to inspect larger areas rapidly. This method provides detailed data recording and three-dimensional imaging capabilities, allowing for the precise detection of surface and subsurface defects, including SCC [148].

Remote field testing (RFT) is effective for assessing defects at various depths by inducing currents on both the external and internal surfaces of a tube, making it suitable for evaluating thick-walled structures. Pulsed eddy current testing (PEC) involves sending short pulses of current into the material rather than using continuous AC. This approach enhances sensitivity for detecting SCC and is valuable for inspecting components beneath insulation. PEC is widely utilized in industries such as oil and gas, power generation, and offshore operations, and it performs well in challenging environments, including dirty, rough, cold, and high-temperature conditions. PEC is also effective for assessing flow-accelerated corrosion (FAC), corrosion under fireproofing (CUF), and corrosion under insulation (CUI) [161,162]. Magneto-optical imaging of eddy currents offers real-time imaging over large areas, which is advantageous for quickly detecting SCC and other subsurface defects. This method allows for effective monitoring of extensive regions, enhancing the overall detection capabilities of ECT [148].

Despite its advantages, ECT has limitations in detecting SCC. The technique's effectiveness can decrease for defects located in ferromagnetic materials due to the effects of magnetic permeability, which can distort eddy currents and reduce sensitivity. Additionally, ECT's ability to detect deeper defects diminishes with increasing depth, and the surface finish of the material can also impact performance. While ECT may not match the spatial resolution or depth penetration of ultrasonic techniques, it remains a valuable tool for detecting SCC, especially in multilayer structures and complex geometries [148]. Addressing these limitations requires considerable expertise in probe design and data interpretation.

### 6.3.4. Radiographic Testing

Radiographic testing (RT) is a crucial NDT method extensively used to detect SCC. This technique is highly valued for its ability to assess the internal structure of components and materials without causing damage. RT is particularly effective in identifying SCC, which can be difficult to detect due to its often-subtle and internal nature [147,148]. RT employs penetrating radiation to create images of the internal structure of an object. By passing radiation through the object and capturing the transmitted radiation on a detection medium, such as photographic film or a digital detector, RT reveals variations in material density and thickness. These variations produce images that can indicate internal features, such as cracks or corrosion, which are crucial for identifying SCC [163]. Typically, RT uses X-rays or gamma rays as radiation sources. X-rays are generated by accelerating

electrons and directing them toward a target, producing high-energy photons that can penetrate materials up to approximately 200 mm of steel equivalent. X-ray machines come in various configurations with adjustable energy levels to accommodate different inspection needs. Gamma rays, produced from radioactive isotopes like iridium-192 and cobalt-60, are also employed, especially for their portability and compactness in field applications [147]. Another significant RT technique is neutron radiography, which is particularly effective for detecting SCC. Neutrons, sensitive to hydrogen, can identify fine cracks and localized corrosion that may not be visible with other radiographic methods. Neutron radiography is enhanced by techniques such as gray-level stretching, beam flattening, and frame averaging, which improve the quality and clarity of the images [148].

RT's versatility extends beyond SCC detection. It is used in pipeline corrosion detection within the process industry, pitting and localized corrosion identification, and rebar corrosion inspection in civil structures. RT is also applied to inspect welds, castings, assemblies, adhesive bonds, plastics, wood, composite materials, and electronic components. The technique can accommodate a range of object sizes, from small components like integrated circuit chips to large items such as rocket motor casings. RT is especially effective at identifying volumetric defects, such as voids and porosities, which can signal underlying SCC [147].

Despite its advantages, RT has limitations in SCC detection. It requires access to both sides of the component, which may not always be feasible. RT is less effective at detecting linear defects, such as cracks, unless they align with the radiation beam. The precision of thickness measurements is generally  $\pm 10\%$  for pit depth, and surface debris or scale can impact the accuracy of SCC detection. Additionally, neutron radiography can be affected by scattered radiation, complicating accurate measurement [148]. The relatively high cost of RT and the need for stringent safety measures due to the hazardous nature of radiation are also considerations. Managing radiation exposure and adhering to safety protocols is essential to protect personnel. Nonetheless, advancements in radiographic technology, including improvements in radiation sources, digital imaging, and Compton scattering techniques, have addressed many of these limitations and expanded the applications of RT [147].

In conclusion, RT remains an essential tool for detecting SCC and assessing the integrity of various components and structures. Its ability to provide detailed internal images and identify subtle defects makes it invaluable for maintaining safety and performance in industrial applications. While there are limitations, ongoing technological advancements continue to enhance the effectiveness and broaden the scope of RT, reinforcing its role as a key method in NDT and inspection.

#### 6.3.5. Magnetic Particle Testing

Magnetic particle testing (MPT) is a crucial NDT technique used to identify surface and near-surface discontinuities in ferromagnetic materials. This method is particularly significant for detecting early signs of SCC, a phenomenon where materials undergo brittle fracture due to the combined effects of tensile stress and a corrosive environment. MPT operates on the principle that ferromagnetic materials become magnetized when subjected to a magnetic field. Defects within these materials disrupt the magnetic flux lines, causing a leakage flux that becomes visible on the surface. Fine magnetic particles, such as iron filings or specialized magnetic powders, are then applied. These particles cluster around areas of magnetic flux leakage, creating a visible indication pattern that reveals the defect's location, size, and shape [146,147].

The MPT procedure involves several essential steps: cleaning the component's surface to remove contaminants; magnetizing the component using methods such as AC, direct current (DC), half-wave direct current (HWDC), or permanent magnets and electromagnets;

applying magnetic particles; inspecting for defects; and finally, demagnetizing and cleaning the component to remove residual particles. Effective detection relies on the proper alignment of the magnetic flux with the defect orientation, which may necessitate multiple inspections to cover various potential orientations. High currents are often required for larger components, necessitating careful management to prevent localized overheating at electrical contact points [147].

MPT is particularly effective in identifying surface-breaking cracks and corrosion-induced defects that are critical in the context of SCC. It can detect various forms of discontinuities, such as grinding cracks, heat treatment cracks, and other surface flaws that may contribute to SCC. This technique is applicable to a range of ferromagnetic materials, including finished products, billets, hot-rolled bars, castings, and forgings. However, MPT is limited to ferromagnetic materials, and thorough post-inspection procedures are necessary to ensure that all residual magnetic particles are removed and the component is demagnetized [146].

Recent advancements in MPT technology have enhanced its ability to detect smaller and more subtle defects. Vasylenko et al. [164] have introduced a technique utilizing luminescent ferrofluids made from  $\text{CoFe}_2\text{O}_4$  nanoparticles, sized between 5 and 11 nm. These luminescent ferrofluids offer improved sensitivity and contrast compared to standard magnetic powders. At a concentration of 3.1 g/L, these ferrofluids can detect minute defects, such as an artificial ring defect of 10 mm in diameter with an opening width of 1.2  $\mu\text{m}$ , on steel plates. This improved detection capability is crucial for identifying small-scale defects associated with SCC, where early detection is essential for preventing material failure [164].

In summary, MPT remains a robust and effective method for detecting surface and near-surface defects in ferromagnetic materials, with ongoing advancements further enhancing its effectiveness in identifying critical flaws related to SCC.

#### 6.4. Predictive Models for Assessing SCC

Incorporating predictive modeling and simulation techniques for SCC not only enhances the practical value of managing SCC but also bridges the gap between theoretical understanding and real-world application. Modern computational methods, such as the finite element method (FEM), molecular dynamics (MD), and machine learning, have revolutionized how we predict and manage SCC in complex systems.

##### 6.4.1. Finite Element Method

The finite element method (FEM) is an advanced computational technique used to simplify complex problems by breaking them into smaller, more manageable sub-regions. This method is particularly essential for studying SCC in pipelines. By discretizing pipeline structures into finite elements, the FEM enables detailed simulations of mechanical stresses and their interactions with corrosive environments, which is crucial for understanding SCC. SCC is influenced by material properties, stress levels, and environmental conditions [165,166].

SCC occurs when a material subjected to tensile stress is exposed to a corrosive environment. The FEM is particularly valuable in this context, as it allows for the precise modeling and prediction of how stress concentrations impact SCC. For example, Turnbull et al. [167] utilized the FEM to analyze stress–strain distributions around pitting pits on cylindrical specimens. Their research showed that stress was concentrated at the bases of the pits, while strain was most significant at the pit shoulders. This information is crucial, as it indicates the most likely sites for crack initiation and propagation. Adjusting the mesh density in simulations enabled the accurate modeling of corrosion progression and its effect on stress distribution.

FEM simulations have also been employed to investigate the effects of hydrogen diffusion on corrosion. Hydrogen can diffuse into metals and exacerbate cracking, a phenomenon extensively studied using the FEM. Research confirmed that hydrogen atom bias plays a significant role in the initiation and propagation of intergranular cracks. Specifically, a reduction in grain boundary binding energy increased the percentage of failure cells, and higher displacement under constant binding energy also raised the failure unit percentage [168,169]. These findings support traditional theories of hydrogen-induced intergranular cracking [170,171]. Simulations using the Abaqus method with two-dimensional linear and secondary bonding cells have contributed to developing a system for predicting critical internal stress values in high-strength steels with specific corrosion defect sizes, which has been applied in pipeline safety assessments in Canada [172].

The FEM is not merely a theoretical tool but has practical applications in pipeline integrity management. Studies have shown that stress concentrations, such as those caused by deeper dents, lead to increased corrosion rates and accelerated crack initiation and propagation. This effect is particularly pronounced in high-pressure gas transmission pipelines, where internal pressures exacerbate stress levels and heighten SCC risk [165].

In practice, the FEM helps engineers evaluate the impact of external loads and internal pressures on pipeline integrity. By simulating these conditions, engineers can identify high-risk areas for SCC and develop targeted maintenance and reinforcement strategies. For example, the FEM has been used extensively in the TransCanada pipeline system to assess various stressors impacting pipeline segments and guide maintenance and reinforcement efforts [165].

Furthermore, the FEM is invaluable for analyzing SCC on complex surfaces and irregular pitting corrosion patterns. It provides insights into localized corrosion processes and their effects on material integrity. This capability is essential for estimating pipeline lifespan, evaluating maintenance interventions, and making informed decisions about reinforcement measures to enhance pipeline durability [165].

In summary, the FEM is a powerful tool for understanding and managing SCC in pipelines. It allows for detailed simulations of stress and corrosion interactions, provides insights into the effects of material properties and environmental conditions, and supports practical applications in pipeline integrity management. This comprehensive approach helps engineers predict and mitigate the risks associated with SCC, ensuring safer and more reliable pipeline operations.

#### 6.4.2. Molecular Dynamics

Molecular dynamics (MD) simulations provide a valuable approach for modeling atomic and molecular interactions over time, making them particularly effective for studying SCC. These simulations track the positions and velocities of atoms based on classical mechanics principles, enabling researchers to explore dynamic behaviors at the atomic scale. MD simulations are primarily divided into two types: ab initio molecular dynamics (AIMD) and classical molecular dynamics (classical MD). AIMD combines quantum mechanical calculations with molecular dynamics to achieve high precision, though it is computationally expensive, limiting its application to smaller systems and shorter time scales. In contrast, classical MD uses empirical force fields, which are less computationally demanding and allow for the simulation of larger systems and longer time scales [165].

In SCC research, MD simulations are essential for understanding phase interfaces, corrosion mechanisms, and the effectiveness of corrosion inhibitors. For instance, simulations have demonstrated that water droplets on graphene coatings maintain a consistent contact angle, with a single graphene layer exhibiting significant hydrophobic properties. MD simulations also provide insights into how metal surfaces interact with corrosive agents, such as the formation of a non-bonded water network on gold that affects passivation stability [173]. Furthermore, MD research has been used to evaluate corrosion

inhibitors like olmesartan and ketosulfone, revealing their effectiveness under various conditions [174,175].

MD simulations are also valuable for elucidating failure mechanisms associated with SCC. Studies have shown that radiation damage and stress concentrations from vacancy formation contribute to SCC [176]. Simulations of failure in galvanized iron and copper have revealed that stretching of the zinc lattice and the resistance of specific copper interfaces to temperature and load changes are key factors [177,178]. Despite their advantages, MD simulations have limitations, such as reliance on empirical force fields and the high computational cost of AIMD. Nonetheless, they remain a powerful tool for advancing our understanding of SCC and developing effective strategies for corrosion mitigation.

#### 6.4.3. Machine Learning for Assessing SCC

In the field of SCC growth estimation, ongoing research is crucial for developing reliable predictive models. The complexity and variability of SCC progression have led to increasing interest in artificial intelligence (AI) as a tool for understanding and managing SCC in pipelines. AI is transforming how we assess corrosion risks in critical infrastructure. For instance, Zhang et al. have employed AI models, such as Multilayer Perceptron (MLP) and Long Short-Term Memory (LSTM), to enhance prediction accuracy by correlating SCC-induced crack widths with steel weight loss in reinforced concrete (RC). Their approach, which includes analyzing reinforcement bar cross-sections, improves evaluation precision and cost efficiency [165].

AI's capabilities extend to predicting corrosion rates and crack growth. Advanced techniques like Principal Component Analysis (PCA), Particle Swarm Optimization (PSO), Feed-Forward Artificial Neural Networks (FFANNs), Gradient Boosting Machine (GBM), Random Forest (RF), and Deep Neural Networks (DNNs) have significantly advanced the estimation of SCC progression in aging infrastructure. By training these models on historical SCC data, researchers can forecast SCC onset and growth rates under various conditions [179,180]. For example, AI methods have been applied to study SCC in carbon steel and pipelines, with Ossai's analysis of over 8300 records providing valuable insights into estimating the SCC depth [165,181].

Machine learning (ML) involves developing systems that improve their performance over time based on data-driven learning [22]. Michie et al. [182] describe ML as a process where algorithms learn from data patterns rather than relying on explicit programming [182]. The effectiveness of ML models depends on data quality and the extent of human intervention, such as providing accurate labels or feedback. The choice of methodology affects prediction accuracy and efficiency: PCA reduces data dimensionality but might overlook important details [183], and PSO effectively optimizes model parameters [184], while FFANNs and DNNs handle complex relationships with high precision but require extensive data and computational resources [185]. GBM and RF use ensemble learning to enhance stability, though they may encounter difficulties with very-high-dimensional data [186,187]. Choosing the right technique depends on specific SCC assessment needs, data characteristics, and available computational resources.

ML models also play a vital role in SCC protection and inhibitor optimization. They assist in managing complex protection strategies, reducing preparation and testing costs, and predicting optimal inhibitor formulations [165]. Additionally, deep learning-based image processing techniques, such as the Accurate Metallic Corrosion Detector (AMCD) developed by Yu et al., are increasingly used to automate SCC assessment [10]. Forkan's image recognition model has achieved high accuracy [188], Ao's tool for Al-Zn-Mg alloys predicts mechanical performance changes with notable precision [189], and Dogan's deep transfer learning model effectively distinguishes SCC damage from other structural issues, facilitating targeted repairs [190]. These advancements not only improve SCC detection accuracy but also significantly reduce labor costs. Advanced ML techniques are set to enhance global efforts in managing pipeline integrity and predicting SCC [22].

## 7. Prevention of SCC

Pipeline companies, industry groups, and researchers in the United States and Canada have extensively studied methods to prevent or mitigate SCC in pipelines prior to failures. To address SCC, various prevention strategies can be utilized, including proper material selection, electrochemical methods, chemical methods, physical methods, and thermal methods. Effective management of SCC also requires the integration of stress management and environmental controls. Figure 6 illustrates the key factors in preventing both internal and external SCC in pipelines.

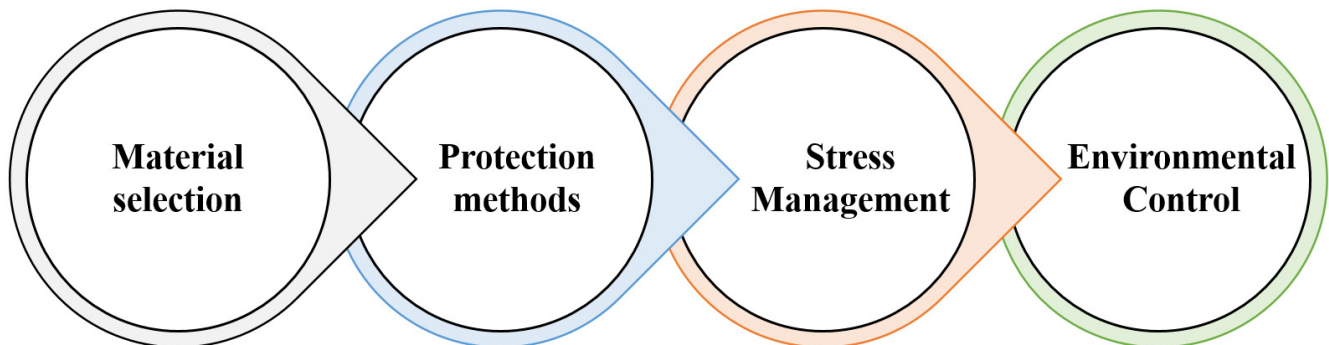


**Figure 6.** Factors that must be considered to prevent SCC development in pipelines.

### 7.1. Material Selection

Proper material selection plays a crucial role in preventing SCC in pipelines. Factors to consider include choosing materials with low susceptibility to SCC, high quality, appropriate toughness, and favorable microstructures. Recent studies indicate that higher API steel grades generally exhibit increased strength but also higher susceptibility to SCC. Conversely, lower-carbon steels exhibit varying levels of susceptibility, often correlating increased steel hardness with greater vulnerability to SCC. Steels of higher quality typically demonstrate reduced susceptibility to SCC.

Moreover, steels with acicular ferrite and bainite microstructures generally show lower susceptibility to SCC. Single-phase microstructures, devoid of precipitates, typically exhibit greater resistance to SCC than multiphase structures. SCC originates predominantly on the metal surface from existing cracks or pitting, while HE manifests at crack tips or between areas of hydrogen accumulation, primarily along grain boundaries and defective crystalline regions. The microstructure and alloy composition, influenced significantly by heat treatment, play critical roles in SCC development. HE reduces steel strength, particularly lowering the critical stress intensity factor, which accelerates fracture propagation, especially with smaller crack sizes.

The specific alloy elements in carbon steel pipelines significantly influence SCC mechanisms, evolving over time due to material aging. After approximately two decades of service life, carbon steel pipelines typically exhibit a ferrite–pearlite microstructure susceptible to SCC. Despite their susceptibility, these steels often contain sulfur, leading to MnS inclusions and other types, such as calcium sulfides, oxides, and aluminum oxides. Inclusions enriched in  $\text{Al}_2\text{O}_3$  and  $\text{SiO}_2$  impart an incoherent, brittle nature to the metal matrix, promoting microcrack formation primarily at grain boundaries and around inclusions [70,191,192].

A study by Liu et al. [193] emphasized the significance of inclusions as the primary sites for crack initiation. Additionally, research by Asahi et al. [191] indicates that quenched-tempered (QT) and thermomechanically controlled processing (TMCP) treatments on X52, X65, and X80 steels result in more homogeneous microstructures, reducing susceptibility to SCC. The microstructure of carbon steel pipelines plays a pivotal role in SCC initiation and propagation. Eliminating inclusions or precipitates can enhance SCC resistance by removing potential nucleation sites for corrosion pits [140,193,194].

Effective suppression of IGC in high-chromium steels involves minimizing carbon content to prevent carbide precipitation, enhancing corrosion resistance in welded joints like those made of 03Cr18Ni11 steel. Practical strength requirements often necessitate carbon content between 0.08% and 0.12%, exceeding solubility limits. Carbide-forming elements such as titanium, niobium, and molybdenum, with stronger carbon affinity than chromium, prevent M<sub>23</sub>C<sub>6</sub> formation, retaining chromium in solid solution and preserving corrosion resistance, albeit at the expense of reduced ductility and increased strength. Experimental studies on enhancing corrosion resistance via molybdenum nanopowder concentration in weld pools during arc welding reveal varied microstructures depending on the concentration. Molybdenum and tungsten nanopowders yield the most corrosion-resistant samples [53].

Forming a favorable weld metal structure by introducing ferritic elements significantly mitigates fractures in dual-phase austenitic–ferritic structures. Primary ferrite presence enhances SCC resistance by replenishing chromium-depleted areas with high diffusion rates [195–197]. Controlling weld metal structures poses challenges, especially in welding and surfacing dissimilar materials. The Schaeffler diagram assists in determining weld metal structures, especially for overlaying corrosion-resistant steel onto low-carbon or low-alloy steel substrates. Selecting materials and welding regimes within specific C<sub>req</sub> (18–24%) and Ni<sub>eq</sub> (7–18%) ranges ensures favorable A+F structures, minimizing crack susceptibility [53].

In welding dissimilar metals like low-carbon steel to AISI304 corrosion-resistant steel, AISI309 steel with higher alloying elements (25% Cr and 12% Ni) is recommended to achieve a similar composition in the weld metal. AISI309 subcoats are often used for surfacing dissimilar metals. Research on enhancing steel-grade EP-302 and welding materials for power plant equipment includes silicon doping to improve heat and liquid metal corrosion resistance, which is critical in environments with lead-bismuth coolant temperatures up to 450 °C. Microstructural analysis of Cr–Ni–Nb austenitic–ferritic welded joints containing silicon underscores the importance of the ferrite phase content in optimizing weld joint processability. Delta-ferrite transformation into the sigma phase after prolonged aging at 500–600 °C highlights the necessity of temperature–time control for maintaining weld joint SCC resistance [53]. Research on low-nickel austenitic steel 08Cr18Ni5 identifies weld metal compositions and temperature–time regions resistant to SCC during welding and emphasizes that low carbon content and high chromium, manganese, niobium, and nitrogen levels contribute to minimizing microcrack susceptibility during welding [55].

## 7.2. Electrochemical Methods

Electrochemical techniques, such as cathodic protection, passivation, and anodization, are highly effective in mitigating SCC in pipelines. These methods employ electrical currents or potential differences to drive chemical reactions on the metal's surface, leading to protective changes that improve resistance to both corrosion and SCC. Implementing these techniques is essential for preserving the structural integrity of metallic systems in corrosive environments.

### 7.2.1. Cathodic Protection

Cathodic protection systems are essential for extending the life of external coatings and mitigating damage using either impressed current or sacrificial anodes. The primary principle behind cathodic protection is to reduce the electrochemical potential of the metal surface, thereby suppressing the anodic reaction that causes metal dissolution. This is achieved by making the metal structure the cathode of an electrochemical cell. Impressed current systems involve applying an external current from an inert anode to the metal structure, while sacrificial anode systems use more reactive metals, such as zinc or magnesium, which corrode in place of the protected structure. A critical aspect of

cathodic protection is the prevention of HE, a process where hydrogen atoms diffuse into the metal and cause brittleness, especially in high-strength steels. This risk is heightened in environments where water can dissociate under the influence of the protective current, releasing hydrogen. Proper control of the applied potential is essential to minimize hydrogen generation.

The effectiveness of cathodic protection systems is influenced by several factors, including the nature of the coating, the soil or seawater composition, and seasonal changes that affect temperature and moisture levels. For example, high soil resistivity can reduce the current output from sacrificial anodes, requiring careful design and monitoring. The NACE SP0169 standard provides comprehensive guidelines for the design, installation, and maintenance of cathodic protection systems for buried or submerged pipelines. Methods such as ASTM G95, ASTM G80, ASTM G42, and ASTM G8 are employed to assess the condition and effectiveness of these systems, particularly in detecting coating disbondment that could lead to localized corrosion and SCC. Regular monitoring and maintenance are crucial to ensure the continued effectiveness of these systems in preventing corrosion and SCC [5].

### 7.2.2. Passivation

Passivation is a chemical process designed to enhance the formation of a thin, stable oxide layer on metals, especially stainless steel. This passive layer, primarily consisting of chromium oxide, serves as a protective barrier against oxygen and other corrosive agents, effectively mitigating both general and localized corrosion that can lead to SCC. Typically, the process involves immersing the metal in an acidic solution, such as nitric or citric acid, to remove contaminants and facilitate the development of the oxide layer. The success of passivation is influenced by various factors, including the type and concentration of passivating agents, the temperature of the treatment solution, and the duration of the process. For example, higher concentrations of  $\text{HNO}_3$  can result in a more uniform and thicker oxide layer, though excessive treatment may cause undesirable etching of the metal surface.

In marine environments, chloride ions can infiltrate weak points in the passive film, leading to pitting and crevice corrosion that precede SCC. Consequently, it is essential to monitor the quality and integrity of the passive layer in such conditions. Recent research highlights that the composition and microstructure of the oxide layer are critical to its protective effectiveness. For instance, chromium-rich oxides offer superior resistance to chloride-induced pitting. Advances in surface analysis techniques have allowed for more precise investigations of oxide layers, contributing to the optimization of passivation processes [198–200].

### 7.2.3. Anodization

Anodization is an electrochemical technique commonly used to enhance the surface properties of aluminum and its alloys. In this process, the metal is submerged in an electrolytic solution, typically sulfuric acid, and an electric current is applied. This results in the formation of a thick, stable anodic oxide layer on the metal's surface, which acts as a protective barrier against environmental degradation and SCC. The anodized layer is generally significantly thicker and more durable than naturally occurring oxides. Its properties can be adjusted by varying factors such as the composition of the electrolyte, temperature, and current density. For example, sulfuric acid generates thicker, more porous layers that are ideal for dyeing, while chromic acid produces thinner, denser layers with superior corrosion resistance. Additionally, the anodized layer can be sealed with hot water or steam to hydrate the oxide and enhance its protective qualities. Anodization not only improves corrosion resistance but also increases surface hardness

and wear resistance, making it valuable for applications requiring robust surface finishes. However, chloride ions can degrade the protective layer, leading to pitting and SCC under specific conditions. Therefore, further treatments, such as sealing or applying organic coatings, may be necessary to improve the durability of the anodized surface [201,202].

Both passivation and anodization effectively prevent SCC by forming stable protective oxide layers. These methods address the root cause of SCC—localized corrosion—by providing a resilient surface capable of withstanding severe environmental conditions. Nevertheless, the effectiveness of these electrochemical methods can be diminished if the protective layers are mechanically damaged or exposed to highly aggressive environments. High temperatures, mechanical stress, or contact with harsh chemicals can degrade these protective layers and increase the risk of SCC [203,204]. In summary, the strategic use of electrochemical methods such as cathodic protection, passivation, and anodization represents a comprehensive approach to mitigating SCC in various metallic structures. These techniques enhance metal surface protection, extend component lifespan, and ensure reliability in challenging environments. Continued research and development to optimize these methods and explore new electrochemical treatments are crucial for advancing corrosion prevention strategies and extending the service life of critical infrastructure.

### 7.3. Chemical Methods

Chemical approaches, such as the use of inhibitors and coatings, are essential for improving the corrosion resistance of metals and preventing SCC. These techniques involve applying chemical substances either directly to the metal surface or to the environment surrounding it to reduce the likelihood of corrosion and SCC. By implementing these methods, researchers and engineers can significantly decrease the risk of corrosion-induced failures in metallic structures, thereby enhancing their durability and reliability in demanding conditions [204].

#### 7.3.1. Coatings

Coatings are vital for safeguarding carbon steel pipelines against SCC, a significant threat to pipeline integrity. These coatings act as physical barriers, preventing direct exposure of the metal surface to corrosive elements, which helps reduce the likelihood of SCC. Choosing the right coating is crucial for effective SCC protection. Organic coatings, particularly epoxy resin coatings, are well researched for their desirable attributes, including minimal shrinkage, resistance to chemicals, and mechanical durability. These coatings are widely employed in industrial contexts, such as on marine vessels and buried pipelines, to combat corrosion and lower the risk of hydrogen-induced SCC [205,206]. The primary function of these coatings is to establish a protective layer that isolates the metal from external factors, thereby minimizing SCC risk [207–210].

Among the coatings applied to external pipeline surfaces, Fusion-Bonded Epoxy (FBE) is distinguished by its exceptional mechanical strength and adhesion, making it suitable for large-diameter pipelines that undergo considerable handling and installation stresses. Despite its effectiveness, FBE coatings can be prone to blistering and shielding effects when used with cathodic protection systems. Liquid epoxy is noted for its robust corrosion protection and excellent adhesion, making it widely applicable in various industrial environments. Urethane and polyurethane coatings offer flexibility and impact resistance, which help protect against physical damage and corrosion. Historically, asphalt and coal tar were prized for their durability and water resistance; however, their use has diminished due to environmental concerns. Polyethylene (PE) and polyolefin resin coatings provide additional protective benefits, while ceramic and composite coatings offer high-temperature resistance and durability, though they can be brittle and require careful application [207,208,211–213].

The success of coatings in preventing SCC depends on factors such as their mechanical properties, water permeability, electrical insulation, and resistance to environmental degradation. Adequate surface preparation is essential to achieve the optimal adhesion and long-term effectiveness of the coating system. Moreover, coatings must be compatible with pipeline materials to avoid detrimental interactions that could compromise their protective capabilities. Environmental factors, including soil and atmospheric conditions, as well as residual stresses from pipeline operations, also influence coating performance and SCC risk. Ensuring that coatings meet these criteria and are applied properly is critical for maximizing their protective efficacy and reducing SCC risk [207].

### 7.3.2. New Trends in SCC Prevention by Coatings

Organic protective coatings are extensively used to combat SCC. Recent developments have led to the creation of coatings tailored to address the specific challenges posed by SCC. These advanced coatings enhance their effectiveness by sealing defects and preventing corrosion reactions, thereby minimizing the need for external maintenance [214].

#### Self-Healing Coatings

Self-healing mechanisms in smart coatings can be categorized into autonomous and non-autonomous types, both of which are crucial for combating SCC. Autonomous self-healing involves integrating polymerizable healing agents or corrosion inhibitors into the coating matrix. These substances are activated when the coating is damaged, thereby restoring its integrity and preventing SCC. For instance, encapsulated agents such as isocyanates, epoxies, and curing agents like tetraethylenepentamine (TEPA) are triggered upon damage to seal cracks and halt further corrosion [214]. Conversely, non-autonomous self-healing requires external stimuli, such as changes in pH or electrochemical signals, to initiate chemical reactions that repair the coating. Conductive polymers, including polypyrrole (PPy) and polyaniline (PANI), are utilized for their ability to undergo redox reactions, which helps to passivate the steel surface and reduce SCC [215,216].

#### Advanced Coating Materials

Recent advancements in materials science feature self-healing polymers such as AQALIC CS-7S, which absorb water and expand to mend scratches upon contact, thereby mitigating SCC in coating defects. Additionally, metallic-polymeric coatings, such as those combining zinc with polyethylene oxide-b-polystyrene (PEO113-b-PS218) nanoaggregates, exhibit self-healing properties due to their amphiphilic nature, effectively serving as barriers against environments that promote SCC. Furthermore, ceramic materials, including TiC/Al<sub>2</sub>O<sub>3</sub> and Ti<sub>2</sub>AlC, demonstrate self-healing capabilities triggered by oxidation. These materials self-heal when exposed to elevated temperatures and oxygen, replenishing defects with protective oxides and thus lowering the risk of SCC [217].

#### Environmental Sustainability

Environmental sustainability and ecological regulations advocate for the incorporation of natural macromolecules and biopolymers—such as chitosan, lignin, cellulose, and nanocellulose—in coating engineering, which can also aid in the prevention of SCC. When chitosan is used in conjunction with an epoxy matrix, it imparts combined anticorrosive and antibacterial effects, thereby enhancing the integrity of protective coatings and mitigating SCC [217]. Lignin serves as a natural ultraviolet (UV) absorber, improving UV stability and prolonging the lifespan of coatings, which, in turn, offers extended protection against SCC [218]. Additionally, cellulose microfibrils and nanofibrils, when infused with healing agents, can be integrated into polymeric matrices to create advanced self-healing epoxy coatings. These innovative materials not only repair mechanical damage but also bolster the defense against SCC by maintaining a strong barrier against corrosive agents [219,220].

### Nanomaterial Additives

Integrating functional nanomaterials into coating formulations can greatly improve their performance, enhancing resistance to SCC. Carbon-based nanomaterials, such as carbon nanotubes (CNTs), graphene, and graphene oxide, enhance the mechanical stability of epoxy matrices, thereby decreasing their vulnerability to stress and strain that could induce SCC. Additionally, nano-silica contributes to improved corrosion resistance, fracture toughness, and tensile strength, further increasing the coating's resilience against SCC. The incorporation of polymeric matrices with metal oxide nanoparticles, nano-clays, and nano-ceramics results in nanocomposite coatings with enhanced properties, offering superior protection against SCC by boosting both mechanical and chemical resistance [217,221,222].

### SCC-Specific Strategies

Advanced coatings that feature self-healing and stimuli-responsive technologies offer a promising approach to reducing SCC. These coatings are designed to identify the initial formation of cracks and either release repair agents to address the damage or modify their properties to halt further crack development. By incorporating corrosion inhibitors such as phosphates, nitrites, and rare-earth metal salts, these coatings can counteract the corrosive elements that exacerbate SCC. Additionally, the integration of nanomaterials into these coatings enhances their mechanical properties, increasing their resistance to the stresses that lead to SCC [217,223].

The adoption of such advanced self-healing and stimuli-responsive coatings in refinery systems is expected to improve anticorrosive performance and extend the lifespan of protective systems, thereby reducing the occurrence of SCC and prolonging the service life of essential infrastructure.

#### 7.3.3. Inhibitors

Corrosion inhibitors are specialized chemical compounds introduced in minimal quantities to corrosive environments to protect metallic materials from deterioration. These substances function by either creating a protective film on the metal surface or neutralizing corrosive agents in the environment. They are particularly effective in controlled environments such as cooling systems and oil pipelines. Corrosion inhibitors can be classified into several types, including anodic, cathodic, passivating, film-forming, vapor phase, and adsorption-based inhibitors. Among these, organic inhibitors, especially those containing polar functional groups with nitrogen, sulfur, and/or oxygen, have proven effective in both acidic and alkaline conditions. The adsorption of these inhibitors on metal surfaces is influenced by factors such as functional groups, steric effects, aromaticity, electron density, and the electronic structure of the inhibitors. These compounds form a protective adsorbate layer on the metal, thereby reducing corrosion rates by shielding the surface from aggressive solutions [224].

Additionally, inhibitors can effectively prevent SCC in metals by forming a protective layer on the metal surface. Organic inhibitors with polar functional groups containing nitrogen, sulfur, and/or oxygen have shown significant effectiveness against SCC in steel under both acidic and alkaline conditions. The efficiency of these inhibitors is affected by several factors, including their functional groups, steric effects, aromaticity, electron density, and electronic structure, which influence their adsorption on the metal surface. By altering the electrode potential of the metal or isolating it from the corrosive environment, inhibitors can substantially lower the risk of SCC. It is noteworthy that higher concentrations of inhibitors might be required to prevent SCC compared to those needed for general corrosion control. Furthermore, paints and coatings containing inhibitors can enhance SCC resistance by preventing corrosive solutions from penetrating the coating and reaching the metal underneath. Recent advancements in chemical additives have been specifically aimed at addressing SCC in applications such as fuel ethanol storage and distribution systems [225,226].

Despite extensive research on corrosion inhibitors for general corrosion in acidic media, there is a significant lack of studies focusing on SCC. While plant extracts have shown promise as environmentally friendly corrosion inhibitors, their effectiveness against SCC remains largely unexplored. A primary challenge in this area is the inadequate mechanistic understanding of these extracts, as most studies use crude formulations without a detailed analysis of individual components. This gap hinders the selection of effective SCC inhibitors. Future research should explore the effects of substituent groups, investigate synergistic interactions among inhibitors, and assess factors influencing SCC inhibition. Additionally, analyzing corrosion product formation in the presence of inhibitors and employing nanotechnology, such as graphene-based composites, could enhance inhibition strategies. Incorporating quantum chemical calculations and molecular mechanics simulations will aid in elucidating inhibition mechanisms. By concentrating on SCC and utilizing eco-friendly materials, researchers can develop effective and cost-efficient solutions for preventing SCC in stainless steel across various industries.

#### 7.4. Physical Methods

Physical methods encompass mechanical processes designed to modify the properties of metals or their surfaces to improve their resistance to SCC.

##### 7.4.1. Physical Vapor Deposition

Physical vapor deposition (PVD) is a sophisticated coating technique widely employed to mitigate SCC in metallic components. This process involves the vaporization of a solid material, which is then deposited onto a substrate to create a thin, protective film. PVD is especially effective in enhancing the corrosion resistance of materials, making it a preferred choice for applications vulnerable to SCC. The coatings produced by PVD are known for their strong adhesion, consistent thickness, and durability, resulting in hard, wear-resistant surfaces. These coatings establish a dense, impermeable layer that shields the substrate from corrosive agents, thereby lowering the risk of both corrosion and SCC. PVD coatings can be applied to a variety of substrates, including metals, ceramics, and alloys, providing not only enhanced corrosion resistance but also improved mechanical properties. Research has demonstrated that PVD-coated tools can significantly influence the susceptibility of materials to SCC. For example, studies have revealed that PVD-coated cutting tools can diminish SCC risk in super duplex stainless steel during machining operations. This highlights the effectiveness of PVD in reducing SCC by improving the surface characteristics of the materials. In conclusion, PVD is a highly effective method for applying protective coatings that enhance the resistance of metals to corrosion and SCC. By creating a robust barrier on the substrate, PVD coatings play a crucial role in extending the lifespan and reliability of metallic structures in environments susceptible to SCC [227,228].

##### 7.4.2. Other Physical Methods

While PVD and thermal spray coating are among the most prevalent and effective methods for preventing SCC, they are not the only techniques available. Other physical approaches can also contribute to SCC prevention, though their effectiveness and appropriateness may depend on the specific application and environmental conditions.

Chemical vapor deposition (CVD) is a technique that deposits thin films onto metal surfaces via chemical reactions with vaporized precursor gases. In this process, precursor gases containing the desired elements are introduced into a reactor, where they decompose on a heated substrate, forming a solid coating with a controlled composition, thickness, and uniformity [204]. CVD coatings are especially effective in mitigating SCC. These coatings create a durable protective barrier that improves the metal's resistance to SCC, which is essential for use in corrosive environments. The conformal nature of CVD

coatings ensures comprehensive coverage, preventing the initiation and propagation of SCC. Moreover, CVD can also be used to apply functional coatings, such as protective, wear-resistant, or catalytic films, further enhancing the surface properties and performance of metal substrates [229].

Plasma treatments have gained prominence in surface engineering, particularly for electronic devices. Techniques such as plasma etching and deposition offer precise control over surface characteristics, including roughness, wettability, and chemical composition. These treatments are effective for removing contaminants, activating surfaces to improve adhesion, or modifying surface energy to enhance the wetting behavior of coatings or adhesives. Recent studies have explored plasma treatments with various gas compositions and process parameters to optimize the surface properties of electronic components for specific applications. For instance, plasma surface modification has been utilized to improve the adhesion of wire bonding and soldering materials to electronic substrates, thereby enhancing the reliability of these interconnections [230,231].

Laser surface engineering encompasses techniques that use lasers to modify the surface properties of metals. Methods such as laser cladding, laser alloying, laser hardening, and laser surface texturing enable precise, localized treatment, allowing control over characteristics like hardness, wear resistance, and thermal performance. These techniques are widely used in tooling, automotive components, and aerospace structures. Regarding SCC, laser surface treatments can significantly enhance resistance. For example, laser cladding can apply protective coatings that reduce metals' susceptibility to SCC by modifying their surface chemistry and microstructure. Similarly, laser hardening can increase surface hardness and diminish the likelihood of crack propagation in corrosive environments [232].

#### 7.5. Thermal Methods

Thermal methods for mitigating SCC involve the application of protective coatings through various thermal spraying techniques, each offering distinct advantages suited to specific applications and environments. Among these techniques, high-velocity oxygen fuel (HVOF) spraying is particularly effective in reducing SCC.

Thermal spray coatings are applied to metal surfaces using high-velocity methods to form a protective layer that shields the underlying material from corrosive conditions. The HVOF spraying technique is especially noteworthy in this regard. It employs the combustion of fuel gas and oxygen to generate a high-velocity jet that deposits molten or semi-molten particles onto the surface at supersonic speeds. The resulting coatings are dense, have low porosity, and demonstrate excellent adhesion to the substrate. This dense and well-adhered coating effectively blocks corrosive agents that could otherwise cause SCC [228,233]. The effectiveness of HVOF spraying in preventing SCC is largely due to its ability to produce durable coatings that resist corrosion and remain intact under severe conditions. In comparison to other thermal spray methods, HVOF coatings provide superior protection owing to their density and strong adhesion, which significantly decreases the likelihood of corrosion pathways penetrating the protective layer.

In addition to HVOF, aluminum- and zinc-based thermal spray coatings have shown impressive performance in SCC prevention. These coatings establish a physical barrier that isolates the metal from the corrosive environment, effectively hindering the initiation and propagation of stress corrosion cracks. The electrochemical properties of aluminum and zinc further enhance the coatings' overall corrosion resistance. Furthermore, the high-velocity impact of particles during the HVOF process creates compressive residual stresses on the surface, counteracting the tensile stresses that contribute to crack formation [228]. The effectiveness of thermal spray coatings in preventing SCC depends on several factors, including the coating thickness, porosity, and adhesion to the substrate. Thicker coatings generally offer better protection, while coatings with lower porosity and higher adhesion

provide improved integrity and durability. Optimal performance is achieved through a careful selection of coating materials and the precise control of spraying parameters to align with the specific environmental conditions and stress factors encountered by the components [228].

#### Additive Manufacturing

Additive manufacturing (AM), often known as 3D printing, is a progressive technology that fabricates objects layer by layer based on digital 3D design data. AM encompasses a variety of processes, including those that use lasers, electron beams, or plasma to deposit, fuse, or solidify materials. This technology offers substantial benefits compared to conventional manufacturing methods, such as the capability to produce intricate components directly from CAD models, reduced material waste, and shorter production times. By the end of 2020, the AM market was anticipated to reach USD 21 billion, which spurred extensive research aimed at improving AM processes, particularly in addressing SCC [234].

Studies on selective laser melting (SLM) have examined how different process parameters—such as scanning speed, laser power, and energy density—affect the microstructure of ASS, including aspects like grain size and porosity. These microstructural features are critical, as they impact the stability of the passive film, which is essential for corrosion resistance and SCC mitigation. Therefore, optimizing SLM parameters is crucial for enhancing corrosion resistance and reducing SCC vulnerability. Research on direct laser deposition (DLD) has explored how heat treatments and chromium content influence passive film formation. Heat treatment is significant for enhancing the development of protective passive films and decreasing SCC susceptibility by improving the overall microstructure. New AM technologies, including advanced 3D printing techniques, provide innovative solutions for reducing SCC. These technologies allow for the production of complex component designs that minimize stress concentrations—a key factor in SCC. They also support the creation of novel materials and coatings specifically designed to withstand corrosive environments. Additionally, AM enables the integration of protective coatings during production and facilitates in situ repairs, thus prolonging the lifespan of components in harsh conditions. The integration of sensors within components for the real-time monitoring of environmental conditions and structural health aids in the early detection of SCC. Rapid prototyping accelerates the development of new materials and designs, thus hastening the application of SCC prevention measures. Nevertheless, challenges related to material performance, manufacturing consistency, and cost need to be addressed to fully realize AM's potential in SCC prevention. Research into other AM methods, such as wire arc additive manufacturing (WAAM) and droplet-based 3D printing, is still emerging. Understanding their effects on corrosion behavior and SCC is limited but essential for ensuring the durability of metal parts produced by AM [234,235].

#### 7.6. Environmental Considerations

SCC is influenced by various environmental factors, including soil composition, transported fluids, and external and internal conditions, each contributing distinct corrosion mechanisms. SCC raises substantial economic, environmental, and safety concerns, necessitating global monitoring. Of particular concern are ions such as  $\text{CO}_2$ ,  $\text{H}_2\text{S}$ , temperature, partial pressure, and naphthenic acid content [42,236,237].

SCC predominantly occurs in environments with nearly neutral to high pH levels, characterized by carbonate-rich conditions influenced by environmental and physicochemical parameters [237]. Susceptibility to SCC increases with greater levels of cathodic polarization, akin to the overprotection effect observed in carbon steel [238–240]. For instance, near-neutral-pH SCC in carbon steel pipelines is linked to the breakdown of tape coatings,

facilitating carbonate formation from CO<sub>2</sub> [45,209,240,241]. Conversely, elevated pH levels contribute to SCC failures associated with carbonate (CO<sub>3</sub><sup>2-</sup>), bicarbonate (HCO<sub>3</sub><sup>-</sup>), and alkaline conditions [44,51]. Additionally, dissolved CO<sub>2</sub> in water forms corrosive carbonic acid, impacting carbon steel [242]. HIC in carbon steels, exacerbated by acidic soil solutions or sulfate-reducing bacteria, also poses a risk [193,210,243]. Damaged pipeline coatings underlie extreme conditions, particularly with defective coatings compromising cathodic protection, compounded by mechanical damage during construction [144,244].

Effective control of tensile stress is critical in preventing SCC initiation and propagation in susceptible materials. This management involves proper heat treatment, cold expansion techniques, and control of pressure fluctuations. Mitigating SCC in vulnerable materials requires a comprehensive assessment of external and internal environmental factors. Key considerations include removing corrosive species from transported fluids and preventing stagnant pipeline water accumulation. Soils with elevated carbonate levels are particularly prone to SCC and require appropriate preventive measures [5].

Variations in the physicochemical properties of soils, such as water content, oxygen availability, air–solid interfaces, and seasonal fluctuations in specific geographical regions, create highly corrosive environments [245]. The corrosion behavior of carbon steel surfaces is influenced by abrupt environmental changes, such as seasonal variations and altered soil properties, and the effectiveness of cathodic protection systems [5]. Therefore, electrochemical interactions at the soil–pipeline steel interface, mechanical property fluctuations, and ion concentration variations within the soil are anticipated. In geological and scientific investigations, natural soil samples are typically collected approximately 1.2 m deep along the pipeline right-of-way (ROW) to assess significant external corrosion damage [246]. Romanoff's study examined the impact of external corrosion on various metals in different U.S. soils, while Cole and Marney emphasized the influences of electrochemical reactions, oxide formation, and factors such as temperature, void spaces, pH, salinity, and moisture on corrosion processes in soil environments [5,247].

In practical applications, preventing I-SCC in carbon steel pipelines often involves deploying field separators to remove corrosive elements such as gases, hydrocarbons, high-salinity water (e.g., oilfield-produced water), solids, metals, and sediments from sludge. This process includes desalting and dehydration procedures [248]. Fluid composition factors like dissolved oxygen, organic acids, water content, gas and liquid densities, viscosity, microorganism presence, suspended solids, field debris, CO<sub>2</sub> levels, and H<sub>2</sub>S content influence I-SCC occurrence. Additionally, pipeline operational conditions such as inner wall and fluid temperatures, gas and liquid flow rates, erosion and deposition rates, heat transfer characteristics, surface shear stress, flow turbulence intensity, and pressure dynamics during hydrocarbon production, gathering, storage, and transportation stages all play critical roles. Fouling propensity significantly impacts pressure dynamics throughout these stages, affecting operational costs and product yields.

Therefore, implementing corrosion prevention measures is imperative. These measures include chemical treatments such as corrosion inhibitor programs, direct methods like corrosion coupons and failure frequency analysis, and inline inspection using UT, RT, and smart pigs. Indirect techniques encompass monitoring water content, pressure, temperature, hydrogen flux, gas composition, solid and liquid analysis, inhibitor presence, and microbiological factors [248]. In the context of oil pipelines, inline cleaning systems employing pig tools are commonly used to address fouling tendencies, while gas pipelines employ spheres for similar purposes [5].

## 8. Conclusions

This comprehensive review examines the critical issue of SCC in the oil and gas industry, focusing on CI-SCC. The study highlights the intricate interplay between environmental conditions and material properties contributing to SCC, emphasizing the heightened risk under specific operational scenarios. The findings indicate that SCC can initiate at relatively low temperatures, around 20 °C, with rapid crack propagation

observed as temperatures exceed 60 °C. The presence of chloride ions is particularly detrimental, with concentrations above 100 ppm significantly increasing susceptibility to SCC. For instance, a 100 ppm increase in chloride concentration can elevate crack growth rates by approximately 40%, underscoring the critical role of environmental control in managing SCC risks. Mitigation strategies, including corrosion-resistant alloys and protective coatings, have proven effective in reducing SCC incidence by up to 50% under controlled experimental conditions. Cathodic protection and targeted corrosion inhibitors further contribute to risk reduction, decreasing SCC occurrences by about 30%. Advanced monitoring techniques play a vital role in early detection and preventative maintenance schedules. The study also highlights the significance of environmental pH and temperature in influencing SCC behavior. Environments with a pH lower than 4 were found to double the rate of SCC compared to those at neutral pH. Additionally, temperature variations between 50 °C and 100 °C in high-chloride environments (over 200 ppm) were linked to a 60% increase in SCC frequency. This review emphasizes the importance of a comprehensive approach to SCC management, involving strategic material selection, continuous environmental monitoring, and proactive maintenance. By adopting this integrated approach, industry stakeholders can significantly enhance the resilience of their infrastructure, reducing economic losses and environmental hazards. The findings provide compelling evidence that proactive SCC management is essential for maintaining the structural integrity and operational reliability of assets in the oil and gas sector, thereby safeguarding against significant economic losses and environmental hazards.

**Author Contributions:** Conceptualization, M.V., P.K., J.K. and Z.G.; methodology, M.V. and P.K.; software, M.V. and P.K.; validation, M.V., P.K., J.K. and Z.G.; formal analysis, P.K. and J.K.; investigation, M.V. and P.K.; resources, M.V. and P.K.; data curation, P.K. and J.K.; writing—original draft preparation, M.V.; writing—review and editing, M.V., P.K. and J.K.; visualization, M.V.; supervision, M.V. and P.K.; project administration, P.K. and J.K.; funding acquisition, P.K. All authors have read and agreed to the published version of the manuscript.

**Funding:** This publication is a result of the project “Modern trends in the processing of energy raw materials” (8232201) carried out at ORLEN UniCRE a.s.

**Institutional Review Board Statement:** Not applicable.

**Informed Consent Statement:** Not applicable.

**Data Availability Statement:** No new data were created or analyzed in this study.

**Conflicts of Interest:** Authors Mohammadtaghi Vakili, Petr Koutník, Jan Kohout and Zahra Gholami are employed by ORLEN UniCRE a.s. The authors of the paper declare that the research was conducted in the absence of any commercial or financial relationships that could be construed as a potential conflict of interest. The affiliated company was not involved in the study design, collection, analysis, interpretation of data, the writing of this article or the decision to submit it for publication.

## References

1. Byun, T.S.; Garrison, B.E.; McAlister, M.R.; Chen, X.; Gussev, M.N.; Lach, T.G.; Le Coq, A.; Linton, K.; Joslin, C.B.; Carver, J.K.; et al. Mechanical behavior of additively manufactured and wrought 316L stainless steels before and after neutron irradiation. *J. Nucl. Mater.* **2021**, *548*, 152849. [[CrossRef](#)]
2. Martin, M.L.; Dadfarnia, M.; Nagao, A.; Wang, S.; Sofronis, P. Enumeration of the hydrogen-enhanced localized plasticity mechanism for hydrogen embrittlement in structural materials. *Acta Mater.* **2018**, *165*, 734–750. [[CrossRef](#)]
3. Parikin, P.; Dani, M.; Dimiyati, A.; Purnamasari, N.D.; Sugeng, B.; Panitra, M.; Insani, A.; Priyanto, T.; Mustofa, S.; Syahbuddin, S.; et al. Effect of Arc Plasma Sintering on the Structural and Microstructural Properties of Fe-Cr-Ni Austenitic Stainless Steels. *Makara J. Technol.* **2021**, *25*, 71–78. [[CrossRef](#)]
4. Nuthalapati, S.; Kee, K.; Pedapati, S.R.; Jumbri, K. A review of chloride induced stress corrosion cracking characterization in austenitic stainless steels using acoustic emission technique. *Nucl. Eng. Technol.* **2024**, *56*, 688–706. [[CrossRef](#)]
5. Quej-Ake, L.M.; Rivera-Olvera, J.N.; Domínguez-Aguilar, Y.d.R.; Avelino-Jiménez, I.A.; Garibay-Febles, V.; Zapata-Peñasco, I. Analysis of the Physicochemical, Mechanical, and Electrochemical Parameters and Their Impact on the Internal and External SCC of Carbon Steel Pipelines. *Materials* **2020**, *13*, 5771. [[CrossRef](#)] [[PubMed](#)]

6. Muraleedharan, P. 6—Metallurgical Influences on Stress Corrosion Cracking. In *Corrosion of Austenitic Stainless Steels*; Khatak, H.S., Raj, B., Eds.; Woodhead Publishing: Cambridgeshire, UK, 2002; pp. 139–165.
7. Serafim, F.M.; Alabi, W.O.; Oguocha, I.N.; Odeshi, A.G.; Evitts, R.; Gerspacher, R.J.; Ohaeri, E.G. Stress corrosion cracking behavior of selected stainless steels in saturated potash brine solution at different temperatures. *Corros. Sci.* **2020**, *178*, 109025. [[CrossRef](#)]
8. Alireza, K. Stress Corrosion Cracking Behavior of Materials. In *Engineering Failure Analysis*; Kary, T., Ed.; IntechOpen: Rijeka, Croatia, 2020; Chapter 3.
9. Mohtadi-Bonab, M.A. Effects of Different Parameters on Initiation and Propagation of Stress Corrosion Cracks in Pipeline Steels: A Review. *Metals* **2019**, *9*, 590. [[CrossRef](#)]
10. Galvão, T.L.P.; Novell-Leruth, G.; Kuznetsova, A.; Tedim, J.; Gomes, J.R.B. Elucidating Structure–Property Relationships in Aluminum Alloy Corrosion Inhibitors by Machine Learning. *J. Phys. Chem. C* **2020**, *124*, 5624–5635. [[CrossRef](#)]
11. Yan, X.; Rong, H.; Fan, W.; Yang, J.; Zhou, C.; Li, S.; Zhao, X. Effect and simulation of tensile stress on corrosion behavior of 7050 aluminum alloy in a simulated harsh marine environment. *Eng. Fail. Anal.* **2024**, *156*, 107843. [[CrossRef](#)]
12. Khodamorad, S.H.; Alinezhad, N.; Fatmehsari, D.H.; Ghahtan, K. Stress corrosion cracking in Type.316 plates of a heat exchanger. *Case Stud. Eng. Fail. Anal.* **2016**, *5*, 59–66. [[CrossRef](#)]
13. Zhang, W.; Dunbar, L.; Tice, D. Monitoring of stress corrosion cracking of sensitised 304H stainless steel in nuclear applications by electrochemical methods and acoustic emission. *Energy Mater.* **2008**, *3*, 59–71. [[CrossRef](#)]
14. Beavers, J.; Bubenik, T.A. 12—Stress corrosion cracking. In *Trends in Oil and Gas Corrosion Research and Technologies*; El-Sherik, A.M., Ed.; Woodhead Publishing: Boston, MA, USA, 2017; pp. 295–314.
15. Manfredi, C.; Otegui, J. Failures by SCC in buried pipelines. *Eng. Fail. Anal.* **2002**, *9*, 495–509. [[CrossRef](#)]
16. Fang, B.Y.; Atrens, A.; Wang, J.Q.; Han, E.H.; Zhu, Z.Y.; Ke, W. Review of stress corrosion cracking of pipeline steels in “low” and “high” pH solutions. *J. Mater. Sci.* **2003**, *38*, 127–132. [[CrossRef](#)]
17. Shehata, M.T.; Elboujdaini, M.; Revie, R.W. *Initiation of Stress Corrosion Cracking and Hydrogen-Induced Cracking in Oil and Gas Line-Pipe Steels*; Springer: Dordrecht, The Netherlands, 2008.
18. Sen, R.R.F.M. Characteristics, causes, and management of circumferential stress-corrosion cracking. In Proceedings of the 10th International Pipeline Conference IPC2014-33059, Calgary, AB, Canada, 29 September–3 October 2014.
19. Yahi, S.; Bensmaili, A.; Haddad, A.; Benmohamed, M. Experimental Approach to Monitoring the Degradation Status of Pipelines Transporting Hydrocarbons. *Eur. J. Eng. Sci. Technol.* **2021**, *4*, 34–44. [[CrossRef](#)]
20. Xie, M.; Tian, Z. A review on pipeline integrity management utilizing in-line inspection data. *Eng. Fail. Anal.* **2018**, *92*, 222–239. [[CrossRef](#)]
21. Khasanova, A. Corrosion cracking under main pipelines stress. *J. Physics Conf. Ser.* **2022**, *2176*, 012051. [[CrossRef](#)]
22. Hussain, M.; Zhang, T.; Chaudhry, M.; Jamil, I.; Kausar, S.; Hussain, I. Review of Prediction of Stress Corrosion Cracking in Gas Pipelines Using Machine Learning. *Machines* **2024**, *12*, 42. [[CrossRef](#)]
23. Vanboven, G.; Chen, W.; Rogge, R. The role of residual stress in neutral pH stress corrosion cracking of pipeline steels. Part I: Pitting and cracking occurrence. *Acta Mater.* **2007**, *55*, 29–42. [[CrossRef](#)]
24. Vakili, M.; Koutník, P.; Kohout, J. Corrosion by Polythionic Acid in the Oil and Gas Sector: A Brief Overview. *Materials* **2023**, *16*, 7043. [[CrossRef](#)] [[PubMed](#)]
25. Vakili, M.; Koutník, P.; Kohout, J. Addressing Hydrogen Sulfide Corrosion in Oil and Gas Industries: A Sustainable Perspective. *Sustainability* **2024**, *16*, 1661. [[CrossRef](#)]
26. Withers, P.J.; Bhadeshia, H. Residual stress. Part 1—measurement techniques. *Mater. Sci. Technol.* **2001**, *17*, 355–365. [[CrossRef](#)]
27. Freitas, V.L.d.A.; de Albuquerque, V.H.C.; Silva, E.d.M.; Silva, A.A.; Tavares, J.M.R. Nondestructive characterization of microstructures and determination of elastic properties in plain carbon steel using ultrasonic measurements. *Mater. Sci. Eng. A* **2010**, *527*, 4431–4437. [[CrossRef](#)]
28. Beavers, J.A.; Johnson, J.T.; Sutherby, R.L. Materials factors influencing the initiation of near-neutral pH SCC on underground pipelines. In *International Pipeline Conference*; American Society of Mechanical Engineers: New York, NY, USA, 2000.
29. Chen, W.; Vanboven, G.; Rogge, R. The role of residual stress in neutral pH stress corrosion cracking of pipeline steels—Part II: Crack dormancy. *Acta Mater.* **2007**, *55*, 43–53. [[CrossRef](#)]
30. Khalifeh, A.; Banaraki, A.D.; Daneshmanesh, H.; Paydar, M. Stress corrosion cracking of a circulation water heater tubesheet. *Eng. Fail. Anal.* **2017**, *78*, 55–66. [[CrossRef](#)]
31. Ghosh, S.; Rana, V.P.S.; Kain, V.; Mittal, V.; Baveja, S. Role of residual stresses induced by industrial fabrication on stress corrosion cracking susceptibility of austenitic stainless steel. *Mater. Des.* **2011**, *32*, 3823–3831. [[CrossRef](#)]
32. Kannan, M.B.; Shukla, P. Stress corrosion cracking (SCC) of copper and copper-based alloys. In *Stress Corrosion Cracking*; Elsevier: Amsterdam, The Netherlands, 2011; pp. 409–426.

33. Alyousif, O.M.; Nishimura, R. The Effect of Applied Stress on Environment-Induced Cracking of Aluminum Alloy 5052-H3 in 0.5 M NaCl Solution. *Int. J. Corros.* **2012**, *2012*, 894875. [[CrossRef](#)]
34. Kan, W.; Pan, H. Failure analysis of a stainless steel hydrotreating reactor. *Eng. Fail. Anal.* **2011**, *18*, 110–116. [[CrossRef](#)]
35. Alireza, K. Stress Corrosion Cracking Damages. In *Failure Analysis*; Huang, Z.-M., Hemeda, S., Eds.; IntechOpen: Rijeka, Croatia, 2019; Chapter 3.
36. Fairweather, N.; Platts, N.; Tice, D. Stress-corrosion crack initiation of type 304 stainless steel in atmospheric environments containing chloride: Influence of surface condition, relative humidity, temperature and thermal sensitization. In *NACE Corrosion*; NACE: New Orleans, LA, USA, 2008.
37. Hayashibara, H.; Mayuzumi, M.; Mizutani, Y.; Tani, J.I. Effects of temperature and humidity on atmospheric stress corrosion cracking of 304 stainless steel. In *NACE Corrosion*; NACE: Houston, TX, USA, 2008.
38. Singh, P.M.; Ige, O.; Mahmood, J. Stress corrosion cracking of 304L stainless steel in sodium sulfide containing caustic solutions. *J. Corros. Sci. Eng.* **2003**, *59*, 843–850. [[CrossRef](#)]
39. Rodríguez, J.J.; Hernández, F.S.; González, J.E. The effect of environmental and meteorological variables on atmospheric corrosion of carbon steel, copper, zinc and aluminium in a limited geographic zone with different types of environment. *Corros. Sci.* **2003**, *45*, 799–815. [[CrossRef](#)]
40. Iakovleva, E.; Mäkilä, E.; Salonen, J.; Sitarz, M.; Sillanpää, M. Industrial products and wastes as adsorbents for sulphate and chloride removal from synthetic alkaline solution and mine process water. *Chem. Eng. J.* **2015**, *259*, 364–371. [[CrossRef](#)]
41. Liu, Y.; Wang, J.; Liu, L.; Wang, F. Study of the failure mechanism of an epoxy coating system under high hydrostatic pressure. *Corros. Sci.* **2013**, *74*, 59–70. [[CrossRef](#)]
42. Arafin, M.; Szpunar, J. Effect of bainitic microstructure on the susceptibility of pipeline steels to hydrogen induced cracking. *Mater. Sci. Eng. A* **2011**, *528*, 4927–4940. [[CrossRef](#)]
43. Mustapha, A.; Charles, E.; Hardie, D. Evaluation of environment-assisted cracking susceptibility of a grade X100 pipeline steel. *Corros. Sci.* **2012**, *54*, 5–9. [[CrossRef](#)]
44. Oskuie, A.; Shahrabi, T.; Shahriari, A.; Saebnoori, E. Electrochemical impedance spectroscopy analysis of X70 pipeline steel stress corrosion cracking in high pH carbonate solution. *Corros. Sci.* **2012**, *61*, 111–122. [[CrossRef](#)]
45. Maocheng, Y.; Jin, X.; Libao, Y.; Tangqing, W.; Cheng, S.; Wei, K. EIS analysis on stress corrosion initiation of pipeline steel under disbonded coating in near-neutral pH simulated soil electrolyte. *Corros. Sci.* **2016**, *110*, 23–34. [[CrossRef](#)]
46. Kang, Y.; Chen, W.; Kania, R.; Van Boven, G.; Worthingham, R. Simulation of crack growth during hydrostatic testing of pipeline steel in near-neutral pH environment. *Corros. Sci.* **2011**, *53*, 968–975. [[CrossRef](#)]
47. Marshakov, A.; Ignatenko, V.; Bogdanov, R.; Arabey, A. Effect of electrolyte composition on crack growth rate in pipeline steel. *Corros. Sci.* **2014**, *83*, 209–216. [[CrossRef](#)]
48. Mohtadi-Bonab, M.A.; Eskandari, M.; Karimdadashi, R.; Szpunar, J.A. Effect of different microstructural parameters on hydrogen induced cracking in an API X70 pipeline steel. *Met. Mater. Int.* **2017**, *23*, 726–735. [[CrossRef](#)]
49. Mohtadi-Bonab, M.; Eskandari, M.; Szpunar, J. Role of cold rolled followed by annealing on improvement of hydrogen induced cracking resistance in pipeline steel. *Eng. Fail. Anal.* **2018**, *91*, 172–181. [[CrossRef](#)]
50. Fan, Z.; Hu, X.; Liu, J.; Li, H.; Fu, J. Stress corrosion cracking of L360NS pipeline steel in sulfur environment. *Petroleum* **2017**, *3*, 377–383. [[CrossRef](#)]
51. Wang, J.Q.; Atrens, A. SCC initiation for X65 pipeline steel in the “high” pH carbonate/bicarbonate solution. *Corros. Sci.* **2003**, *45*, 2199–2217. [[CrossRef](#)]
52. Chen, W. 30—Modeling and prediction of stress corrosion cracking of pipeline steels. In *Trends in Oil and Gas Corrosion Research and Technologies*; El-Sherik, A.M., Ed.; Woodhead Publishing: Boston, MA, USA, 2017; pp. 707–748.
53. Krivonosova, E.A. A Review of Stress Corrosion Cracking of Welded Stainless Steels. *OALib* **2018**, *5*, 1. [[CrossRef](#)]
54. Adair, S.T.; Attwood, P.A. In-service stress corrosion cracking of AISI 316L stainless steel in an H<sub>2</sub>S environment. *Corros. Eng. Sci. Technol.* **2014**, *49*, 396–400. [[CrossRef](#)]
55. Yazovskikh, V.M.; Krivonosova, E.K. Structure Formation and Properties of Corrosion-Resistant Steel with Treatment by a Highly Concentrated Energy Source. *Metallurgist* **2016**, *59*, 912–916. [[CrossRef](#)]
56. Krivonosova, E.A.; Sinkina, E.A.; Gorchakov, A.I. Effect of the type of electrode coating on the corrosion resistance of weld metal in 08Cr18Ni10Ti steel. *Weld. Int.* **2013**, *27*, 489–492. [[CrossRef](#)]
57. Ghosh, G.; Rostron, P.; Garg, R.; Panday, A. Hydrogen induced cracking of pipeline and pressure vessel steels: A review. *Eng. Fract. Mech.* **2018**, *199*, 609–618. [[CrossRef](#)]
58. Truman, J.E. Stress-corrosion cracking of martensitic and ferritic stainless steels. *Int. Met. Rev.* **1981**, *26*, 301–349. [[CrossRef](#)]
59. Mohtadi-Bonab, M.; Szpunar, J.; Basu, R.; Eskandari, M. The mechanism of failure by hydrogen induced cracking in an acidic environment for API 5L X70 pipeline steel. *Int. J. Hydrogen Energy* **2015**, *40*, 1096–1107. [[CrossRef](#)]

60. Mohtadi-Bonab, M.; Eskandari, M. A focus on different factors affecting hydrogen induced cracking in oil and natural gas pipeline steel. *Eng. Fail. Anal.* **2017**, *79*, 351–360. [[CrossRef](#)]
61. Mohtadi-Bonab, M.A.; Eskandari, M.; Ghaednia, H.; Das, S. Effect of Microstructural Parameters on Fatigue Crack Propagation in an API X65 Pipeline Steel. *J. Mater. Eng. Perform.* **2016**, *25*, 4933–4940. [[CrossRef](#)]
62. Mohtadi-Bonab, M.; Eskandari, M.; Sanayei, M.; Das, S. Microstructural aspects of intergranular and transgranular crack propagation in an API X65 steel pipeline related to fatigue failure. *Eng. Fail. Anal.* **2018**, *94*, 214–225. [[CrossRef](#)]
63. Shi, X.; Yan, W.; Wang, W.; Shan, Y.; Yang, K. Novel Cu-bearing high-strength pipeline steels with excellent resistance to hydrogen-induced cracking. *Mater. Des.* **2016**, *92*, 300–305. [[CrossRef](#)]
64. Baba, K.; Mizuno, D.; Yasuda, K.; Nakamichi, H.; Ishikawa, N. Effect of Cu Addition in Pipeline Steels on Prevention of Hydrogen Permeation in Mildly Sour Environments. *Corrosion* **2016**, *72*, 1107–1115. [[CrossRef](#)] [[PubMed](#)]
65. Zhu, M.; Du, C.; Li, X.; Liu, Z.; Wang, S.; Zhao, T.; Jia, J. Effect of Strength and Microstructure on Stress Corrosion Cracking Behavior and Mechanism of X80 Pipeline Steel in High pH Carbonate/Bicarbonate Solution. *J. Mater. Eng. Perform.* **2014**, *23*, 1358–1365. [[CrossRef](#)]
66. González, J.; Gutiérrez-Solana, F.; Varona, J.M. The effects of microstructure, strength level, and crack propagation mode on stress corrosion cracking behavior of 4135 steel. *Met. Mater. Trans. A* **1996**, *27*, 281–290. [[CrossRef](#)]
67. Mohtadi-Bonab, M.; Eskandari, M.; Szpunar, J. Effect of arisen dislocation density and texture components during cold rolling and annealing treatments on hydrogen induced cracking susceptibility in pipeline steel. *J. Mater. Res.* **2016**, *31*, 3390–3400. [[CrossRef](#)]
68. Fang, B.; Wang, J.; Xiao, S.; Han, E.-H.; Zhu, Z.; Ke, W. Stress corrosion cracking of X-70 pipeline steels by eletropulsing treatment in near-neutral pH solution. *J. Mater. Sci.* **2005**, *40*, 6545–6552. [[CrossRef](#)]
69. Lu, B.T.; Luo, J.L. Crack Initiation and Early Propagation of X70 Steel in Simulated Near-Neutral pH Groundwater. *Corrosion* **2006**, *62*, 723–731. [[CrossRef](#)]
70. Contreras, A.; Hernández, S.; Orozco-Cruz, R.; Galvan-Martínez, R. Mechanical and environmental effects on stress corrosion cracking of low carbon pipeline steel in a soil solution. *Mater. Des.* **2012**, *35*, 281–289. [[CrossRef](#)]
71. Hänninen, H.E. 6.01—Stress Corrosion Cracking. In *Comprehensive Structural Integrity*; Milne, I., Ritchie, R.O., Karihaloo, B., Eds.; Pergamon: Oxford, UK, 2003; pp. 1–29.
72. El-Amoush, A.S.; Zamil, A.; Jaber, D.; Ismail, N. Stress corrosion cracking of the pre-immersed tin brass heat exchanger tube in an ammoniacal solution. *Mater. Des.* **2014**, *56*, 842–847. [[CrossRef](#)]
73. Popović, M.; Romhanji, E. Stress corrosion cracking susceptibility of Al–Mg alloy sheet with high Mg content. *J. Mater. Process. Technol.* **2002**, *125*, 275–280. [[CrossRef](#)]
74. Jones, R.H.; Baer, D.R.; Danielson, M.J.; Vetrano, J.S. Role of Mg in the stress corrosion cracking of an Al–Mg alloy. *Met. Mater. Trans. A* **2001**, *32*, 1699–1711. [[CrossRef](#)]
75. Rao, A.U.; Vasu, V.; Govindaraju, M.; Srinadh, K.S. Stress corrosion cracking behaviour of 7xxx aluminum alloys: A literature review. *Trans. Nonferrous Met. Soc. China* **2016**, *26*, 1447–1471. [[CrossRef](#)]
76. Pilchak, A.; Young, A.; Williams, J. Stress corrosion cracking facet crystallography of Ti–8Al–1Mo–1V. *Corros. Sci.* **2010**, *52*, 3287–3296. [[CrossRef](#)]
77. Parnian, N. Failure analysis of austenitic stainless steel tubes in a gas fired steam heater. *Mater. Des.* **2012**, *36*, 788–795. [[CrossRef](#)]
78. Pal, S.; Ibrahim, R.N.; Raman, R. S. Studying the effect of sensitization on the threshold stress intensity and crack growth for chloride stress corrosion cracking of austenitic stainless steel using circumferential notch tensile technique. *Eng. Fract. Mech.* **2012**, *82*, 158–171. [[CrossRef](#)]
79. Singh, R.; Sachan, D.; Verma, R.; Goel, S.; Jayaganthan, R.; Kumar, A. Mechanical behavior of 304 Austenitic stainless steel processed by cryogenic rolling. *Mater. Today: Proc.* **2018**, *5*, 16880–16886. [[CrossRef](#)]
80. Kappes, M.A. Localized corrosion and stress corrosion cracking of stainless steels in halides other than chlorides solutions: A review. *Corros. Rev.* **2020**, *38*, 1–24. [[CrossRef](#)]
81. Knyazeva, M.; Pohl, M. Duplex Steels. Part II: Carbides and Nitrides. *Met. Microstruct. Anal.* **2013**, *2*, 343–351. [[CrossRef](#)]
82. Rodríguez, M.A. Corrosion control of nuclear steam generators under normal operation and plant-outage conditions: A review. *Corros. Rev.* **2020**, *38*, 195–230. [[CrossRef](#)]
83. Féron, D. 2—Overview of nuclear materials and nuclear corrosion science and engineering. In *Nuclear Corrosion Science and Engineering*; Féron, D., Ed.; Woodhead Publishing: Cambridge, UK, 2012; pp. 31–56.
84. Shiwa, M.; Masuda, H.; Yamawaki, H.; Ito, K.; Enoki, M. Acoustic emission monitoring of micro cell corrosion testing in type 304 stainless steels. *Strength Fract. Complex.* **2011**, *7*, 71–78. [[CrossRef](#)]
85. Mackey, E.D.; Seacord, T.F. Guidelines for Using Stainless Steel in the Water and Desalination Industries. *J.-Am. Water Work. Assoc.* **2017**, *109*, E158–E169. [[CrossRef](#)]
86. Yoon, H.; Ha, H.-Y.; Lee, T.-H.; Kim, S.-D.; Jang, J.H.; Moon, J.; Kang, N. Pitting Corrosion Resistance and Repassivation Behavior of C-Bearing Duplex Stainless Steel. *Metals* **2019**, *9*, 930. [[CrossRef](#)]

87. Maziasz, P.J.; Busby, J.T. 2.09—Properties of Austenitic Steels for Nuclear Reactor Applications. In *Comprehensive Nuclear Materials*; Konings, R.J.M., Ed.; Elsevier: Oxford, UK, 2012; pp. 267–283.
88. Pal, S.; Bhadauria, S.S.; Kumar, P. Pitting Corrosion Behavior of F304 Stainless Steel Under the Exposure of Ferric Chloride Solution. *J. Bio-Tribo-Corros.* **2019**, *5*, 91. [[CrossRef](#)]
89. Jung, R.-H.; Tsuchiya, H.; Fujimoto, S. XPS characterization of passive films formed on Type 304 stainless steel in humid atmosphere. *Corros. Sci.* **2012**, *58*, 62–68. [[CrossRef](#)]
90. Sastry, K.Y.; Narayanan, R.; Shamantha, C.R.; Sundaresan, S.; Seshadri, S.K.; Radhakrishnan, V.M.; Iyer, K.J.L.; Sundararajan, S. Stress corrosion cracking of maraging steel weldments. *Mater. Sci. Technol.* **2003**, *19*, 375–381. [[CrossRef](#)]
91. Cui, C.; Ma, R.; Martínez-Pañeda, E. A phase field formulation for dissolution-driven stress corrosion cracking. *J. Mech. Phys. Solids* **2021**, *147*, 104254. [[CrossRef](#)]
92. Ahmad, Z. Chapter 4—Types of corrosion: Materials and Environments. In *Principles of Corrosion Engineering and Corrosion Control*; Ahmad, Z., Ed.; Butterworth-Heinemann: Oxford, UK, 2006; pp. 120–270.
93. Nguyen, T.-T.; Bolivar, J.; Réthoré, J.; Baietto, M.-C.; Fregonese, M. A phase field method for modeling stress corrosion crack propagation in a nickel base alloy. *Int. J. Solids Struct.* **2017**, *112*, 65–82. [[CrossRef](#)]
94. Jawan, H.A. Some Thoughts on Stress Corrosion Cracking of (7xxx) Aluminum Alloys. *Int. J. Mater. Sci. Eng.* **2019**, *7*, 40–51. [[CrossRef](#)]
95. Li, Z.; Lu, Y.; Wang, X. Modeling of stress corrosion cracking growth rates for key structural materials of nuclear power plant. *J. Mater. Sci.* **2020**, *55*, 439–463. [[CrossRef](#)]
96. Alkateb, M.; Tadić, S.; Sedmak, A.; Ivanović, I.; Marković, S. Crack Growth Rate Analysis of Stress Corrosion Cracking. *Teh. Vjesn.-Tech. Gaz.* **2021**, *28*, 240–247. [[CrossRef](#)]
97. Lynch, S.P. 1—Mechanistic and fractographic aspects of stress-corrosion cracking (SCC). In *Stress Corrosion Cracking*; Raja, V.S., Shoji, T., Eds.; Woodhead Publishing: Cambridge, UK, 2011; pp. 3–89.
98. Zaferani, S.H.; Miresmaeili, R.; Pourcharmi, M.K. Mechanistic models for environmentally-assisted cracking in sour service. *Eng. Fail. Anal.* **2017**, *79*, 672–703. [[CrossRef](#)]
99. Pereira, H.B.; Panossian, Z.; Baptista, I.P.; Azevedo, C.R.d.F. Investigation of Stress Corrosion Cracking of Austenitic, Duplex and Super Duplex Stainless Steels under Drop Evaporation Test using Synthetic Seawater. *Mater. Res.* **2019**, *22*, e20180211. [[CrossRef](#)]
100. Galvele, J. Surface mobility mechanism of stress-corrosion cracking. *Corros. Sci.* **1993**, *35*, 419–434. [[CrossRef](#)]
101. Chatterjee, U.K. Stress corrosion cracking and component failure: Causes and prevention. *Sadhana* **1995**, *20*, 165–184. [[CrossRef](#)]
102. Pal, S.; Bhadauria, S.S.; Kumar, P. Studies on Stress Corrosion Cracking of F304 Stainless Steel in Boiling Magnesium Chloride Solution. *J. Bio-Tribo-Corros.* **2021**, *7*, 62. [[CrossRef](#)]
103. Almubarak, A.; Abuhaimed, W.; Almazrouee, A. Corrosion Behavior of the Stressed Sensitized Austenitic Stainless Steels of High Nitrogen Content in Seawater. *Int. J. Electrochem.* **2013**, *2013*, 970835. [[CrossRef](#)]
104. Wu, K.; Briffod, F.; Ito, K.; Shinozaki, I.; Chivavibul, P.; Enoki, M. In-Situ Observation and Acoustic Emission Monitoring of the Initiation-to-Propagation Transition of Stress Corrosion Cracking in SUS420J2 Stainless Steel. *Mater. Trans.* **2019**, *60*, 2151–2159. [[CrossRef](#)]
105. Song, M.; Wang, M.; Lou, X.; Rebak, R.B.; Was, G.S. Radiation damage and irradiation-assisted stress corrosion cracking of additively manufactured 316L stainless steels. *J. Nucl. Mater.* **2019**, *513*, 33–44. [[CrossRef](#)]
106. Zinkle, S.J.; Was, G.S. Materials challenges in nuclear energy. *Acta Mater.* **2013**, *61*, 735–758. [[CrossRef](#)]
107. Mayuzumi, M.; Arai, T.; Hide, K. Chloride Induced Stress Corrosion Cracking of Type 304 and 304L Stainless Steels in Air. *Zairyo-Kankyo* **2003**, *52*, 166–170. [[CrossRef](#)]
108. Xie, X.; Ning, D.; Chen, B.; Lu, S.; Sun, J. Stress corrosion cracking behavior of cold-drawn 316 austenitic stainless steels in simulated PWR environment. *Corros. Sci.* **2016**, *112*, 576–584. [[CrossRef](#)]
109. Yeom, H.; Dabney, T.; Pocquette, N.; Ross, K.; Pfefferkorn, F.E.; Sridharan, K. Cold spray deposition of 304L stainless steel to mitigate chloride-induced stress corrosion cracking in canisters for used nuclear fuel storage. *J. Nucl. Mater.* **2020**, *538*, 152254. [[CrossRef](#)]
110. Roffey, P.; Davies, E. The generation of corrosion under insulation and stress corrosion cracking due to sulphide stress cracking in an austenitic stainless steel hydrocarbon gas pipeline. *Eng. Fail. Anal.* **2014**, *44*, 148–157. [[CrossRef](#)]
111. Shoji, T.; Lu, Z.; Peng, Q. Factors affecting stress corrosion cracking (SCC) and fundamental mechanistic understanding of stainless steels. In *Stress Corrosion Cracking*; Elsevier: Amsterdam, The Netherlands, 2011; pp. 245–272.
112. Caines, S.; Khan, F.; Shirokoff, J. Analysis of pitting corrosion on steel under insulation in marine environments. *J. Loss Prev. Process. Ind.* **2013**, *26*, 1466–1483. [[CrossRef](#)]
113. Al-Moubaraki, A.H.; Obot, I.B. Corrosion challenges in petroleum refinery operations: Sources, mechanisms, mitigation, and future outlook. *J. Saudi Chem. Soc.* **2021**, *25*, 101370. [[CrossRef](#)]
114. Hao, W.; Liu, Z.; Wu, W.; Li, X.; Du, C.; Zhang, D. Electrochemical characterization and stress corrosion cracking of E690 high strength steel in wet-dry cyclic marine environments. *Mater. Sci. Eng. A* **2018**, *710*, 318–328. [[CrossRef](#)]

115. Xie, Y.; Zhang, J. Chloride-induced stress corrosion cracking of used nuclear fuel welded stainless steel canisters: A review. *J. Nucl. Mater.* **2015**, *466*, 85–93. [[CrossRef](#)]
116. Mayuzumi, M.; Tani, J.; Arai, T. Chloride induced stress corrosion cracking of candidate canister materials for dry storage of spent fuel. *Nucl. Eng. Des.* **2008**, *238*, 1227–1232. [[CrossRef](#)]
117. Wataru, M.; Takeda, H.; Shirai, K.; Saegusa, T. Thermal hydraulic analysis compared with tests of full-scale concrete casks. *Nucl. Eng. Des.* **2008**, *238*, 1213–1219. [[CrossRef](#)]
118. Navidi, W.; Shayer, Z. An application of stochastic modeling to pitting of Spent Nuclear Fuel canisters. *Prog. Nucl. Energy* **2018**, *107*, 48–56. [[CrossRef](#)]
119. Newman, R.C. 2001 W.R. Whitney Award Lecture: Understanding the Corrosion of Stainless Steel. *Corrosion* **2001**, *57*, 1030–1041. [[CrossRef](#)]
120. Andresen, P.L. Effects of Temperature on Crack Growth Rate in Sensitized Type 304 Stainless Steel and Alloy 600. *Corrosion* **1993**, *49*, 714–725. [[CrossRef](#)]
121. Truman, J. The influence of chloride content, pH and temperature of test solution on the occurrence of stress corrosion cracking with austenitic stainless steel. *Corros. Sci.* **1977**, *17*, 737–746. [[CrossRef](#)]
122. Akpanyung, K.; Loto, R.; Fajobi, M. An overview of ammonium chloride (NH<sub>4</sub>Cl) corrosion in the refining unit. In *Journal of Physics: Conference Series*; IOP Publishing: Bristol, UK, 2019. [[CrossRef](#)]
123. Ashida, Y.; Daigo, Y.; Sugahara, K. An Industrial Perspective on Environmentally Assisted Cracking of Some Commercially Used Carbon Steels and Corrosion-Resistant Alloys. *Jom* **2017**, *69*, 1381–1388. [[CrossRef](#)]
124. Fujisawa, R.; Nishimura, K.; Nishida, T.; Sakaiharu, M.; Kurata, Y.; Watanabe, Y. Corrosion behavior of ni base alloys and 316 stainless steel in less oxidizing or reducing SCW containing HCl. *Corrosion* **2006**, *62*, 270–274. [[CrossRef](#)]
125. Ford, F.P.; Silverman, M. The Prediction of Stress Corrosion Cracking of Sensitized 304 Stainless Steel in 0.01M Na<sub>2</sub>SO<sub>4</sub> at 97 C. *Corrosion* **1980**, *36*, 558–565. [[CrossRef](#)]
126. Tani, J.-I.; Mayuzumi, M.; Hara, N. Stress corrosion cracking of stainless-steel canister for concrete cask storage of spent fuel. *J. Nucl. Mater.* **2008**, *379*, 42–47. [[CrossRef](#)]
127. Matsumoto, S.; Uchiya, G.; Ozawa, M.; Kobayashi, Y.; Shirato, K. Research Committee on Ruthenium and Technetium Chemistry in PUREX System, Organized by the Atomic Energy Society of Japan. *Radiochemistry* **2003**, *45*, 219–224. [[CrossRef](#)]
128. Turnbull, A.; Zhou, S. Impact of temperature excursion on stress corrosion cracking of stainless steels in chloride solution. *Corros. Sci.* **2008**, *50*, 913–917. [[CrossRef](#)]
129. Oldfield, J.W.; Todd, B. Room temperature stress corrosion cracking of stainless steels in indoor swimming pool atmospheres. *Br. Corros. J.* **1991**, *26*, 173–182. [[CrossRef](#)]
130. Baker, H.R.; Bloom, M.C.; Bolster, R.N.; Singleterry, C.R. Film and pH Effects in the Stress Corrosion Cracking of Type 304 Stainless Steel. *Corrosion* **2013**, *26*, 420–426. [[CrossRef](#)]
131. Korovin, Y.M.; Ulanovskii, I.B. Effect of Oxygen Concentration and pH on Electrode Potential of Stainless Steels and Operation of Microcouples. *Corrosion* **2013**, *22*, 16–20. [[CrossRef](#)]
132. Tani, J.-I.; Mayuzumi, M.; Hara, N. Initiation and Propagation of Stress Corrosion Cracking of Stainless Steel Canister for Concrete Cask Storage of Spent Nuclear Fuel. *Corrosion* **2009**, *65*, 187–194. [[CrossRef](#)]
133. Feliu, S.; Morcillo, M.; Feliu, S. The prediction of atmospheric corrosion from meteorological and pollution parameters—I. Annual corrosion. *Corros. Sci.* **1993**, *34*, 403–414. [[CrossRef](#)]
134. Kosaki, A. Evaluation method of corrosion lifetime of conventional stainless steel canister under oceanic air environment. *Nucl. Eng. Des.* **2008**, *238*, 1233–1240. [[CrossRef](#)]
135. Chen, P.C.-S.; Shinohara, T.; Tsujikawa, S. Applicability of the Competition Concept in Determining the Stress Corrosion Cracking Behavior of Austenitic Stainless Steels in Chloride Solutions. *Zair.-Kankyo/Corros. Eng.* **1997**, *46*, 313–320. [[CrossRef](#)]
136. Yu, H.; Na, E.; Chung, S. Assessment of stress corrosion cracking susceptibility by a small punch test. *Fatigue Fract. Eng. Mater. Struct.* **1999**, *22*, 889–896. [[CrossRef](#)]
137. Bruchhausen, M.; Altstadt, E.; Austin, T.; Dymacek, P.; Holmström, S.; Jeffs, S.; Lacalle, R.; Lancaster, R.; Matocha, K.; Petzova, J. European standard on small punch testing of metallic materials. In *Pressure Vessels and Piping Conference*; American Society of Mechanical Engineers: New York, NY, USA, 2017.
138. Salazar, M.; Espinosa-Medina, M.A.; Hernández, P.; Contreras, A. Evaluation of SCC susceptibility of supermartensitic stainless steel using slow strain rate tests. *Corros. Eng. Sci. Technol.* **2011**, *46*, 464–470. [[CrossRef](#)]
139. Contreras, A.; Quej-Aké, L.M.; Lizárraga, C.R.; Pérez, T. The Role of Calcareous Soils in SCC of X52 Pipeline Steel. *MRS Online Proc. Libr. (OPL)* **2015**, *1766*, 95–106. [[CrossRef](#)]
140. Velazquez, Z.; Guzman, E.; Espinosa-Medina, M.; Contreras, A. Stress Corrosion Cracking Behavior of X60 Pipe Steel in Soil Environment. *MRS Online Proc. Libr. (OPL)* **2009**, *1242*, S4-P131. [[CrossRef](#)]
141. Contreras, A.; Salazar, M.; Albitar, A.; Galván, R.; Vega, O. Assessment of stress corrosion cracking on pipeline steels weldments used in the petroleum industry by slow strain rate tests. In *Arc Welding*; Sudnik, W., Ed.; IntechOpen: Zagreb, Croatia, 2011; pp. 127–150.

142. Quej-Aké, L.M.; Galván-Martínez, R.; Contreras-Cuevas, A. Electrochemical and Tension Tests Behavior of API 5L X60 Pipeline Steel in a Simulated Soil Solution. *Mater. Sci. Forum* **2013**, *755*, 153–161. [[CrossRef](#)]
143. Cheng, Y.F. *Stress Corrosion Cracking of Pipelines*; John Wiley & Sons: Hoboken, NJ, USA, 2013.
144. Afanasyev, A.; Mel'nikov, A.A.; Konovalov, S.V.; Vaskov, M.I. The Analysis of the Influence of Various Factors on the Development of Stress Corrosion Defects in the Main Gas Pipeline Walls in the Conditions of the European Part of the Russian Federation. *Int. J. Corros.* **2018**, *2018*, 1258379. [[CrossRef](#)]
145. Kamachi Mudali, U.; Jayaraj, J.; Raman, R.K.S.; Raj, B. Corrosion: An Overview of Types, Mechanism, and Requisites of Evaluation. In *Non-Destructive Evaluation of Corrosion and Corrosion-Assisted Cracking*; Wiley: Hoboken, NJ, USA, 2019; pp. 56–74.
146. Silva, M.I.; Malitckii, E.; Santos, T.G.; Vilaça, P. Review of conventional and advanced non-destructive testing techniques for detection and characterization of small-scale defects. *Prog. Mater. Sci.* **2023**, *138*, 101155. [[CrossRef](#)]
147. Venkatraman, B.; Raj, B. Nondestructive Testing: An Overview of Techniques and Application for Quality Evaluation. In *Non-Destructive Evaluation of Corrosion and Corrosion-Assisted Cracking*; Wiley: Hoboken, NJ, USA, 2019; pp. 1–55.
148. Reddy, M.S.B.; Ponnamma, D.; Sadasivuni, K.K.; Aich, S.; Kailasa, S.; Parangusan, H.; Ibrahim, M.; Eldeib, S.; Shehata, O.; Ismail, M.; et al. Sensors in advancing the capabilities of corrosion detection: A review. *Sensors Actuators A Phys.* **2021**, *332*, 113086. [[CrossRef](#)]
149. Atamturktur, H.S.; Gilligan, C.R.; Salyards, K.A. Detection of internal defects in concrete members using global vibration characteristics. *ACI Mater. J.* **2013**, *110*, 529–538.
150. Yi, D.; Pei, C.; Liu, T.; Chen, Z. Inspection of cracks with focused angle beam laser ultrasonic wave. *Appl. Acoust.* **2019**, *145*, 1–6. [[CrossRef](#)]
151. Howard, R.; Cegla, F. Detectability of corrosion damage with circumferential guided waves in reflection and transmission. *NDT E Int.* **2017**, *91*, 108–119. [[CrossRef](#)]
152. Demo, J.; Rajamani, R. Corrosion Sensing. In *Corrosion Processes: Sensing, Monitoring, Data Analytics, Prevention/Protection, Diagnosis/Prognosis and Maintenance Strategies*; Vachtsevanos, G., Natarajan, K., Rajamani, R., Sandborn, P., Eds.; Springer International Publishing: Cham, Switzerland, 2020; pp. 83–104.
153. Megid, W.A.; Chainey, M.-A.; Lebrun, P.; Hay, D.R. Monitoring fatigue cracks on eyebars of steel bridges using acoustic emission: A case study. *Eng. Fract. Mech.* **2019**, *211*, 198–208. [[CrossRef](#)]
154. Delaunois, F.; Tshimombo, A.; Stanciu, V.; Vitry, V. Monitoring of chloride stress corrosion cracking of austenitic stainless steel: Identification of the phases of the corrosion process and use of a modified accelerated test. *Corros. Sci.* **2016**, *110*, 273–283. [[CrossRef](#)]
155. Mazille, H.; Rothea, R.; Tronel, C. An acoustic emission technique for monitoring pitting corrosion of austenitic stainless steels. *Corros. Sci.* **1995**, *37*, 1365–1375. [[CrossRef](#)]
156. Jones, R.H.; Friesel, M.A. Acoustic Emission During Pitting and Transgranular Crack Initiation in Type 304 Stainless Steel. *Corrosion* **1992**, *48*, 751–758. [[CrossRef](#)]
157. Kim, Y.; Fregonese, M.; Mazille, H.; Féron, D.; Santarini, G. Ability of acoustic emission technique for detection and monitoring of crevice corrosion on 304L austenitic stainless steel. *NDT E Int.* **2003**, *36*, 553–562. [[CrossRef](#)]
158. Shaikh, H.; Amirthalingam, R.; Anita, T.; Sivaibharasi, N.; Jaykumar, T.; Manohar, P.; Khatak, H. Evaluation of stress corrosion cracking phenomenon in an AISI type 316LN stainless steel using acoustic emission technique. *Corros. Sci.* **2007**, *49*, 740–765. [[CrossRef](#)]
159. Light, G. Nondestructive evaluation technologies for monitoring corrosion. In *Techniques for Corrosion Monitoring*; Elsevier: Amsterdam, The Netherlands, 2021; pp. 285–304.
160. Sophian, A.; Tian, G.; Fan, M. Pulsed Eddy Current Non-destructive Testing and Evaluation: A Review. *Chin. J. Mech. Eng.* **2017**, *30*, 500–514.
161. Kelidari, Y.; Kashafi, M.; Mirjalili, M.; Seyedi, M.; Krause, T.W. Eddy current technique as a nondestructive method for evaluating the degree of sensitization of 304 stainless steel. *Corros. Sci.* **2020**, *173*, 108742. [[CrossRef](#)]
162. Mardaninejad, R.; Safizadeh, M.S. Gas Pipeline Corrosion Mapping Through Coating Using Pulsed Eddy Current Technique. *Russ. J. Nondestruct. Test.* **2019**, *55*, 858–867. [[CrossRef](#)]
163. Edalati, K.; Rastkhah, N.; Kermani, A.; Seiedi, M.; Movafeghi, A. The use of radiography for thickness measurement and corrosion monitoring in pipes. *Int. J. Press. Vessel. Pip.* **2006**, *83*, 736–741. [[CrossRef](#)]
164. Vasylenko, I.V.; Kazakevych, M.L.; Pavlishchuk, V.V. Design of Ferrofluids and Luminescent Ferrofluids Derived from CoFe<sub>2</sub>O<sub>4</sub> Nanoparticles for Nondestructive Defect Monitoring. *Theor. Exp. Chem.* **2019**, *54*, 365–368. [[CrossRef](#)]
165. Li, S.; Li, C.; Wang, F. Computational experiments of metal corrosion studies: A review. *Mater. Today Chem.* **2024**, *37*, 101986. [[CrossRef](#)]
166. Xu, D.; Pei, Z.; Yang, X.; Li, Q.; Zhang, F.; Zhu, R.; Cheng, X.; Ma, L. A Review of Trends in Corrosion-Resistant Structural Steels Research—From Theoretical Simulation to Data-Driven Directions. *Materials* **2023**, *16*, 3396. [[CrossRef](#)]

167. Turnbull, A.; Wright, L.; Crocker, L. New insight into the pit-to-crack transition from finite element analysis of the stress and strain distribution around a corrosion pit. *Corros. Sci.* **2010**, *52*, 1492–1498. [[CrossRef](#)]
168. Scheider, I.; Pfuff, M.; Dietzel, W. Simulation of hydrogen assisted stress corrosion cracking using the cohesive model. *Eng. Fract. Mech.* **2008**, *75*, 4283–4291. [[CrossRef](#)]
169. Raykar, N.; Maiti, S.; Raman, R.S. Modelling of mode-I stable crack growth under hydrogen assisted stress corrosion cracking. *Eng. Fract. Mech.* **2011**, *78*, 3153–3165. [[CrossRef](#)]
170. Wei, X.; Dong, C.; Chen, Z.; Xiao, K.; Li, X. The effect of hydrogen on the evolution of intergranular cracking: A cross-scale study using first-principles and cohesive finite element methods. *RSC Adv.* **2016**, *6*, 27282–27292. [[CrossRef](#)]
171. Álvarez, D.; Blackman, B.; Guild, F.; Kinloch, A. Mode I fracture in adhesively-bonded joints: A mesh-size independent modelling approach using cohesive elements. *Eng. Fract. Mech.* **2014**, *115*, 73–95. [[CrossRef](#)]
172. Xu, L.; Cheng, Y.F. A direct assessment of failure pressure of high-strength steel pipelines with considerations of the synergism of corrosion defects, internal pressure and soil strain. In *NACE Corrosion*; NACE: Orlando, FL, USA, 2013.
173. Criscenti, L.J.; Cygan, R.T.; Kooser, A.S.; Moffat, H.K. Water and Halide Adsorption to Corrosion Surfaces: Molecular Simulations of Atmospheric Interactions with Aluminum Oxyhydroxide and Gold. *Chem. Mater.* **2008**, *20*, 4682–4693. [[CrossRef](#)]
174. Praveen, B.M.; Alhadhrani, A.; Prasanna, B.M.; Hebbar, N.; Prabhu, R. Anti-Corrosion Behavior of Olmesartan for Soft-Cast Steel in 1 mol dm<sup>-3</sup> HCl. *Coatings* **2021**, *11*, 965. [[CrossRef](#)]
175. Matad, P.B.; Mokshanatha, P.B.; Hebbar, N.; Venkatesha, V.T.; Tandon, H.C. Ketosulfone Drug as a Green Corrosion Inhibitor for Mild Steel in Acidic Medium. *Ind. Eng. Chem. Res.* **2014**, *53*, 8436–8444. [[CrossRef](#)]
176. Beyerlein, I.; Caro, A.; Demkowicz, M.; Mara, N.; Misra, A.; Uberuaga, B. Radiation damage tolerant nanomaterials. *Mater. Today* **2013**, *16*, 443–449. [[CrossRef](#)]
177. Bhattacharya, B.; Kumar, G.D.; Agarwal, A.; Erkoç, Ş.; Singh, A.; Chakraborti, N. Analyzing Fe–Zn system using molecular dynamics, evolutionary neural nets and multi-objective genetic algorithms. *Comput. Mater. Sci.* **2009**, *46*, 821–827. [[CrossRef](#)]
178. Wang, F.; Liu, Y.; Zhu, T.; Gao, Y.; Zhao, J. Nanoscale interface of metals for withstanding momentary shocks of compression. *Nanoscale* **2010**, *2*, 2818–2825. [[CrossRef](#)]
179. Yan, L.; Diao, Y.; Lang, Z.; Gao, K. Corrosion rate prediction and influencing factors evaluation of low-alloy steels in marine atmosphere using machine learning approach. *Sci. Technol. Adv. Mater.* **2020**, *21*, 359–370. [[CrossRef](#)]
180. Salami, B.A.; Rahman, S.M.; Oyehan, T.A.; Maslehuiddin, M.; Al Dulaijan, S.U. Ensemble machine learning model for corrosion initiation time estimation of embedded steel reinforced self-compacting concrete. *Measurement* **2020**, *165*, 108141. [[CrossRef](#)]
181. Ossai, C.I. A Data-Driven Machine Learning Approach for Corrosion Risk Assessment—A Comparative Study. *Big Data Cogn. Comput.* **2019**, *3*, 28. [[CrossRef](#)]
182. Fulkerson, B.; Michie, D.; Spiegelhalter, D.J.; Taylor, C.C. Machine Learning, Neural and Statistical Classification. *Technometrics* **1995**, *37*, 459. [[CrossRef](#)]
183. Polikreti, K.; Argyropoulos, V.; Charalambous, D.; Vossou, A.; Perdikatsis, V.; Apostolaki, C. Tracing correlations of corrosion products and microclimate data on outdoor bronze monuments by Principal Component Analysis. *Corros. Sci.* **2009**, *51*, 2416–2422. [[CrossRef](#)]
184. Khayati, G.R.; Rajabi, Z.; Ehteshamzadeh, M.; Beirami, H. A Hybrid Particle Swarm Optimization with Dragonfly for Adaptive ANFIS to Model the Corrosion Rate in Concrete Structures. *Int. J. Concr. Struct. Mater.* **2022**, *16*, 28. [[CrossRef](#)]
185. Memon, A.M.; Imran, I.H.; Alhems, L.M. Neural network based corrosion modeling of Stainless Steel 316L elbow using electric field mapping data. *Sci. Rep.* **2023**, *13*, 13088. [[CrossRef](#)]
186. Li, Q.; Xia, X.; Pei, Z.; Cheng, X.; Zhang, D.; Xiao, K.; Wu, J.; Li, X. Long-term corrosion monitoring of carbon steels and environmental correlation analysis via the random forest method. *npj Mater. Degrad.* **2022**, *6*, 1. [[CrossRef](#)]
187. Wei, B.; Xu, J.; Pang, J.; Huang, Z.; Wu, J.; Cai, Z.; Yan, M.; Sun, C. Prediction of electrochemical impedance spectroscopy of high-entropy alloys corrosion by using gradient boosting decision tree. *Mater. Today Commun.* **2022**, *32*, 104047. [[CrossRef](#)]
188. Forkan, A.R.M.; Kang, Y.-B.; Jayaraman, P.P.; Liao, K.; Kaul, R.; Morgan, G.; Ranjan, R.; Sinha, S. CorrDetector: A framework for structural corrosion detection from drone images using ensemble deep learning. *Expert Syst. Appl.* **2022**, *193*, 116461. [[CrossRef](#)]
189. Ao, M.; Ji, Y.; Sun, X.; Guo, F.; Xiao, K.; Dong, C. Image Deep Learning Assisted Prediction of Mechanical and Corrosion Behavior for Al-Zn-Mg Alloys. *IEEE Access* **2022**, *10*, 35620–35631. [[CrossRef](#)]
190. Dogan, G.; Arslan, M.H.; Ilki, A. Detection of damages caused by earthquake and reinforcement corrosion in RC buildings with Deep Transfer Learning. *Eng. Struct.* **2023**, *279*, 115629. [[CrossRef](#)]
191. Asahi, H.; Kushida, T.; Kimura, M.; Fukai, H.; Okano, S. Role of Microstructures on Stress Corrosion Cracking of Pipeline Steels in Carbonate-Bicarbonate Solution. *Corrosion* **1999**, *55*, 644–652. [[CrossRef](#)]
192. Gonzalez-Rodriguez, J.G.; Casales, M.; Salinas-Bravo, V.M.; Albarran, J.L.; Martinez, L. Effect of Microstructure on the Stress Corrosion Cracking of X-80 Pipeline Steel in Diluted Sodium Bicarbonate Solutions. *Corrosion* **2002**, *58*, 584–590. [[CrossRef](#)]
193. Liu, Z.; Li, X.; Du, C.; Lu, L.; Zhang, Y.; Cheng, Y. Effect of inclusions on initiation of stress corrosion cracks in X70 pipeline steel in an acidic soil environment. *Corros. Sci.* **2009**, *51*, 895–900. [[CrossRef](#)]

194. Al-Mansour, M.; Alfantazi, A.; El-Boujdaini, M. Sulfide stress cracking resistance of API-X100 high strength low alloy steel. *Mater. Des.* **2009**, *30*, 4088–4094. [[CrossRef](#)]
195. Lu, Z.P.; Shoji, T.; Takeda, Y. Effects of water chemistry on stress corrosion cracking of 316NG weld metals in high temperature water. *Corros. Eng. Sci. Technol.* **2015**, *50*, 41–48. [[CrossRef](#)]
196. Honeycombe, J.; Gooch, T.G. Corrosion and Stress Corrosion of Arc Welds in 18% Chromium–2% Molybdenum–Titanium Stabilised Stainless Steel. *Br. Corros. J.* **1983**, *18*, 25–34. [[CrossRef](#)]
197. Kuroda, T.; Matsuda, F.; Bunno, K. Stress corrosion cracking of duplex stainless steel in high-temperature/high-pressure water. *Weld. Int.* **1995**, *9*, 788–796. [[CrossRef](#)]
198. Baroux, B. Passivation and localized corrosion of stainless steels. In *Passivity of Metals and Semiconductors*; Froment, M., Ed.; Elsevier: Amsterdam, The Netherlands, 1983; pp. 531–545.
199. Kain, V. 5—Stress corrosion cracking (SCC) in stainless steels. In *Stress Corrosion Cracking*; Raja, V.S., Shoji, T., Eds.; Woodhead Publishing: Cambridge, UK, 2011; pp. 199–244.
200. Pan, Y.; Sun, B.; Liu, Z.; Wu, W.; Li, X. Hydrogen effects on passivation and SCC of 2205 DSS in acidified simulated seawater. *Corros. Sci.* **2022**, *208*, 110640. [[CrossRef](#)]
201. Runge, J.M.; Runge, J.M. A brief history of anodizing aluminum. In *The Metallurgy of Anodizing Aluminum: Connecting Science to Practice*; Springer International Publishing: Cham, Switzerland, 2018; pp. 65–148.
202. Zhu, H.; Li, J. Advancements in corrosion protection for aerospace aluminum alloys through surface treatment. *Int. J. Electrochem. Sci.* **2024**, *19*, 100487. [[CrossRef](#)]
203. Minagar, S.; Berndt, C.C.; Wang, J.; Ivanova, E.; Wen, C. A review of the application of anodization for the fabrication of nanotubes on metal implant surfaces. *Acta Biomater.* **2012**, *8*, 2875–2888. [[CrossRef](#)]
204. Rezayat, M.; Karamimoghadam, M.; Moradi, M.; Casalino, G.; Rovira, J.J.R.; Mateo, A. Overview of Surface Modification Strategies for Improving the Properties of Metastable Austenitic Stainless Steels. *Metals* **2023**, *13*, 1268. [[CrossRef](#)]
205. Fürstner, R.; Barthlott, W.; Neinhuis, C.; Walzel, P. Wetting and Self-Cleaning Properties of Artificial Superhydrophobic Surfaces. *Langmuir* **2005**, *21*, 956–961. [[CrossRef](#)] [[PubMed](#)]
206. Bellido-Aguilar, D.A.; Zheng, S.; Huang, Y.; Zeng, X.; Zhang, Q.; Chen, Z. Solvent-Free Synthesis and Hydrophobization of Biobased Epoxy Coatings for Anti-Icing and Anticorrosion Applications. *ACS Sustain. Chem. Eng.* **2019**, *7*, 19131–19141. [[CrossRef](#)]
207. Cheng, Y. Fundamentals of hydrogen evolution reaction and its implications on near-neutral pH stress corrosion cracking of pipelines. *Electrochimica Acta* **2007**, *52*, 2661–2667. [[CrossRef](#)]
208. Yan, M.; Wang, J.; Han, E.; Ke, W. Local environment under simulated disbanded coating on steel pipelines in soil solution. *Corros. Sci.* **2008**, *50*, 1331–1339. [[CrossRef](#)]
209. Yan, M.; Sun, C.; Xu, J.; Wu, T.; Yang, S.; Ke, W. Stress corrosion of pipeline steel under occluded coating disbondment in a red soil environment. *Corros. Sci.* **2015**, *93*, 27–38. [[CrossRef](#)]
210. Chen, X.; Wang, G.; Gao, F.; Wang, Y.; He, C. Effects of sulphate-reducing bacteria on crevice corrosion in X70 pipeline steel under disbanded coatings. *Corros. Sci.* **2015**, *101*, 1–11. [[CrossRef](#)]
211. Beavers, J.A.; Thompson, N.G. External Corrosion of Oil and Natural Gas Pipelines. In *ASM Handbook*; ASM International: Materials Park, OH, USA, 2006; pp. 1015–1026.
212. Fu, A.; Tang, X.; Cheng, Y. Characterization of corrosion of X70 pipeline steel in thin electrolyte layer under disbanded coating by scanning Kelvin probe. *Corros. Sci.* **2009**, *51*, 186–190. [[CrossRef](#)]
213. Quej, L.; Mireles, M.; Galván-Martínez, R.; Contreras, A. Electrochemical characterization of X60 steel exposed to different soils from South of México. In *Materials Characterization*; Springer: Berlin/Heidelberg, Germany, 2015; pp. 101–116.
214. Zhang, F.; Ju, P.; Pan, M.; Zhang, D.; Huang, Y.; Li, G.; Li, X. Self-healing mechanisms in smart protective coatings: A review. *Corros. Sci.* **2018**, *144*, 74–88. [[CrossRef](#)]
215. Stankiewicz, A.; Szczygieł, I.; Szczygieł, B. Self-healing coatings in anti-corrosion applications. *J. Mater. Sci.* **2013**, *48*, 8041–8051. [[CrossRef](#)]
216. Karpakam, V.; Kamaraj, K.; Sathiyarayanan, S.; Venkatachari, G.; Ramu, S. Electrosynthesis of polyaniline–molybdate coating on steel and its corrosion protection performance. *Electrochimica Acta* **2011**, *56*, 2165–2173. [[CrossRef](#)]
217. Solovyeva, V.A.; Almuhammadi, K.H.; Badeghaish, W.O. Current Downhole Corrosion Control Solutions and Trends in the Oil and Gas Industry: A Review. *Materials* **2023**, *16*, 1795. [[CrossRef](#)]
218. Nikafshar, S.; McCracken, J.; Dunne, K.; Nejad, M. Improving UV-Stability of epoxy coating using encapsulated halloysite nanotubes with organic UV-Stabilizers and lignin. *Prog. Org. Coat.* **2021**, *151*, 105843. [[CrossRef](#)]
219. Nawaz, M.; Habib, S.; Khan, A.; Shakoor, R.A.; Kahraman, R. Cellulose microfibrils (CMFs) as a smart carrier for autonomous self-healing in epoxy coatings. *New J. Chem.* **2020**, *44*, 5702–5710. [[CrossRef](#)]
220. Tanvir, A.; El-Gawady, Y.H.; Al-Maadeed, M. Cellulose nanofibers to assist the release of healing agents in epoxy coatings. *Prog. Org. Coatings* **2017**, *112*, 127–132. [[CrossRef](#)]

221. Rafiee, M.A.; Rafiee, J.; Wang, Z.; Song, H.; Yu, Z.-Z.; Koratkar, N. Enhanced Mechanical Properties of Nanocomposites at Low Graphene Content. *ACS Nano* **2009**, *3*, 3884–3890. [[CrossRef](#)] [[PubMed](#)]
222. Varzeghani, H.N.; Amraei, I.A.; Mousavi, S.R. Dynamic Cure Kinetics and Physical-Mechanical Properties of PEG/Nanosilica/Epoxy Composites. *Int. J. Polym. Sci.* **2020**, *2020*, 7908343. [[CrossRef](#)]
223. Ahmadi, Z. Epoxy in nanotechnology: A short review. *Prog. Org. Coatings* **2019**, *132*, 445–448. [[CrossRef](#)]
224. Loto, R.T.; Leramo, R.; Oyebade, B. Synergistic Combination Effect of *Salvia officinalis* and *Lavandula officinalis* on the Corrosion Inhibition of Low-Carbon Steel in the Presence of  $\text{SO}_4^{2-}$  and  $\text{Cl}^-$ -Containing Aqueous Environment. *J. Fail. Anal. Prev.* **2018**, *18*, 1429–1438. [[CrossRef](#)]
225. Aslam, R.; Mobin, M.; Zehra, S.; Aslam, J. A comprehensive review of corrosion inhibitors employed to mitigate stainless steel corrosion in different environments. *J. Mol. Liq.* **2022**, *364*, 119992. [[CrossRef](#)]
226. Zhang, Y.; Pan, Y.; Li, P.; Zeng, X.; Guo, B.; Pan, J.; Hou, L.; Yin, X. Novel Schiff base-based cationic Gemini surfactants as corrosion inhibitors for Q235 carbon steel and printed circuit boards. *Colloids Surfaces A: Physicochem. Eng. Asp.* **2021**, *623*, 126717. [[CrossRef](#)]
227. Sivapragash, M.; Kumaradhas, P.; Vettivel, S.; Retnam, B.S.J. Optimization of PVD process parameter for coating AZ91D magnesium alloy by Taguchi grey approach. *J. Magnes. Alloy.* **2018**, *6*, 171–179. [[CrossRef](#)]
228. Daroonparvar, M.; Bakhsheshi-Rad, H.R.; Saberi, A.; Razzaghi, M.; Kasar, A.K.; Ramakrishna, S.; Menezes, P.L.; Misra, M.; Ismail, A.F.; Sharif, S.; et al. Surface modification of magnesium alloys using thermal and solid-state cold spray processes: Challenges and latest progresses. *J. Magnes. Alloy.* **2022**, *10*, 2025–2061. [[CrossRef](#)]
229. Zhang, M.; Zhou, T.; Li, H.; Liu, Q. UV-durable superhydrophobic ZnO/SiO<sub>2</sub> nanorod arrays on an aluminum substrate using catalyst-free chemical vapor deposition and their corrosion performance. *Appl. Surf. Sci.* **2023**, *623*, 157085. [[CrossRef](#)]
230. Deng, K.; Wang, X.; Huang, S.; Li, P.; Jiang, Q.; Yin, H.; Fan, J.; Wei, K.; Zheng, Y.; Shi, J.; et al. Effective Suppression of Amorphous Ga<sub>2</sub>O and Related Deep Levels on the GaN Surface by High-Temperature Remote Plasma Pretreatments in GaN-Based Metal-Insulator-Semiconductor Electronic Devices. *ACS Appl. Mater. Interfaces* **2023**, *15*, 25058–25065. [[CrossRef](#)]
231. Kencana, S.D.; Kuo, Y.-L.; Yen, Y.-W.; Schellkes, E.; Chuang, W. Improving the solder wettability via atmospheric plasma technology. In Proceedings of the 2019 IEEE 69th Electronic Components and Technology Conference (ECTC), Las Vegas, NV, USA, 28–31 May 2019.
232. Ramezani, M.; Ripin, Z.M.; Pasang, T.; Jiang, C.-P. Surface Engineering of Metals: Techniques, Characterizations and Applications. *Metals* **2023**, *13*, 1299. [[CrossRef](#)]
233. Liu, B.; Xiao, F.; Zhu, H.; Tang, M. Promising WC-30WB-10Co Cemented Carbide Coating with Improved Density and Hardness Deposited by High Velocity Oxy-Fuel Spraying: Microstructure and Mechanical Properties. *J. Mater. Eng. Perform.* **2023**, *32*, 6405–6411. [[CrossRef](#)]
234. Ko, G.; Kim, W.; Kwon, K.; Lee, T.-K. The Corrosion of Stainless Steel Made by Additive Manufacturing: A Review. *Metals* **2021**, *11*, 516. [[CrossRef](#)]
235. Pasco, J.; Lei, Z.; Aranas, C. Additive Manufacturing in Off-Site Construction: Review and Future Directions. *Buildings* **2022**, *12*, 53. [[CrossRef](#)]
236. Kong, D.-J.; Wu, Y.-Z.; Long, D. Stress Corrosion of X80 Pipeline Steel Welded Joints by Slow Strain Test in NACE H<sub>2</sub>S Solutions. *J. Iron Steel Res. Int.* **2013**, *20*, 40–46. [[CrossRef](#)]
237. Javidi, M.; Horeh, S.B. Investigating the mechanism of stress corrosion cracking in near-neutral and high pH environments for API 5L X52 steel. *Corros. Sci.* **2014**, *80*, 213–220. [[CrossRef](#)]
238. Liu, Z.; Li, X.; Cheng, Y. Electrochemical state conversion model for occurrence of pitting corrosion on a cathodically polarized carbon steel in a near-neutral pH solution. *Electrochimica Acta* **2011**, *56*, 4167–4175. [[CrossRef](#)]
239. Li, M.; Cheng, Y. Corrosion of the stressed pipe steel in carbonate–bicarbonate solution studied by scanning localized electrochemical impedance spectroscopy. *Electrochimica Acta* **2008**, *53*, 2831–2836. [[CrossRef](#)]
240. Liu, Z.; Li, X.; Cheng, Y. Mechanistic aspect of near-neutral pH stress corrosion cracking of pipelines under cathodic polarization. *Corros. Sci.* **2012**, *55*, 54–60. [[CrossRef](#)]
241. Fu, A.; Cheng, Y. Electrochemical polarization behavior of X70 steel in thin carbonate/bicarbonate solution layers trapped under a disbanded coating and its implication on pipeline SCC. *Corros. Sci.* **2010**, *52*, 2511–2518. [[CrossRef](#)]
242. Yin, Z.F.; Zhao, W.Z.; Feng, Y.R.; Zhu, S.D. Characterisation of CO<sub>2</sub> corrosion scale in simulated solution with Cl<sup>-</sup> ion under turbulent flow conditions. *Corros. Eng. Sci. Technol.* **2009**, *44*, 453–461. [[CrossRef](#)]
243. Liu, Z.; Li, X.; Du, C.; Zhai, G.; Cheng, Y. Stress corrosion cracking behavior of X70 pipe steel in an acidic soil environment. *Corros. Sci.* **2008**, *50*, 2251–2257. [[CrossRef](#)]
244. Dong, C.; Fu, A.; Li, X.; Cheng, Y. Localized EIS characterization of corrosion of steel at coating defect under cathodic protection. *Electrochimica Acta* **2008**, *54*, 628–633. [[CrossRef](#)]
245. Quej-Ake, L.; Marín-Cruz, J.; Contreras, A. Electrochemical study of the corrosion rate of API steels in clay soils. *Anti-Corrosion Methods Mater.* **2017**, *64*, 61–68. [[CrossRef](#)]
246. Quej-Aké, L.; Nava, N.; Espinosa-Medina, M.A.; Liu, H.B.; Alamilla, J.L.; Sosa, E. Characterisation of soil/pipe interface at a pipeline failure after 36 years of service under impressed current cathodic protection. *Corros. Eng. Sci. Technol.* **2015**, *50*, 311–319. [[CrossRef](#)]

- 
247. Cole, I.S.; Marney, D. The science of pipe corrosion: A review of the literature on the corrosion of ferrous metals in soils. *Corros. Sci.* **2021**, *56*, 5–16. [[CrossRef](#)]
248. Liao, K.; Yao, Q.; Wu, X.; Jia, W. A Numerical Corrosion Rate Prediction Method for Direct Assessment of Wet Gas Gathering Pipelines Internal Corrosion. *Energies* **2012**, *5*, 3892–3907. [[CrossRef](#)]

**Disclaimer/Publisher’s Note:** The statements, opinions and data contained in all publications are solely those of the individual author(s) and contributor(s) and not of MDPI and/or the editor(s). MDPI and/or the editor(s) disclaim responsibility for any injury to people or property resulting from any ideas, methods, instructions or products referred to in the content.